MÁSTER UNIVERSITARIO EN INGENIERÍA INDUSTRIAL

TRABAJO FIN DE MÁSTER

NUMERICAL STUDY ON STRUCTURAL RESPONSE OF COMPOSITE WIND TURBINE BLADE SECTIONS WITH ARTIFICIAL DAMAGES

Autor: Blanca Acitores de la Cruz

Director: Kim Branner

Madrid

Abril de 2019

AUTHORIZATION FOR DIGITALIZATION, STORAGE AND DISSEMINATION IN THE NETWORK OF END-OF-DEGREE PROJECTS, MASTER PROJECTS, DISSERTATIONS OR BACHILLERATO REPORTS

1. Declaration of authorship and accreditation thereof.

The author Mr. /Ms. Blanca Acitores de la Cruz

HEREBY DECLARES that he/she owns the intellectual property rights regarding the piece of work: Numerical study on structural failure of composite wind turbine blade sections with artificial damages
that this is an original piece of work, and that he/she holds the status of author, in the sense granted by the Intellectual Property Law.

2. Subject matter and purpose of this assignment.

With the aim of disseminating the aforementioned piece of work as widely as possible using the University's Institutional Repository the author hereby **GRANTS** Comillas Pontifical University, on a royalty-free and non-exclusive basis, for the maximum legal term and with universal scope, the digitization, archiving, reproduction, distribution and public communication rights, including the right to make it electronically available, as described in the Intellectual Property Law. Transformation rights are assigned solely for the purposes described in a) of the following section.

3. Transfer and access terms

Without prejudice to the ownership of the work, which remains with its author, the transfer of rights covered by this license enables:

a) Transform it in order to adapt it to any technology suitable for sharing it online, as well as including metadata to register the piece of work and include "watermarks" or any other security or protection system.

b) Reproduce it in any digital medium in order to be included on an electronic database, including the right to reproduce and store the work on servers for the purposes of guaranteeing its security, maintaining it and preserving its format.

c) Communicate it, by default, by means of an institutional open archive, which has open and cost-free online access.

d) Any other way of access (restricted, embargoed, closed) shall be explicitly requested and requires that good cause be demonstrated.

e) Assign these pieces of work a Creative Commons license by default.

f) Assign these pieces of work a HANDLE (*persistent* URL). by default.

4. Copyright.

The author, as the owner of a piece of work, has the right to:

a) Have his/her name clearly identified by the University as the author

b) Communicate and publish the work in the version assigned and in other subsequent versions using any medium.

c) Request that the work be withdrawn from the repository for just cause.

d) Receive reliable communication of any claims third parties may make in relation to the work and, in particular, any claims relating to its intellectual property rights.

5. Duties of the author.

The author agrees to:

a) Guarantee that the commitment undertaken by means of this official document does not infringe any third party rights, regardless of whether they relate to industrial or intellectual property or any other type.

b) Guarantee that the content of the work does not infringe any third party honor, privacy or image rights.
c) Take responsibility for all claims and liability, including compensation for any damages, which may be brought against the University by third parties who believe that their rights and interests have been infringed by the assignment.
d) Take responsibility in the event that the institutions are found guilty of a rights infringement regarding the work subject to assignment.

6. Institutional Repository purposes and functioning.

The work shall be made available to the users so that they may use it in a fair and respectful way with regards to the copyright, according to the allowances given in the relevant legislation, and for study or research purposes, or any other legal use. With this aim in mind, the University undertakes the following duties and reserves the following powers:

a) The University shall inform the archive users of the permitted uses; however, it shall not guarantee or take any responsibility for any other subsequent ways the work may be used by users, which are non-compliant with the legislation in force. Any subsequent use, beyond private copying, shall require the source to be cited and authorship to be recognized, as well as the guarantee not to use it to gain commercial profit or carry out any derivative works.
b) The University shall not review the content of the works, which shall at all times fall under the exclusive responsibility of the author and it shall not be obligated to take part in lawsuits on behalf of the author in the event of any infringement of intellectual property rights deriving from storing and archiving the works. The author hereby waives any claim against the University due to any way the users may use the works that is not in keeping with the legislation in force.
c) The University shall adopt the necessary measures to safeguard the work in the future.
d) The University reserves the right to withdraw the work, after notifying the author, in sufficiently justified cases, or in the event of third party claims.

Madrid, on 3..... of April 2019....., ...

HEREBY ACCEPTS

Signed.Blanca Acitores de la Cruz.....

Reasons for requesting the restricted, closed or embargoed access to the work in the Institution's Repository

I declare, under my resposability, that the Project presented under the title:

Numerical study on structural failure of composite wind turbine blade sections with artificial damages

in the Engineering School Universidad Pontificia Comillas in the academic year 2018/2019 is original and from my authorship. The information taken from other documents is hereby referenced.

Blanca Acitores de la Cruz Date: 03/ 04/ 2019

Authorizing the Project:

The Project's supervisor

Kim Branner Date: 05/ 03/ 2019

MÁSTER UNIVERSITARIO EN INGENIERÍA INDUSTRIAL

TRABAJO FIN DE MÁSTER

NUMERICAL STUDY ON STRUCTURAL RESPONSE OF COMPOSITE WIND TURBINE BLADE SECTIONS WITH ARTIFICIAL DAMAGES

Autor: Blanca Acitores de la Cruz

Director: Kim Branner

Madrid

Abril de 2019

ESTUDIO NUMÉRICO SOBRE EL FALLO ESTRUCTURAL EN SECCIONES DE PALA DE AEROGENERADORES EÓLICOS MEDIANTE DEFECTOS ARTIFICIALES

Autor: Acitores de la Cruz, Blanca.

Director: Branner, Kim.

Entidad Colaboradora: Laboratorio Nacional Risø de energías renovables.

RESUMEN DEL PROYECTO

1. Introducción

Las palas de los aerogeneradores son los componentes fundamentales de estos para la generación de energía. Por lo tanto, su diseño y optimización es muy importante para garantizar que las cargas que sufren durante su vida útil son soportadas a la vez que aportan la mayor eficiencia posible.

Por otro lado, las palas deben diseñarse minimizando sus reparaciones para así reducir los costes de mantenimiento y operaciones, que pueden suponer hasta un 20-25 % del coste total energético nivelado (LCOE) [1]. Una forma de limitar los costes de mantenimiento y operaciones es disminuyendo el número de defectos en las palas de los aerogeneradores, así como incrementando la investigación sobre ellos para discernir qué defectos requieren reparación inmediata o cuáles pueden mantenerse durante la operación del aerogenerador.

Los materiales compuestos que conforman las palas de los aerogeneradores no tienen las mismas propiedades mecánicas en todas las direcciones del espacio, por lo que su comportamiento varía de una estructura compuesta a otra. En consecuencia, los modos de fallo todavía necesitan mayor investigación [2].

Este proyecto se centrará en el análisis de dos tipos de defectos comunes que se encuentran en las palas de los aerogeneradores. Estos se enfocan principalmente en la falta de adhesivo en dos ubicaciones diferentes de la pala.

El objetivo principal de este proyecto es llevar a cabo un análisis estático de pandeo sobre una sección de una pala comercial. La pala considerada es prismática, está hecha de fibra de vidrio y pertenece a una turbina eólica de 2MW [3].

Otro objetivo importante de este proyecto es poder proporcionar un estudio numérico de las cargas experimentadas por la sección de la pala considerada. Para ello, esta sección es generada mediante un modelo de elementos finitos realizado en Abaqus y su comportamiento de pandeo se comparará con el de la misma sección con defectos. Los defectos que se tienen en cuenta para este estudio son la falta de adhesivo en el borde posterior de la pala y en las juntas del cajón de torsión.

Por último, otro fin de este trabajo es examinar las consecuencias de los defectos sobre la respuesta estructural en diferentes direcciones de carga. Estas direcciones serán ampliadas con respecto a las que son actualmente exigidas por la legislación vigente para el diseño de palas en las turbinas eólicas [4]. Finalmente, el estudio estructural y la comparación entre la pala con y sin defectos se llevará a cabo considerando dos criterios de fallo del material: Tsai-Wu y fallo de adhesivo.

2. Metodología

El modelo 3D de la sección de la pala se genera en Abaqus modificando un archivo de entrada con formato de archivo de texto. El uso de archivos de entrada posibilita el estudio numérico y paramétrico, ya que permite la asigna-

ción y modificación de cualquier parámetro, materiales, geometrías, así como la facilidad para alterar los datos según sea necesario.

El estudio comienza con el diseño de los defectos artificiales y su introducción en el modelo de elementos finitos de la sección de pala. Cada tipo de defecto está diseñado para que algunos parámetros puedan modificarse y así poder variar el tamaño de los defectos. Varios casos de estudio son considerados dentro de cada tipo de defecto. Por un lado, los casos de borde posterior se ilustran en la figura 1, donde tres casos de estudio varían el tamaño del defecto manteniendo una posición centrada en la sección. Por otro lado, la ausencia de adhesivo en el cajón de torsión se estudia en dos regiones diferentes de la sección transversal de la pala: la parte superior derecha del larguero posterior (UR) y la parte inferior izquierda del larguero delantero (LL). Las ubicaciones de ambos defectos junto con la variación de tamaño del defecto en cada caso de estudio se muestran en la figura 2.

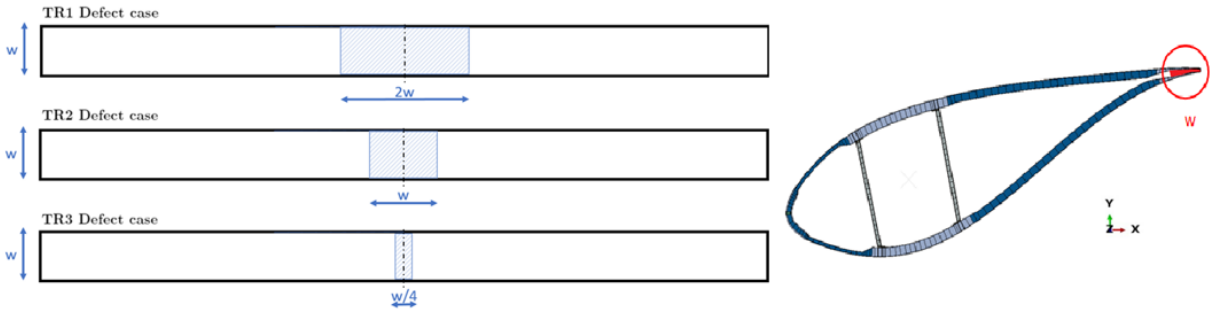

Figura 1: Esquema de los defectos en el borde posterior (izquierda) y situación del defecto en la sección transversal de la pala (derecha).

Los análisis de pandeo se basan en el actual Estándar de diseño de las palas del rotor (DNVGL-ST-0376 Standard) [4]. De acuerdo con esta legislación, todas las partes de la pala deben revisarse para detectar posibles fallos de pandeo en todas las ubicaciones con un determinado factor de seguridad, denominado factor de reducción γ_m en esta norma. Este factor de reducción se ha fijado para este proyecto en 2.2 para el análisis de pandeo lineal y en 1.65 para el análisis de pandeo no lineal. El análisis de pandeo se desarrolla de la misma manera

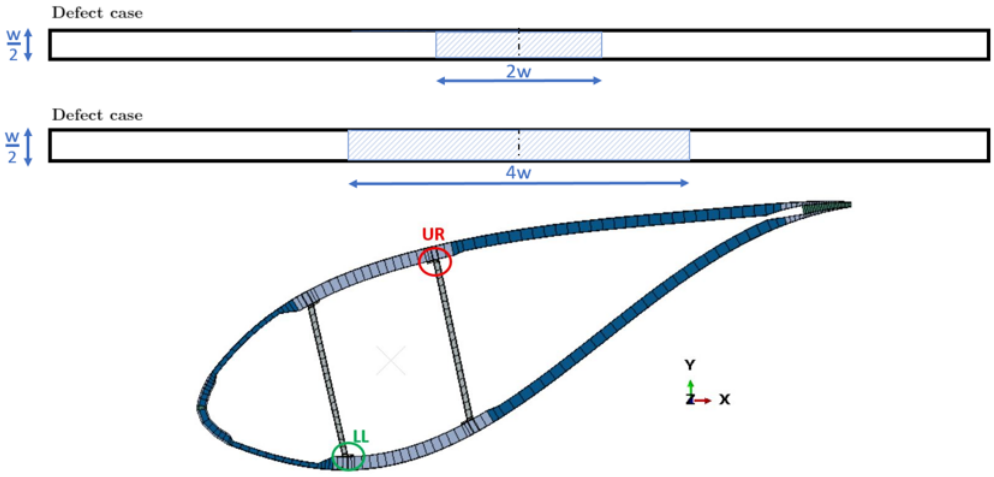

Figura 2: Esquema de defectos en la parte superior derecha del larguero posterior (UR) y en la parte inferior izquierda del larguero delantero (LL), en la figura superior. También se muestra la situación de los defectos en la sección transversal de la pala (figura inferior).

para el estudio de la pala con y sin defectos. Además, este análisis es estático, ya que no se tienen en cuenta velocidades o aceleraciones. En este proyecto se realizan análisis de pandeo tanto lineales como no lineales, ya que los últimos pueden proporcionar mayor precisión.

Las cargas iniciales de este estudio se tomaron de un estudio anterior de la misma pala [3] que investiga su colapso estructural a través de un ensayo a gran escala (pala completa). Estas cargas de entrada son los momentos de batimento y arrastre experimentados en una sección específica de la pala durante su ensayo. Por tanto, estos momentos se aplican en cuatro direcciones de carga determinadas. Adicionalmente, también se estudian otras ocho direcciones de carga que para realizar un análisis de carga combinada. De esta manera, estas direcciones se pueden estudiar suponiendo un envolvente de carga elíptico a partir de las cargas iniciales, lo que lleva a un total de doce direcciones de carga estudiadas, las cuales están separadas 30° entre sí. Este envolvente de carga se ilustra en la figura 3 y las magnitudes de las cargas se calculan con respecto a su dirección de carga específica. El rendimiento de la pala en cada dirección de carga se evaluará comparando el comportamiento de pandeo y el fallo del

material con el factor de reducción exigido por el estándar de diseño actual [4].

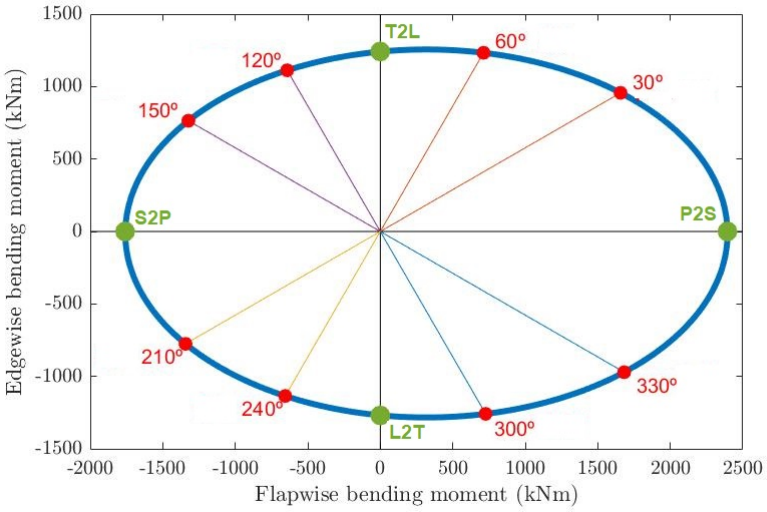

Figura 3: Envolvente de carga con las cargas de diseño para el análisis de pandeo. Las cargas iniciales de batimento y arrastre se muestran en verde mientras que las cargas combinadas se muestran en rojo.

Por otro lado, las condiciones de contorno consideradas son las de una viga simplemente apoyada, ya que es la que mejor se ajusta al comportamiento de una sección media de pala.

Los criterios de fallo relacionan las deformaciones y tensiones de la lámina con las magnitudes de éstas que el material es capaz de soportar. Según el criterio, se define una función F que limita las tensiones y las deformaciones. La estructura falla si las tensiones y las deformaciones creadas por las cargas de entrada hacen que esta función exceda o sea igual a 1 ($F \geq 1$). Dos criterios de fallo son definidos en este proyecto: Tsai-Wu y fallo del adhesivo. Además, se usa el fallo de primera lámina para el análisis de los criterios de fallo, el cual establece que la resistencia del laminado está determinada por la resistencia de cada lámina [5].

Finalmente, para implementar los análisis, se han hecho varias hipótesis:

- Los defectos se configuran con formas rectangulares arbitrarias. Los defectos reales variarían en forma y tamaño.
- Las cuatro cargas extremas a la pala (iniciales) son las únicas cargas conocidas para el estudio. Las magnitudes de carga combinada están determinadas por la envolvente de carga, la cual se aproxima a una elipse que incluye las cargas iniciales.
- Como se mencionó en la sección anterior, el criterio de fallo de primera capa se considera para la determinación del fallo del material.
- El modelo 3D de la pala no restringe el contacto entre las láminas. Por lo tanto, cuando la estructura de la pala se deforma, las láminas pueden penetrar unas con otras. Este comportamiento no es realista.
- Las condiciones de contorno se fijan en los extremos de la pala y proporcionan mayores tensiones que las que se crearían en realidad. Por lo tanto, la región del extremo de la pala no se considera para el análisis de resultados.
- Imperfecciones geométricas de 1 mm de longitud son añadidas al análisis de pandeo no lineal de la pala sin defectos para iniciar el pandeo y proporcionar resultados fiables. Para mantener consistencia, estas imperfecciones también se aplican a los casos de defectos, ya que se supone que son muy pequeñas para ser significativas en comparación con estos.

3. Resultados

3.1. Análisis de la pala sin defectos

ANÁLISIS DE PANDEO LINEAL

Haciendo uso del análisis de elementos finitos, el análisis de pandeo lineal resuelve el problema de autovalores de la matriz de rigidez en cada elemento

de la malla sobre la sección de pala considerada. Por lo tanto, la carga crítica de pandeo se puede calcular mediante la multiplicación de la carga aplicada con el autovalor obtenido (se toma el autovalor más bajo). De esta manera, los autovalores son factores de seguridad que pueden compararse fácilmente con los factores de reducción especificados por la legislación de diseño de las palas de aerogeneradores.

La figura 4 muestra la conformidad de la sección de pala en pandeo con respecto a los requisitos solicitados por la norma de diseño. Las magnitudes de los autovalores se muestran en cada dirección de carga, formando una envolvente de carga similar al de las cargas de diseño para este análisis de pandeo (figura 3). La principal diferencia es que, en lugar de momentos flectores, los autovalores forman la envolvente para así poder ser comparados con el factor de reducción requerido por el Estándar. Por lo tanto, aquellos casos donde los autovalores son más bajos que el factor de reducción solicitado (no cumplen con el Estándar) están incluidos dentro del límite del factor de reducción (elipse roja en la figura). Por el contrario, los autovalores que satisfacen el Estándar, son mayores que el factor de reducción y están en las afueras de esta elipse.

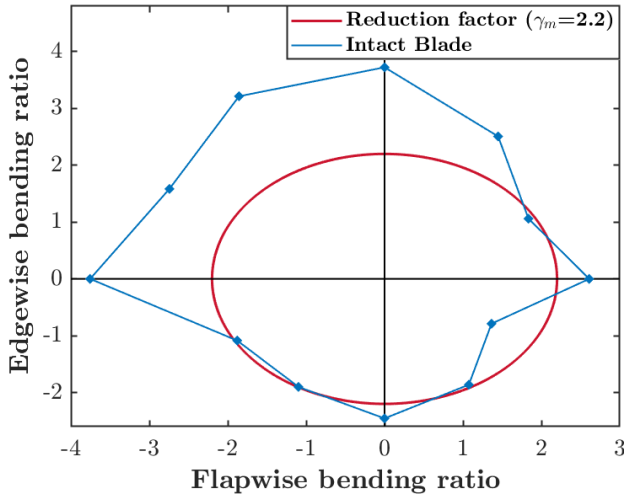

Figura 4: Envolvente para el análisis lineal de pandeo de la pala sin defectos, comparando este con el factor de reducción solicitado por la norma de diseño.

Un resultado importante obtenido es que las direcciones de carga extremas

presentan mayores autovalores que el factor de reducción solicitado $\gamma_m = 2{,}200$, satisfaciendo así los requisitos de diseño. Sin embargo, hay algunos autovalores correspondientes a las direcciones de carga combinada que son inferiores a este factor de reducción, especialmente para las direcciones de carga con $\pm 30°$.

ANÁLISIS DE PANDEO NO LINEAL

El análisis de pandeo no lineal es un estudio incremental que permite tener en cuenta las existencia de imperfecciones y de zonas no lineales. Es más preciso que el análisis de pandeo lineal, por lo que bajo este análisis se estudia el fallo del material y se compara igualmente con los requerimientos de diseño de la pala.

El análisis de pandeo no lineal se muestra en la figura 5. De la misma manera que en el análisis lineal, las direcciones de carga de $\pm 30°$ no satisfacen adecuadamente los requerimientos de diseño. Por otro lado, el criterio de fallo Tsai-Wu es más restrictivo que el criterio de fallo de adhesivo.

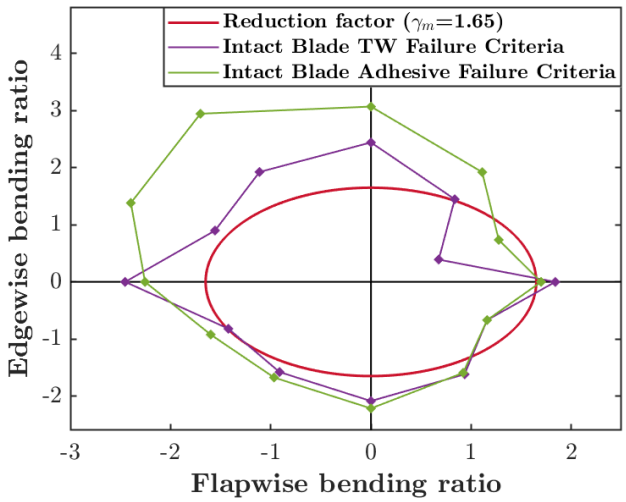

Figura 5: Envolvente para el análisis de pandeo no lineal de la pala sin defectos, comparando este con el factor de reducción solicitado por la norma de diseño.

3.2. Análisis de la pala con defectos

El procedimiento de análisis seguido sobre la pala sin defectos es el mismo que para la pala con defectos. En el análisis de pandeo no lineal, el criterio de fallo de material más restrictivo es el que se emplea para realizar la comparación entre los diferentes casos de defectos con la pala sin defectos y con el factor de reducción exigido.

AUSENCIA DE ADHESIVO EN EL BORDE POSTERIOR DE LA PALA

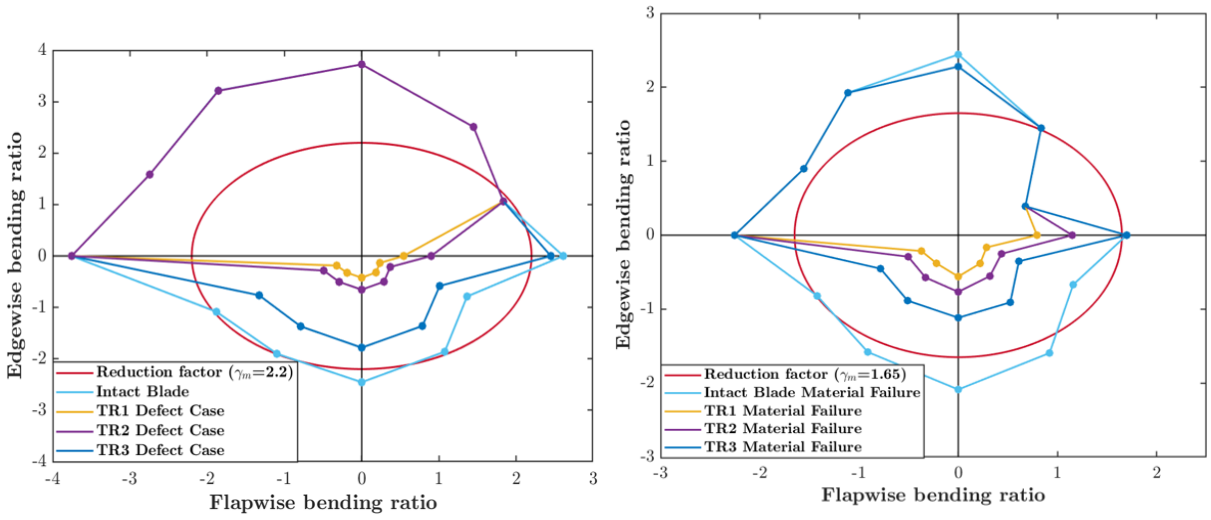

(a) Pandeo lineal

(b) Pandeo no lineal

Figura 6: Análisis de pandeo lineal y no lineal de los casos de defectos en el borde posterior, comparados con el estándar de diseño.

Los análisis de pandeo de todos los casos de defectos en el borde posterior se comparan con el estándar de diseño en la figura 6. Por un lado, el análisis de pandeo lineal (6a) muestra que el rendimiento de la pala se ve afectado por la presencia del defecto únicamente en las direcciones de carga que tienen el defecto en compresión. Sin embargo, las direcciones de carga donde el defecto se encuentra en tensión tienen la misma respuesta de pandeo que la pala sin defectos. Esto se debe a que el pandeo aparece debido a la inestabilidad estructural bajo compresión.

Por otro lado, los análisis de pandeo no lineal presentan una diferencia con respecto a los análisis de pandeo lineal: el defecto reduce también el rendimiento de la pala en la dirección de carga de 90°, que sitúa al defecto en el lado de tensión. Esto se debe a que el análisis de pandeo no lineal se divide en incrementos y el resultado de este análisis contrasta todos los elementos de la malla. Esto tiene como consecuencia que el defecto pueda terminar afectando al rendimiento de la pala incluso si el defecto se encuentra sometido a tensión cuando la carga es aplicada. 90° es la única dirección en el lado de tensión que reduce el rendimiento porque el defecto mantiene la máxima distancia al eje neutro de la estructura.

En ambos análisis de pandeo, es razonable que el rendimiento de la pala empeore cuando se amplía el tamaño del defecto. Sin embargo, incluso en el caso en el que el defecto es más pequeño (12.5 cm de longitud), el rendimiento de la pala es inaceptable, ya que las direcciones de carga con el defecto bajo compresión tienen factores de reducción inferiores a 1.

AUSENCIA DE ADHESIVO EN LAS UNIONES DEL CAJÓN DE TORSIÓN DE LA PALA

- Ausencia de adhesivo en la parte superior derecha del larguero posterior

En este caso, el defecto está bajo compresión entre las direcciones de carga desde 240 a 30°, en sentido contrario a las agujas del reloj. Sin embargo, entre todas estas direcciones de carga en las que el defecto está en compresión, solo 0 y 30° son aquellas en las que el defecto afecta negativamente al rendimiento de la pala. Esto es debido a que en la mayor parte de estas direcciones de carga, el mayor comportamiento de pandeo no se produce cerca del defecto si no en zonas de las palas que están más alejadas del eje neutral (borde posterior). Por consiguiente, el defecto en el larguero posterior soporta menos esfuerzos en dichas direcciones.

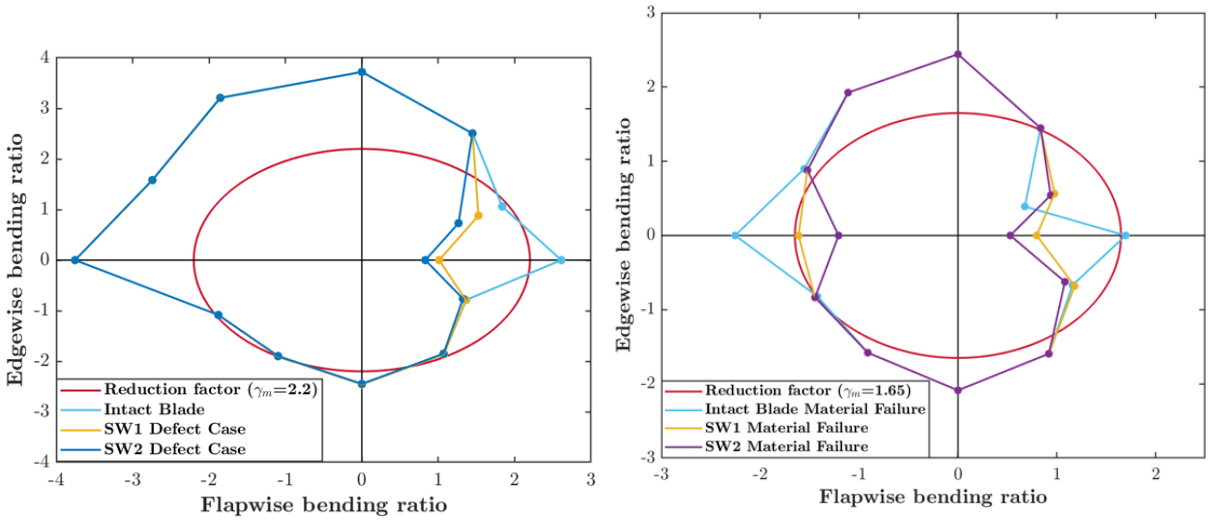

(a) Pandeo lineal

(b) Pandeo no lineal

Figura 7: Análisis de pandeo lineal y no lineal de los casos de defectos en el borde superior derecha del cajón de torsión, comparados con el estándar de diseño.

El análisis de pandeo no lineal se diferencia del análisis de pandeo lineal en dos cosas. En primer lugar, el rendimiento de la pala se ve afectado por el defecto en una dirección de carga diferente a las del análisis lineal. Esta dirección es 180°, lo que significa que este tipo de defecto influye en ambos sentidos del movimiento de batimento. En segundo lugar, la dirección de carga de 30° es un caso especial para este estudio. Los resultados muestran que la pala funcionaría mejor con la presencia de este defecto que sin él (pala sin defectos). La justificación de estos resultados debe estar relacionada con las características e hipótesis del modelo de pala considerado. Sin embargo, la duración del proyecto no ha sido lo suficientemente larga como encontrar la causa de estos resultados.

- Ausencia de adhesivo en la parte inferior izquierda del larguero delantero

En el análisis lineal de este tipo de defecto, el defecto se encuentra en compresión desde 60 a 210°. El rendimiento de la pala disminuye con la presencia del defecto a medida que este aumenta su distancia al eje neutro de la sección transversal de la pala con la dirección de la carga. De esta manera, el rendimiento menor de la pala se produce para la dirección de carga de 180°.

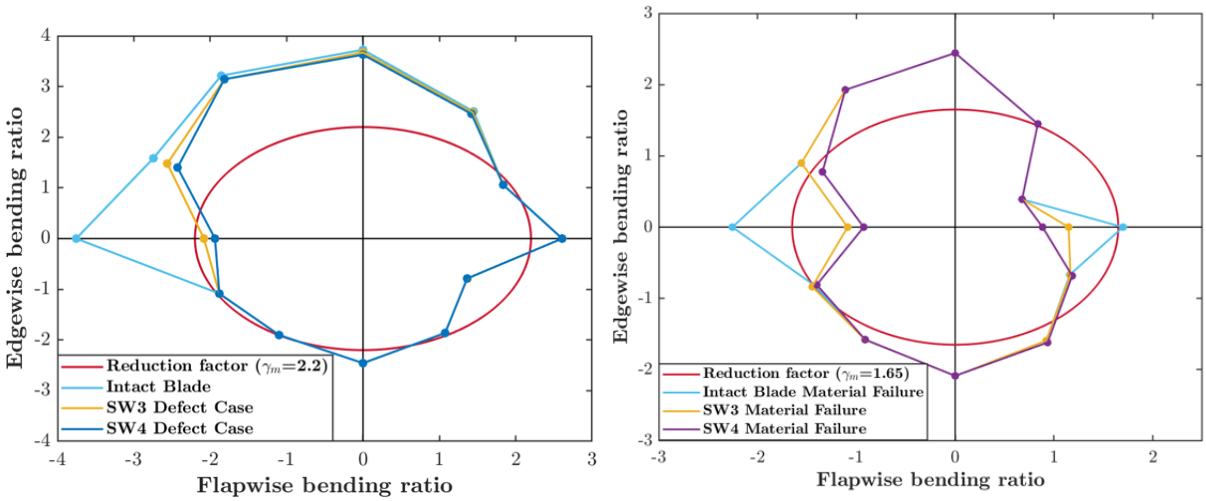

(a) Pandeo lineal

(b) Pandeo no lineal

Figura 8: Análisis de pandeo lineal y no lineal de los casos de defectos en el borde inferior izquierda del cajón de torsión, comparados con el estándar de diseño.

Al igual que en el caso del defecto anterior, el análisis de pandeo no lineal no cumple con la Norma en ambos sentidos del movimiento de batimento, incluso aunque 0° tenga el defecto en la zona de tensión.

4. Conclusiones

Posteriormente a la realización de este estudio, se pueden sacar varias conclusiones:

- El diseño de las palas de los aerogeneradores debe incluir como requisito la carga combinada, ya que se ha demostrado que los factores de seguridad bajo cargas combinadas pueden reducirse considerablemente con respecto a los de las cargas puras de batimento y arrastre.
- Se ha determinado que, en esta sección de pala, las direcciones de carga con $\pm 30°$ desde la dirección positiva del momento de batimento (0 °) son las direcciones más propensas a fallos de pandeo, independientemente de la presencia de defectos.

- Los defectos en el borde posterior disminuyen el rendimiento de la pala en más direcciones de carga bajo compresión que los defectos entre las uniones del cajón de torsión.
- El criterio de fallo Tsai-Wu domina sobre el criterio de fallo de adhesivo, excepto en los casos en los que el adhesivo está presente bajo compresión máxima.

5 References

[1] IRENA. *Renewable Power Generation Costs in 2017*. International Renewable Energy Agency, 2018.

[2] Jr. Charles E. Harris, James H. Starnes and Hampton Virginia Mark J. Shuart, Langley Research Center. Advanced durability and damage tolerance design and analysis methods for composite structures, 06 2003.

[3] Xiao Chen. Experimental investigation on structural collapse of a large composite wind turbine blade under combined bending and torsion. *Composite Structures*, 160:435 – 445, 2017.

[4] DNV GL. *Standard DNVGL-ST-0376, Rotor blades for wind turbines*. 2015.

[5] Dan Zenkert and Mark Battley. *Laminate and Sandwich Structures. Foundations of fibre composites*. DTU Mechanical Engineering Department, 2^{nd} edition, 08 2009.

NUMERICAL STUDY ON STRUCTURAL FAILURE OF COMPOSITE WIND TURBINE BLADE SECTIONS WITH ARTIFICIAL DAMAGES

Author: Acitores de la Cruz, Blanca.

Director: Branner, Kim.

Collaborating entity: Risø National Laboratory of sustainable energy.

PROJECT SUMMARY

1 Introduction

Wind turbine blades are the fundamental components of wind turbines for power generation. Therefore, their design and optimization is mandatory to endure loading throughout their lifetime operation while providing as high efficiency as possible.

Furthermore, the blades must be designed so their reparations can be minimized in order to reduce the cost of operability and maintenance, which can rise up to 20-25% of the total levelized cost of energy (LCOE) [1]. One way of limiting the operability and maintenance costs is by decreasing the defects on blades, as well as having a better understanding about the urgency of blade reparations.

The composite materials of wind turbine blades do not maintain the same mechanical properties in all spatial directions and so, their behaviour changes from one composite structure to another. Consequently, failure modes are still in need of more research [2]. This project will focus on the analysis of two common defects encountered in wind turbine blades, mainly targeting missing adhesive in two different locations.

The main goal of this project is to carry out a generalized static buckling analysis over a blade section from a commercial blade. This considered blade is prismatic, made out of glass fiber and belongs to a 2MW wind turbine [3].

In addition, this project aims to provide a parametric numerical study from previous experimental load inputs over the considered blade section. To do so, the blade section is generated in a finite element model performed in Abaqus and its buckling behaviour is compared to that of the same blade section with defects. The defects that are taken into account for this study are the lack of adhesive in the trailing edge and over the box spar joints.

Furthermore, another scope of this work is to examine the effect of damages on the structural response under load directions which vary from the usual pure flapwise and edgewise loading directions requested by the current blade design legislation [4]. Finally, the structural study and comparison between intact blade and blade with defects is carried out by considering two material failure criteria: Tsai-Wu and adhesive failure.

2 Methodology

The 3D model of the blade section is generated in Abaqus modifying an input file (text file format). Using input files enables the numerical parametric study as it allows the assignation and modification of any parameter, materials, geometries as well as the ease to alter the data as needed.

The study starts with the design of the artificial defects and its introduction in the finite element model of the blade section. Each defect type is designed so that some parameters can be modified in order to consider different defect sizes. Therefore, several defect cases are analyzed within each defect type. Firstly,

trailing edge cases are illustrated in figure 1, where the defect size varies while maintaining a centered position. Secondly, the missing adhesive over the box girder is studied in two different regions: the upper-right (UR) shear web and the lower-left (LL) shear web of the blade cross-section. The locations of both missing adhesive defects together with the defect size variation in each case is shown in figure 2.

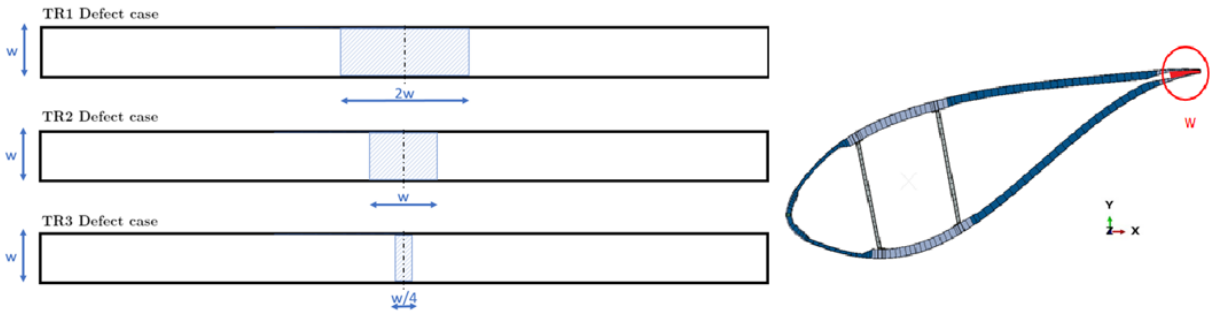

Figure 1: Sketch of trailing edge defect cases (left) and defect location over blade cross-section (right).

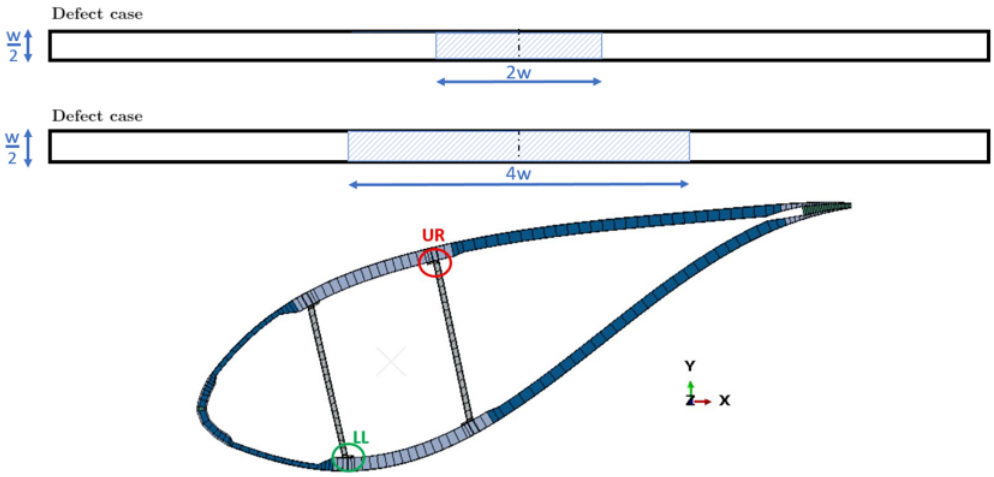

Figure 2: Sketch of upper-right (UR) and lower-left (LL) shear web missing adhesive defects (upper figure) and defects locations over blade cross-section (lower figure).

The buckling analyses is based on the Rotor Blades Design Standard (DNVGL-ST-0376 Standard) [4]. According to this legislation, all parts of the blade shall be checked for buckling failure at all locations with a specified safety factor, referred as reduction factor γ_m. This reduction factor is fixed for this project to

2.2 and 1.65 for linear buckling analysis and nonlinear buckling analysis, respectively. The buckling analyses are developed in the same way over both the intact blade and the blade with defects. The buckling analyses are static, as no velocities or accelerations are considered. In addition, both linear and nonlinear buckling analyses are taken into account in this project, as the latter can provide more accurate results.

The input loads used for this study are taken from a previous study of the same blade [3], which investigates its structural collapse through a full-scale test. The input data considered from this research are the pure flapwise and edgewise bending moments experienced in a specific section of the blade during its test. These input loads configure four loading directions examined under this project. However, other eight loading directions are also studied enabling the study of combined loads. Therefore, an elliptical loading envelope is assumed from the input loads, leading to a total of twelve studied loading directions separated 30° from each other. This loading envelope is illustrated in figure 3 and load magnitudes are calculated according to their specific load direction. Blade performance under each load direction is evaluated by comparing the buckling behaviour and material failure of the blade to the reduction factor requested by the current design standard [4].

Furthermore, the boundary conditions considered are those of a simply supported beam as they adjust best to the behaviour of a middle blade section.

Failure criteria relate the lamina stresses and strains to the allowable values that the material can take. Depending on the criterion, a function F limiting stresses and strains is defined. The structure fails if the stresses and strains created by the input loads make this function exceed or equal 1 ($F \geq 1$). Two failure criteria are defined for this project: Tsai-Wu and adhesive failure criteria. In addition, first ply failure is considered for the analysis of both failure criteria, which states that the strength of the laminate is determined by the strength of

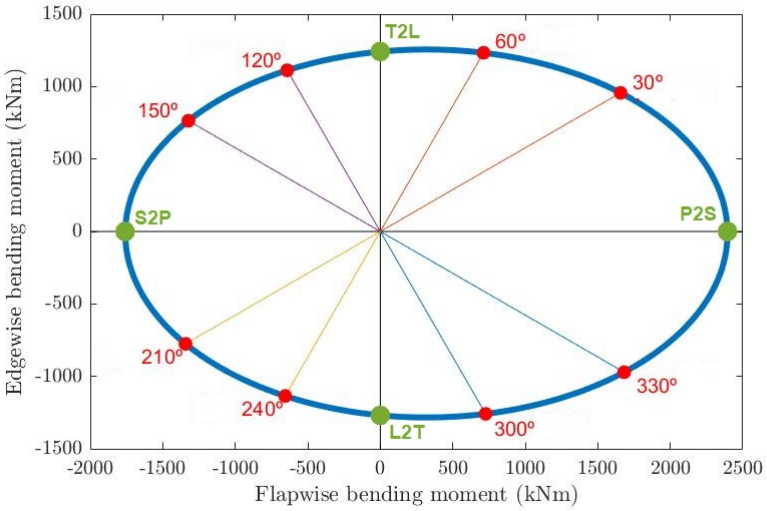

Figure 3: Loading envelope of the design loads for the buckling analyses. Pure flapwise and edgewise loads are shown in green and combined loads are shown in red.

each laminae [5].

Finally, in order to implement the analyses, several assumptions have been made:

- Defects are configured with arbitrary rectangular shapes. Real defects would vary in shape and size.
- The four extreme flapwise and edgewise loads are the only known input for the study. Combined loading magnitudes are determined by the load envelope, which is approximated to an ellipse that includes the four extreme loads.
- As mentioned in the previous section, first-ply failure criterion is considered for material failure.
- The blade model does not restrain the contact between plies. Therefore, when the blade deforms, certain layers can penetrate into others. This behaviour is not realistic.
- The boundary conditions are fixed in the final sections of the blade and

they provide higher stresses than the ones that would be created in a simple middle section of the blade. Therefore, the end region is not considered for the analysis of results.

- Geometric imperfections of 1mm length are added to the nonlinear buckling analysis of the intact blade to trigger buckling and provide trustful results from this method. To maintain consistency, these imperfections are also applied to the defect cases as it is assumed that they are very small to be noticeable compared to the effect of defects.

3 Results

3.1 Intact blade analysis

LINEAR BUCKLING ANALYSIS

Using finite element analysis, linear buckling analysis solves the eigenvalue problem for the stiffness matrix at each element of the grid over the blade section considered. Therefore, the critical buckling load can be calculated by the simple multiplication of the applied load and the obtained eigenvalue (the lower value is taken). Consequently, eigenvalues are indeed safety factors that can be easily compared to the requested values from the blade design legislation.

Figure 4 shows the compliance of the blade section under buckling with respect to the design standard requirements. The magnitudes of the eigenvalues in each load direction are shown, forming a loading envelope similar to the one of the design loads for this buckling analysis (figure 3). The main difference is that, instead of bending loads, eigenvalues are forming the envelope in order to be compared to the reduction factor requested by the Standard. Therefore, the cases in which the eigenvalues are lower than the reduction factor (do not satisfy the Standard) are enclosed in the reduction factor boundary (red ellipse).

On the contrary, the eigenvalues that satisfy the Standard and are higher than the reduction factor are on the outskirts of the ellipse.

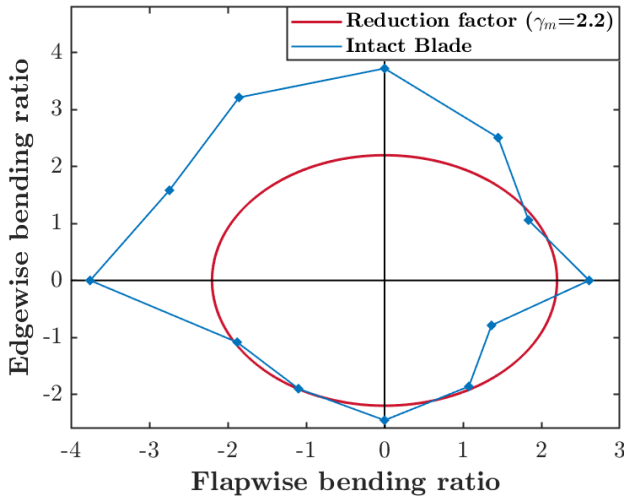

Figure 4: Linear buckling envelope of the intact blade case compared to the reduction factor requested by the Standard.

As an important result, the extreme loading points present higher eigenvalues than the requested reduction factor $\gamma_m = 2.200$, satisfying the blade design requirements. However, there are some eigenvalues over the combined loading directions that are lower than this reduction factor, especially for $\pm 30°$ load directions.

NONLINEAR BUCKLING ANALYSIS

Nonlinear buckling analysis is an incremental study that enables to take imperfections into account as well as unlinearities. It is more precise than linear buckling analysis and so, material failure is studied and compared to blade design compliance in the same way as explained above.

The nonlinear buckling analysis over the intact blade is shown in figure 5. Agreeing with the linear analysis, $\pm 30°$ load directions fail significantly to comply with the blade design requirements. Furthermore, Tsai-Wu failure criterion is shown to be more restrictive than adhesive failure criterion.

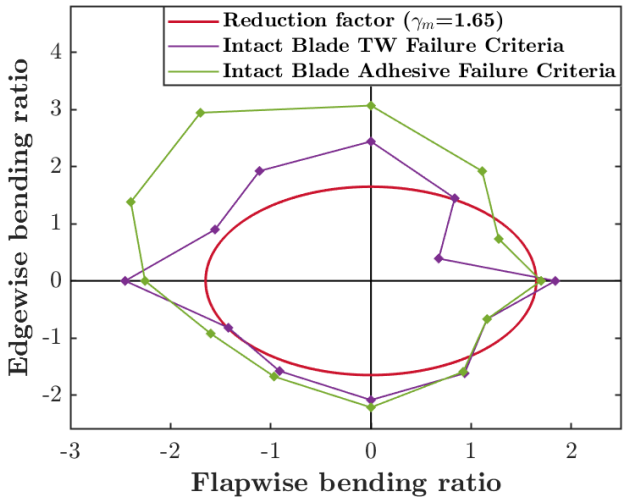

Figure 5: Nonlinear buckling envelope of the intact blade case compared to the reduction factor requested by the Standard.

3.2 Defects analysis

The analysis procedure followed over the intact blade is repeated for the analysis of the defect cases, which are described below. The most restrictive material failure criterion is taken to carry out the comparison between the different defect cases from nonlinear buckling analysis with the intact blade and the requested reduction factor.

TRAILING EDGE MISSING ADHESIVE

The buckling analyses of all trailing edge defect cases are compared to the design standard in figure 6. On the one hand, the linear buckling analyses (6a) show that blade performance is affected by the presence of the defect only in those load directions that encounter the defect over compression. However, the load directions where the defect is placed over the tension side do not vary their buckling response from that of the previous intact blade analysis. This is reasonable as buckling appears due to structural instability under compression.

On the other hand, nonlinear buckling analyses (6b) present one difference with respect to linear buckling analyses: the defect also reduces blade perfor-

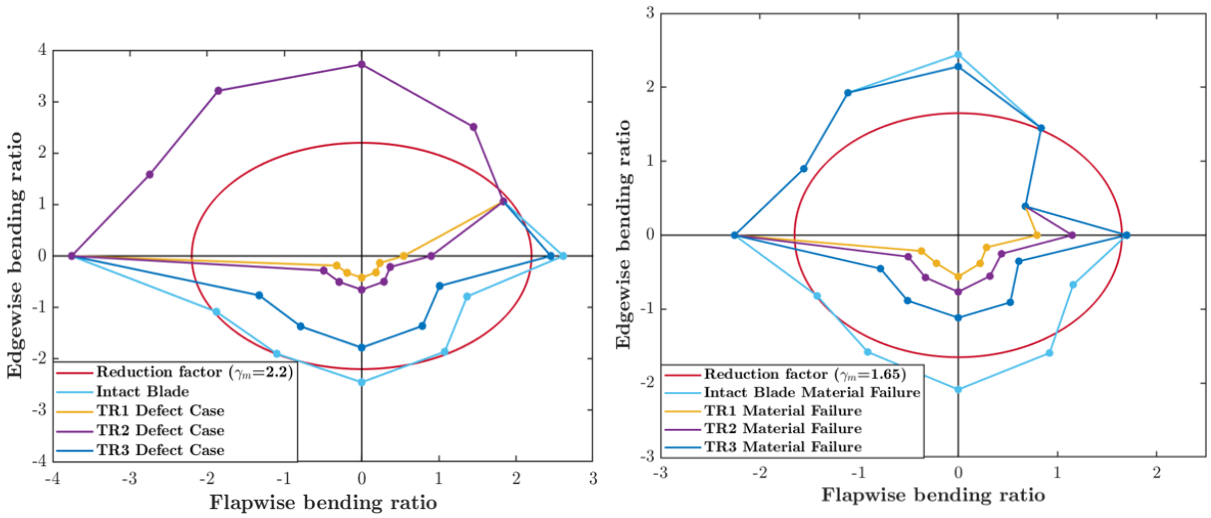

(a) Linear buckling

(b) Nonlinear buckling

Figure 6: Linear and nonlinear buckling analyses of all trailing edge defect cases compared to the design standard.

mance over the 90° load direction, which encounters the defect in the tension side. The reason is that nonlinear buckling analysis is divided into increments and the outcome of the analysis contrasts all the blade elements, showing that the defect may affect blade performance even if it is in tension side. This is the only direction in the tension side where blade performance is reduced because the defect holds the longest distance to neutral axis.

In both buckling analyses, it is reasonable that blade performance is worsen when the defect size is enlarged. However, even in the case where the defect is smaller (12.5cm length), blade performance is unacceptable as the loading directions with the defect under compression have critical bending ratios lower than 1.

BOX GIRDER JUNCTURES MISSING ADHESIVE

- Upper-right shear web missing adhesive

At this location, the defect is under compression from 240 to 30° loading directions, counterclockwise. However, from all the load directions where the

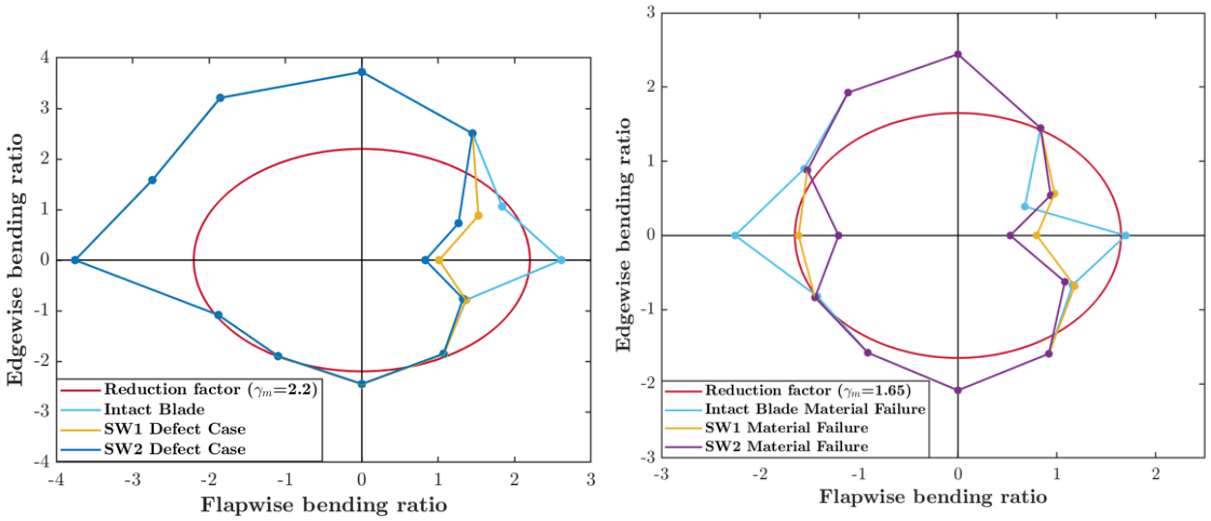

(a) Linear buckling

(b) Nonlinear buckling

Figure 7: Linear and nonlinear buckling envelopes for missing adhesive defect cases over the upper-right shear web, compared to the design standard.

defect is under compression, only 0 and 30° are the ones where the blade performance is worsened by the defect. The reason is that these loading directions do not encounter the greater buckling behaviour over the defect region but in the furthest area from the neutral axis of the blade cross-section (trailing edge). Therefore, the defect on the shear web is not bearing as much load on those directions.

The nonlinear buckling analysis differs from linear buckling analysis in two things. First of all, blade performance is affected by the defect in one different loading direction from the ones stated before. This direction is 180°, meaning that this type of defect has an influence on both directions of pure flapwise movements. Secondly, The 30° loading direction is a special case for this study. As it can be seen, the results show that the blade would perform better with the presence of this defect than without it (intact blade). The justification towards the results under this load direction must be related to the characteristics and assumptions of the studied blade model. However, the project duration has not been long enough to trigger the reason of these results.

- Lower-left shear web missing adhesive

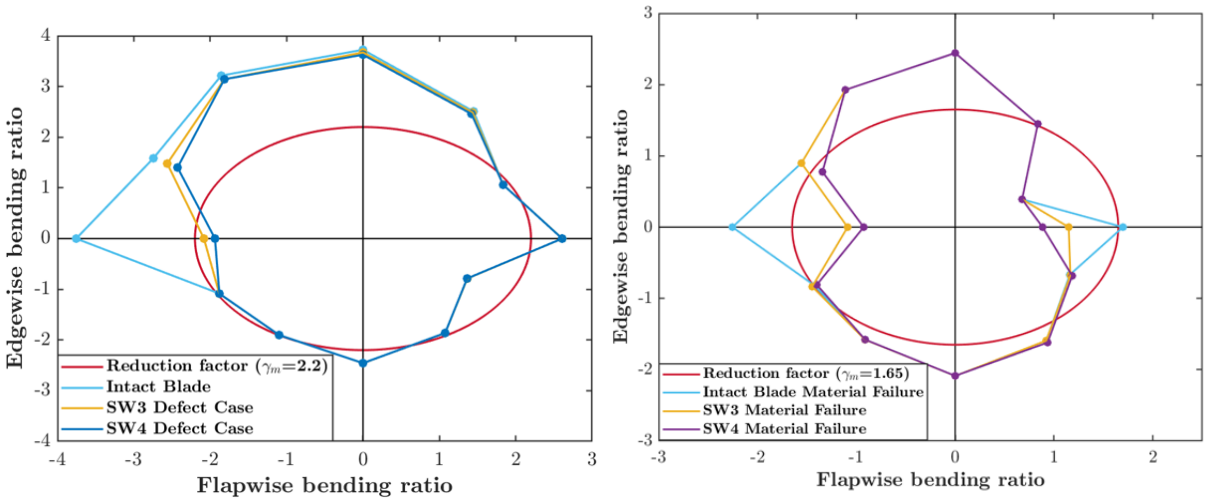

(a) Linear buckling

(b) Nonlinear buckling

Figure 8: Linear and nonlinear buckling envelopes for missing adhesive defect cases over the lower-left shear web, compared to the design standard.

In the linear analysis of this type of defect, the defect is under compression from 60 to 210°. Blade performance is decreased with the presence of the defect as much as this increases its distance to the blade cross-section neutral axis with the increase of load direction. This way, the lowest blade performance is found for 180° loading direction.

Similarly to the previous defect case, the nonlinear buckling analysis of this type of defect fails to comply with the Standard over both directions of pure flapwise movement, even if 0° has the defect under tension.

4 Conclusions

From this study several conclusions can be drawn:

- The design of wind turbine blades should consider combined loading as a requirement as it is shown that safety factors under combined loading can

be considerably reduced from those of pure flapwise and edgewise loads.

- It is found in this blade section that $\pm 30^{\circ}$ from pure positive flapwise bending are the directions most prone to buckling failure, regardless the presence of defects.
- The defects over the trailing edge decrease blade performance in more load directions under compression than that with defects over the spar cap-shear web joints.
- The Tsai-Wu failure criterion is found to dominate over the adhesive failure criterion except the cases where the adhesive is present under maximum compression.

5 References

[1] IRENA. *Renewable Power Generation Costs in 2017*. International Renewable Energy Agency, 2018.

[2] Jr. Charles E. Harris, James H. Starnes and Hampton Virginia Mark J. Shuart, Langley Research Center. Advanced durability and damage tolerance design and analysis methods for composite structures, 06 2003.

[3] Xiao Chen. Experimental investigation on structural collapse of a large composite wind turbine blade under combined bending and torsion. *Composite Structures*, 160:435 – 445, 2017.

[4] DNV GL. *Standard DNVGL-ST-0376, Rotor blades for wind turbines*. 2015.

[5] Dan Zenkert and Mark Battley. *Laminate and Sandwich Structures. Foundations of fibre composites*. DTU Mechanical Engineering Department, 2^{nd} edition, 08 2009.

Acknowledgements

I would first like to thank Xiao Chen for his patience, availability and willingness to assist me on a frequent basis. He helped me setting a thorough planification since the first day and that made possible my day-to-day improvements. In addition, he consistently steered me in the correct direction whenever he thought I needed it. Furthermore, his final feedback and review over my final version of this Thesis helped me to polish the last details.

I would also like to thank Kim Branner for supervising this project and for his help with the necessary mid-reports for my home university, as part of the Double Msc agreement between both universities. The same way, I would like to thank José Ignacio Linares Hurtado for his supervision from Comillas Pontificial University. I would also like to express my gratitude to Philipp Ulrich Haselbach for taking the time to read parts of my Thesis and giving very useful feedback.

It is also my desire to thank the SAC Department in DTU Risø, for including me in their research team, as well as in some social activities throughout the semester.

I must also express my very profound gratitude to my friends for their support and continuous encouragement throughout the process of this Thesis. Especially, I would like to thank my friend Enzo Hacquin for taking the time to read this Thesis and provide me with great advise.

Finally, I would like to thank my parents for their unfailing support throughout the process of my studies and this final step of my education. This accomplishment would not have been possible without them. Thank you.

Contents

Resumen del proyecto **i**

Project summary **xv**

Acknowledgements **xxvii**

Contents **xxix**

List of Figures **xxxi**

List of Tables **xxxvii**

Glossary **xxxix**

1 Introduction **1**

1.1 Motivation and state of the art 1

1.2 Project objectives 2

1.3 Scope of the work 3

2 Blade model **5**

2.1 Abaqus 3D model 5

2.1.1 Abaqus terminology 5

2.1.2 Mesh configuration 8

2.1.3 Material 9

2.1.4 Load conditions 13

2.1.5 Different coordinate systems: from the test to the blade 17

2.1.6 Boundary conditions 19

2.2 Buckling analysis and procedures 21

2.2.1 Configuring the buckling analysis 21

2.2.2 Linear buckling 22

2.2.3 Nonlinear buckling 24

2.2.4 Failure criteria 25

2.2.4.1 Tsai-Wu failure criterion . . . 26
2.2.4.2 Adhesive failure criterion . . . 27
2.3 Assumptions . . . 28

3 Defects design **29**
3.1 Selection of defects . . . 29
3.2 Creation of missing adhesive defects . . . 29
3.3 Design and sizing of defects . . . 30

4 Intact blade analysis **33**
4.1 Linear buckling . . . 33
4.2 Nonlinear buckling . . . 40
4.3 Failure Criteria . . . 42
4.4 Comparison between numerical studies . . . 48

5 Analysis of defects **51**
5.1 Missing adhesive in the trailing edge . . . 51
5.1.1 TR1 defect case . . . 52
5.1.2 TR2 defect case . . . 57
5.1.3 TR3 defect case . . . 58
5.2 Missing adhesive between spar caps and shear webs . . . 59
5.2.1 SW1 defect case . . . 60
5.2.2 SW2 defect case . . . 64
5.2.3 SW3 defect case . . . 67
5.2.4 SW4 defect case . . . 69

6 Conclusions and future work **73**
6.1 Conclusions . . . 73
6.2 Recommendations for future studies . . . 73

A Debonding defects **75**

Bibliography **79**

List of Figures

1.1 3D model of the blade section considered for the study. Different colours in the section stand for different materials. 2

2.1 Element set creation in Abaqus input file. Master element is indicated in red. 7
2.2 Materials used throughout the blade cross section. They are divided into element sets according to their specific function on the blade model. . . . 10
2.3 Blade coordinate system, with its origin at the blade root. This coordinate system is taken to move along with the blade in its rotation and the X and Y axes are exchanged from the ones considered in the DNV GL Standard [1], in order to match the blade model. 14
2.4 Generic loading envelope for a blade section [2]. 14
2.5 Different loading envelopes depending on the type of study/type of loads. Reproduced from [3]. 15
2.6 Loading envelope of the design loads for the buckling analysis. 16
2.7 Different coordinate systems between the blade test and the blade model considered in Abaqus. 18
2.8 Cartesian transformation when *TRANSFORM keyword is used. [4] . . . 18
2.9 2D sketch of the blade section studied with boundary conditions. The external bending moments for uncoupled flapwise and edgewise loads in section 19 are also shown in the blade section. 20
2.10 Linear and nonlinear buckling deformations according to applied load. . . 24
2.11 Representation of the strains and axes directions used in the Tsai-Wu failure criterion [5]. 27

3.1 Creation of missing adhesive defect in Abaqus. Master elements from each element set are indicated in red. 30
3.2 Initial dimensions of studied defects of missing adhesive. 31
3.3 Initial TR and SW adhesive defects representation in the blade model. . 31

4.1 Linear buckling envelope of the intact blade case compared to the reduction factor requested by the Standard. 34
4.2 Linear buckling analysis for P2S 0° load direction over the intact blade. . 35
4.3 Linear buckling analysis for S2P 180° load direction over the intact blade. 36
4.4 Linear buckling analysis for T2L 90° load direction over the intact blade. 37
4.5 Linear buckling analysis for L2T 270° load direction over the intact blade. 38
4.6 Linear buckling analysis for 30° load direction over the intact blade. Element sets according to different type of material configuration in the blade are indicated. 39
4.7 Linear buckling analysis for 60° load direction over the intact blade. . . . 39
4.8 Nonlinear buckling analysis of L2T 270° edgewise loading for the intact blade. 41
4.9 Nonlinear buckling analysis of 210° loading direction for the intact blade. 42
4.10 Nonlinear buckling analysis of P2S 0° flapwise loading for the intact blade. 43
4.11 TW and adhesive failure criteria over the P2S 0° load direction for the intact blade. 44
4.12 Comparison between first-ply failure and final material failure on the blade section, considering the Tsai-Wu failure criterion. P2S 0° load direction for the intact blade. 44
4.13 TW and adhesive failure criteria over the L2T 270° load direction for the intact blade. 45
4.14 Comparison between different material failure locations over the blade section, considering the Tsai-Wu failure criterion. L2T 270° load direction for the intact blade. 46
4.15 TW and adhesive failure criteria over the 210° load direction for the intact blade. 47
4.16 Linear and nonlinear buckling envelopes for the intact blade. 49

5.1 Sketch of trailing edge defect cases. 51
5.2 Linear buckling envelope comparing TR1 defect case with the intact blade. Specific load directions are illustrated over the blade cross section to clarify the mismatch between the intact blade and the defect buckling analyses. Grey colour under these cross sections indicate compression side and the defect is highlighted with a red circle. 53
5.3 Linear buckling analysis of TR1 defect case with P2S 0° loading direction. First buckling mode is shown. 53

5.4 Nonlinear buckling envelope comparing TR1 defect case with the intact blade. Extreme load directions are illustrated over the blade cross section. Grey colour under these cross sections indicates compression side and the defect is highlighted with a red circle. 54
5.5 Final blade deformation and first failure under the TW failure criterion over the nonlinear analysis of P2S 0° loading direction for TR1 defect case. Pressure (P.) and suction (S.) side indicated in the figures. 55
5.6 Final blade deformation and first failure under the TW failure criterion over the nonlinear analysis of L2T 270° loading direction for TR1 defect case. Pressure (P.) and suction (S.) side indicated in the figures. 55
5.7 Final blade deformation and first failure under the TW failure criterion over the nonlinear analysis of T2L 90° loading direction for TR1 defect case. Pressure (P.) and suction (S.) side indicated in the figures. 56
5.8 Buckling envelope comparing TR2 defect case with the intact blade. . . . 57
5.9 Buckling envelope comparing TR3 defect case with the intact blade. . . . 58
5.10 Location of upper-right (UR) and lower-left (LL) adhesive between shear webs and spar caps in blade model. 59
5.11 Sketch of missing adhesive between spar caps and shear webs defects for UR shear web. SW3 and SW4 LL missing adhesive defects share the same size with SW1 and SW2, respectively. 60
5.12 Linear buckling envelope comparing SW1 defect case with the intact blade. Specific load directions are illustrated over the blade cross section to clarify the mismatch between the intact blade and the defect buckling analyses. Grey colour under these cross sections indicates compression side and the defect is highlighted with a red circle. 60
5.13 First buckling mode of the linear analysis on the blade section with SW1 defect case. Flapwise P2S 0° loading direction is applied. Scaling factor=0.12. 61
5.14 Nonlinear buckling envelope comparing SW1 defect case with the intact blade. 62
5.15 The Tsai-Wu failure criterion applied at different increments of the 30° loading direction to the blade section with SW1 type of defect. 63
5.16 Final deformation when 100% of the design load is applied to the blade section with 30° loading direction and SW1 defect case. 63
5.17 Buckling envelope comparing SW2 defect case with the intact blade. . . . 64

5.18 First failure from the Tsai-Wu failure criterion for the P2S 0° loading direction of SW2 defect case. Figure on top shows the complete blade section and the lower figure is a cut of the former image in order to locate the failure, which is enlarged for better visualization. Scaling factor=1. . 65

5.19 Final deformation when 100% of the design load is applied at 0° and 180° loading directions with SW2 type of defect. Pressure (P.) and suction (S.) side indicated in the figures. Scaling factor=1. 66

5.20 Linear buckling envelope comparing SW3 defect case with the intact blade. Specific load directions are illustrated over the blade cross section to clarify the mismatch between the intact blade and the defect buckling analyses. Grey colour under these cross sections indicates compression side and the defect is highlighted with a red circle. 67

5.21 First buckling mode of the linear analysis on the blade section with SW3 defect case. 150° loading direction is applied. Scaling factor=0.12. 68

5.22 First buckling mode of the linear analysis on the blade section with SW3 defect case. Edgewise S2P 180° loading is applied. Scaling factor=0.12. . 68

5.23 Nonlinear buckling envelope comparing SW3 defect case with the intact blade. 68

5.24 Buckling envelope comparing SW4 defect case with the intact blade. . . . 69

5.25 Final blade deformation and first failure under TW failure criterion over the nonlinear analysis of S2P 180° loading direction for SW4 defect case. Pressure (P.) and suction (S.) side indicated in the figures. Scaling factor=1. 70

5.26 Final blade deformation and first failure under TW failure criterion over the nonlinear analysis of 150° loading direction for SW4 defect case. Pressure (P.) and suction (S.) side indicated in the figures. Scaling factor=1. 71

5.27 Blade deformation when 100% of the design load is applied the nonlinear analysis of P2S 0° loading direction for SW4 defect case. Pressure (P.) and suction (S.) side are indicated. Scaling factor=1. 72

A.1 Example of a layer when creating the debonding of the aft panels. 76

A.2 Sketch of debonding defect. 76

A.3 Representation of the debonding defect in the blade model. 76

A.4 Buckling envelope comparing the debonding defect with the intact blade. Specific load directions are illustrated over the blade cross section to clarify the mismatch between the intact blade and the defect buckling analyses. Grey colour under these cross sections indicates compression side and the defect is highlighted with a red rectangle. 77
A.5 Buckling envelope comparing the debonding defect with the intact blade. 78

List of Tables

2.1 Normalized material stiffnesses of the blade section. All magnitudes are relative to the bending stiffness in x-axis of UD composite material. . . . 11
2.2 Design loads taken for the study from the approximation of the loading envelope. . . . 17
2.3 Inputs for *TRANSFORM keyword to rotate the global Abaqus reference axes into the ones of the test conditions. . . . 19
2.4 Reduction factors requested by the Standard [1] for static buckling analyses over the extreme flapwise and edgewise loads. . . . 22

4.1 Eigenvalues from linear buckling analysis for intact blade section at each studied load direction. Cells highlighted in green are the requested load directions by the Standard [1]. In yellow and orange are highlighted the cases for which the Standard is not satisfied ($\gamma_m \leq 2.200$), being the latter the most critical cases. . . . 34
4.2 Loads from nonlinear buckling analysis for each loading direction for the intact blade. Loading ratios not satisfying the Standard ($\gamma_m \geq 1.650$) are shown in red. . . . 41
4.3 Tsai-Wu and adhesive failure criteria for each loading direction of the intact blade model. Loading ratios not satisfying the Standard requirements are shown in red. . . . 48

Glossary

Term	Description
BI	Biaxial fiber
FEA	Finite element analysis
K	Stiffness matrix
F_d	Design load
F_t	Test load
F_v	Viscous load
I	Internal load
L2T	Negative edgewise direction, from leading to trailing edge. 270° loading case in the study.
LCOE	Levelized cost of energy
LL	Lower-left shear web of the blade section
M	Mass matrix
NA	Neutral axis
OM	Operation and maintenance
P	External load
P2S	Positive flapwise direction, from pressure to suction side. 0° loading case in the study.
R	Residue
R_d	Characteristic material design value
S_d	Structural response
S2P	Negative flapwise direction, from suction to pressure side. 180° loading case in the study.
SW	Shear web
t	Nominal stress

Term	Description
T2L	Positive edgewise direction, from trailing to leading edge. 90° loading case in the study.
TR	Trailing edge
TRI	Triaxial fiber
TW	Tsai-Wu
UD	Unidirectional fiber
UR	Upper-right shear web of the blade section
UVARM	Abaqus subroutine that gives the Tsai-Wu failure criterion as an output in this study.
v	Eigenvector from linear buckling analysis
w	Width
ϵ	Nominal strain
λ	Eigenvalue from linear buckling analysis
γ_m	Reduction factor requested by the Rotor Blades for Wind Turbines Standard [1].
σ_{xx}	Element normal stress
σ_{xy}	Element shear stress
θ	Rotation angle from the P2S loading direction in order to configure the load envelope.

CHAPTER 1

Introduction

1.1 Motivation and state of the art

Wind turbine blades are the fundamental components of wind turbine machines for power generation. The failure of just one blade leads to the standstill of the wind turbine and, as a consequence, no electricity is produced [6]. Blade design is of utmost importance so that the rotor blades can endure the loading they are exposed to throughout their lifetime [7].

Furthermore, the blades must be designed so their reparations can easily be carried out in the field of operation [8]. Reliability problems and the cost of operability and maintenance (OM) are the common factors impeding and net gain generated by wind turbines [9]. In fact, wind turbine maintenance costs can rise up to 20-25% of the total levelized cost of energy (LCOE), being this another factor to optimize blades [10]. One way of limiting the OM costs is reducing the defects on blades. A blade may have defects due to environmental impacts (birds, transportation, lightnings), operation or manufacturing processes, fatigue or material properties. This project will focus on defects encountered in wind turbine blades, mainly targeting missing adhesive.

Composite materials are not isotropic which means that their mechanical properties are not the same in all directions. Thus, their behaviour varies from one composite structure to another as their components are normally different [11] and the properties vary according to the proportion of fibres, resin, fibre orientation and manufacturing processes. Due to this fact, failure modes are still in need of more research [8]. As a consequence, further research regarding the sensitivity of blade performance to defects is needed [8].

Moreover, the global analysis of a blade (full blade analysis) in combination with a local in-depth analysis of a specific blade region is currently an underdeveloped method to predict structural failure [8]. As a matter of fact, this study intends to investigate further into this issue. One of the aims is to apply this local and general approach to future global studies.

Finally, combining experimental investigations with finite element methods is key to design damage tolerant composite structures [8]. As a consequence, this project uses experimental load inputs to implement the parametric numerical study over a blade section model in Abaqus.

1.2 Project objectives

This project focuses in the generalized buckling analysis over the considered blade section. The buckling analysis is static, as no velocities or accelerations are coming into play. The blade section is modelled in a finite element model and belongs to a 2MW wind turbine. The blade is made of composite glass fiber and is vacuum infused with epoxy resin. The blade is prebent to 2m at the tip in order to maintain sufficient blade-tower clearance [11]. One of the aims of this study is to be as generic as possible in order to be applicable to other blades and draw general conclusions. Therefore, the blade section considered is simplified from the original tapered blade to a prismatic one. The studied blade section is shown in figure 1.1 and it corresponds to 5m length middle section of the total 47m length full blade.

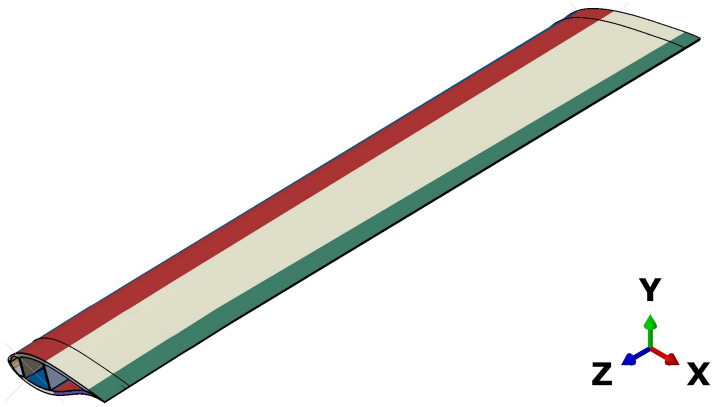

Figure 1.1: 3D model of the blade section considered for the study. Different colours in the section stand for different materials.

The study is fully numerical and performed in Abaqus. The main objectives of this project are the following:

- Parametric modeling of defect types, locations and sizes in a generic section of composite wind turbine blades using solid elements. In order to check the influence of defects on the blade section, two main defects are considered:

  - Missing adhesive from the trailing edge. Trailing edge failure leads to delamination and buckling behaviour when the structure is submitted to edgewise loading [12]. The trailing edge is a very important part of the blade as it highly influences the aerodynamic performance of the airfoil, avoiding stall conditions.
  - Missing adhesive between spar caps and shear webs. The joint between these two components is also extremely important as they provide the strength to flapwise bending for the whole blade.

- Understanding the design load envelope and load combinations of a generic blade section. Different bending moments at several load directions are applied to the blade section with different defects so the final behaviour is compared to the one of the section without defects. The effect of combined loading on top of uncoupled flapwise and edgewise loads is examined under this project.

- Examining the effect of damages on the structural response under different load combinations in order to provide better understanding of the structural design of composite wind turbine blades. Material failure is determined in this study by two failure criteria: Tsai-Wu and adhesive failure.

1.3 Scope of the work

The main scope of this project is to give a better insight into the failure behaviour of wind turbine blades over their buckling response. As stated in the previous section, finite element analysis (FEA) enables to develop a sensitivity analysis over the effect of different defects. However, due to the limited duration of this study, several assumptions have been made over the blade model, which are specified over the project development.

Furthermore, most of the composites research focuses on the edgewise and flapwise loading as the main factor of blade failure due to the high flapwise bending moments experimented. In addition, the current norm [1], at which blade design is subjected to, only requires the satisfaction of certain safety factors under these uncoupled flapwise and edgewise movements. However, it has been proven that combine flap and edgewise loading can lead to maximum bending moments in the ultimate state [3]. Despite this fact, there are few works that focus on the ultimate

strength and collapse of large blades under combined loading state [11]. It is also a more realistic study as wind turbines are hardly subjected to a unique loading mode. As a consequence different loading studies are evaluated in this study. A total of 12 load directions are investigated.

CHAPTER 2

Blade model

This chapter describes the blade section characteristics and loading conditions as well as the necessary terminology to understand the followed procedure in Abaqus. The numerical methods implemented for the buckling study are also detailed under this chapter. Finally, the failure criteria considered to decide over the final structure performance are also examined.

2.1 Abaqus 3D model

The blade model taken for the study belongs to a previous research [11] and it is modified as needed for this project. This way, the blade section considered is 5m long. Its cross section is taken from a 47m blade of 2MW [11] from radial position r =19m to r =24m. The parametric study aims to generalize the effect of common defects. Therefore, the blade considered for analysis is decided to be prismatic, which means that the blade has the same cross section over its whole length.

The 3D model of the blade section is generated in Abaqus modifying an input file. Using input files enables parametric studies to have high flexibility in building and manipulating the model. Creating or modifying the input file allows the assignation of any parameters, materials, geometries as well as the ease to alter the data as needed. Due to these reasons, the overall parametric procedure is faster. The main logic behind the input file is explained next.

2.1.1 Abaqus terminology

The input file is a text file containing keywords and data lines. Abaqus keywords introduce the inputs and options to modify the model. Data lines are the numbers or parameters (assigned variables) requested from keywords. Keywords are distinguished from other parameters or data by a * in the beginning of the word/label. Some examples of keywords are presented below for better understanding. The specific input syntax for keywords and data lines is detailed under Abaqus Analysis Userts Manual [13].

Once the input file is run by Abaqus, several files are created informing about the on-going or finished processes. All given parameters are numerically evaluated in .par and .pes files and code errors are stated in .msg. These files make possible to find a way to track the error and correct it. Furthermore, .sta file indicates the status of the file and if it is completed successfully. Finally, a .odb file is the output database and both the model and results can be visualized in Abaqus CAE/Viewer.

The structure of an input file is divided in two main parts:

1. **MODEL DATA:** Defines all the inputs characterizing the model:

   - **Geometry:** A finite element model is described by nodes and elements. When the input file is created, all nodes and elements need to have a number assigned (different from each other). Moreover, each node number is associated with spatial coordinates and each element is related to the nodes that it is connected to. Nodes and elements are created by the keywords *NODE and *ELEMENT, respectively, and the coordinates or nodes necessary for each case are the data lines following the keyword.

     As the blade section studied is very complex and large, elements are grouped in different element sets. This way, specific characteristics can be assigned to several parts of the blade (material, boundary conditions, loads, requested outputs, etc.). Some keywords enable to copy nodes or elements to other part of the geometry. Others allow to generate different node or element sets from an initial one, called master element/node. This way, layers of elements are generated from a particular element of interest with the *ELSET keyword. An example of this is shown in figure 2.1. The element set is created by specifying the number of elements in the row (xychange in figure), the increment within element and node numbers and the number of total rows (zchange).

     Node and/or element sets have been modified in Matlab and linked to the Abaqus input file (.inp) by means of the keyword *INCLUDE.

   - **Material:** Material properties are introduced under the keyword *MATERIAL. They are associated to different elements of the model. A good assignation of elements sets highly helps this endeavour.

   - **Initial conditions:** Initial stresses or forces when external loads are introduced in the model.

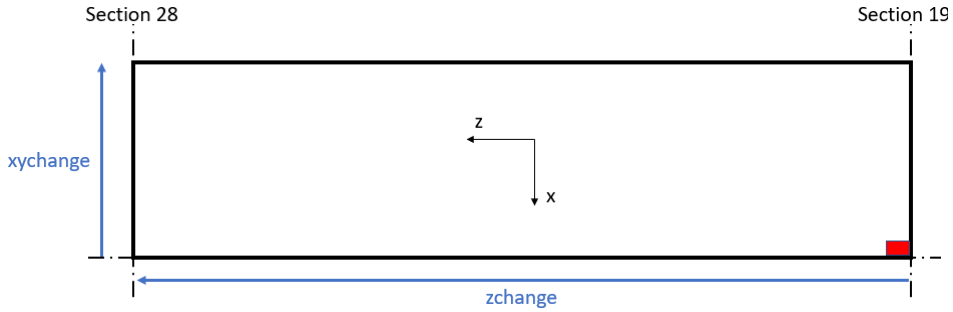

Figure 2.1: Element set creation in Abaqus input file. Master element is indicated in red.

- **Boundary conditions and constraints:** Specific rotational angles or displacements can be assigned to elements or element sets. Boundary conditions are very important for any loading study and so, they are detailed in a later section.

2. **HISTORY DATA:** Defines the necessary inputs to analyze the response of a model when applying external loading. An analysis in Abaqus is developed from one or several steps (keyword: *STEP). A step defines a specific analysis with external loads and certain outputs requested out of it. It is possible to carry out several steps within one study, so the output of the first step is the input of the following one. The data that must be included in the step definition is:

   - **Response type:** Nonlinear, linear, static or dynamic. This study is static as velocities or accelerations are not applied to the blade section. For the buckling study, both linear and nonlinear analyses are compared under this project.

   - **External loading:** Several types of loads are permitted from concentrated or distributed loads to temperature changes (thermal expansion). Only concentrated loads are taken into account in this study.

   - **Outputs:** Variables of interest can be requested as an output to the database. The output can be visualized in the .odb file but it can also be written in a text file.

2.1.2 Mesh configuration

The polygonal mesh is the basis for the Finite Element analysis. It is formed by different polygons that approximate the blade geometry. Each polygon is one element of the mesh, configured by a set of nodes. This particular model is dicretized with hexahedral elements. C3D8R elements with linear shape functions are used.
As a brief summary, FEA is based on applying, through an iterative process, the virtual work principle that minimizes the energy in the system. The goal is to determine, at each node and element, outputs from a structural analysis, buckling in this particular study. Hence, for nonlinear buckling analysis, an external loading is applied to the model with an iterative process where 100% of the input load is reached after certain amount of increments, specified by the user. At each iteration, the displacements occasioned at each node when external loading is applied to the model can be calculated. This way, the outputs of each iteration are inputs for the following one. As a consequence, the higher amount of elements in the mesh, the higher accuracy on the study. However, the computational time also increases, requiring a trade-off between accuracy and elements size.
Three types of elements are used in this study to conform the mesh of the model:

- **Solid elements:** They are usually triangular and tetrahedral elements, suitable for general usage. However, the selected elements are hexahedral, as they provide a solution of equivalent accuracy at lower cost [13]. The type of Abaqus element used is C3D8R, which letters describe its characteristics: continuum stress/strain displacements (C), three dimensional (3D), 8-node linear brick (8) and reduced integration with hourglass control (R) [13]. Reduced integration uses a lower-order integration to form the element stiffness which reduces running time, especially in three dimensional elements. Higher integration is used when distributed loads and/or mass matrix are used. This type of element needs hourglass control as it is one of the drawbacks of having reduced integration. The hourglass problem is produced because the elements with very low integration points may distort in such a way that the strains calculated at the integration points are all zero, which, in turn, leads to uncontrolled

distortion of the mesh [13].

Solid elements are used to model all the blade section elements but those representing the adhesive.

- **Cohesive elements:** The cohesive elements represent the adhesive in the model. In Abaqus, they are represented with a single layer of finite thickness so that the constitutive response of this area directly models the macroscopic properties defining the specific adhesive. In this study, the mechanical behaviour of cohesive elements follows a traction-separation description, further explained in the next section. The type of cohesive element implemented in Abaqus is COH3D8: cohesive element (COH) with three dimensions (3D) and 8 nodes (8) [13].
- **Shell elements:** They are used to model elements whose thickness is significantly smaller than the rest of their dimensions. In this particular model, as the blade section is used to model a real test from a previous study [11], shell elements are used for the element sets in the boundaries of the blade section in order to resemble the clamps that hold the structure during the blade test and the regions that would be in contact with the contiguous sections. The type of Abaqus element applied is S4R: conventional stress/displacement shell (S) with 4 nodes (4) and reduced integration (R) [13]. Conventional shell elements are defined at the reference surface and its specific thickness is provided in the section definition. In addition, reduced integration is used as in solid elements, providing accurate results for reduced computational time. These type of elements account for finite membrane strains and so, they are suitable for large strain analysis [13].

2.1.3 Material

The blade section is formed out of composite glass fiber. Glass fibers have lower stiffness than carbon or aramid fibres but the overall strength properties are good for a relatively low cost. Glass fiber is isotropic (its physical properties are the same in every direction) and it can be characterized by just measuring the longitudinal stiffness and the estimated Poisson's ratio [14].

The wind turbine blade section is formed by two parts on the pressure and suction

side mounted together and stiffed together with two shear webs, that connects the upper and lower part. The upper part is mounted to the lower part with adhesive in the trailing and leading edges as well as in the shear webs connections. Figure 2.2 shows the blade cross section and the different materials it is composed of. The blade section is formed by composites and sandwich panels. Sandwich structures is a specific way of configuring composite materials by joining two very stiff composite material plates with a light but thick core. Sandwich panels provide high stiffness while having low weight. The mechanical properties of composite materials highly depend on the direction of fibers and on the exact quantity of fibers/resin.

According to the type of loading experienced by the blade, different locations on the blade cross section must hold higher resistance to loading. Therefore, different materials are used throughout the blade structure. Material data for this specific blade can't be disclosed but, for the sake of better understanding, their normalized bending stiffnesses can be seen in table 2.1 with respect to the x axis bending stiffness of UD material. Different element sets, corresponding to the ones implemented in Abaqus, are indicated in figure 2.2. Each set is detailed next, justifying the material chosen for each of them.

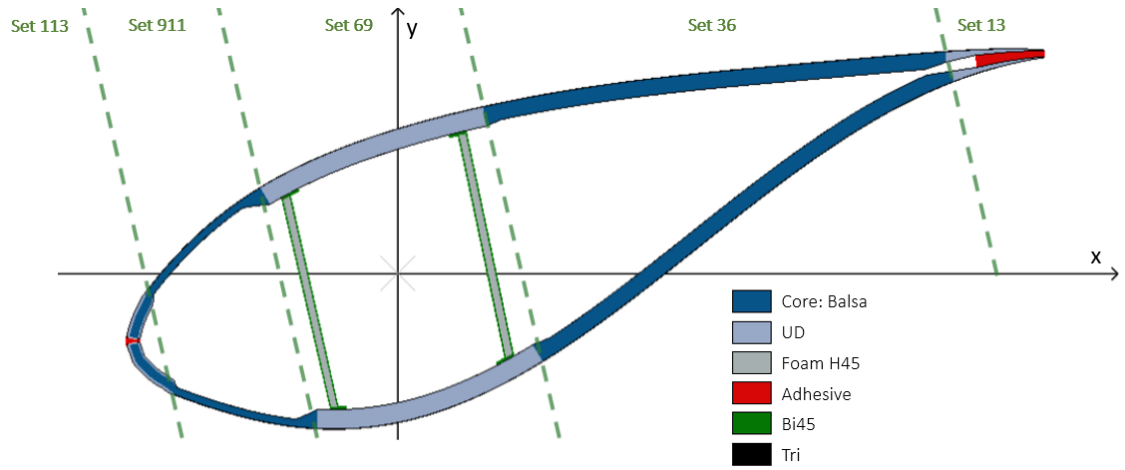

Figure 2.2: Materials used throughout the blade cross section. They are divided into element sets according to their specific function on the blade model.

- **Element set 113: Leading edge**
  The leading edge is formed by the same sandwich panel used in the blade shells. The sandwich panel is formed of Balsa wood as core material and Triaxial glass fiber (Tri) as the skin. Balsa wood is commonly used as a core material as it provides good mechanical properties as well as ease in manufacturing.

	UD	**Bi**	**Tri**	**Core (balsa)**	**Foam**
E_x	1.000	0.321	0.456	0.018	0.001
E_y	0.333	0.321	0.335	0.018	0.001
E_z	0.333	0.321	0.335	0.036	0.001

Table 2.1: Normalized material stiffnesses of the blade section. All magnitudes are relative to the bending stiffness in x-axis of UD composite material.

Together with the trailing edge, the leading edge carries the edgewise bending, experienced around the y-axis. Therefore, it is configured so that bending stiffness is higher in this direction in order to avoid buckling and failure. As its core material (Balsa) possesses low stiffness, additional Unidirectional glass fiber (UD) composite material outside the sandwich panel helps bearing the bending load with its higher bending stiffness in the y direction.

- **Element set 911 and 36: Blade shells**
  As mentioned before, these sections are formed by sandwich panels. They do not carry as high loads as the leading and trailing edges. Thus, this combination of materials is enough for this set of the blade.

- **Element set 69: Box spar**
  The box spar contains the spar caps and the shear webs. Spar caps are formed by the union of two composite materials: mainly unidirectional glass fiber and triaxial glass fiber as the outer layer. They resist the flapwise loading (around x-axis) experienced by the blade and, consequently, their bending stiffness in x axis needs to be high. As seen in table 2.1, UD provides the highest bending stiffness in x direction.

  Shear webs take the shear loading experienced by the blade. They are composed of a sandwich structure of foam as a core and Biaxial glass fiber (Bi) in the skin. Biaxial glass fiber is used in the shear webs as its shear bending stiffness is higher than that of the rest of materials.

- **Element set 13: Trailing edge**
  It carries high edgewise loading together with leading edge and shells and, as a matter of being the thinner part of the cross section, it is a very sensible part for the blade performance. Furthermore, its optimization is necessary to reduce, as much as possible, turbulent flow at the tip of the blade section. Hence, triaxial and unidirectional glass fiber are used for this part. Its elevated

bending stiffness together with the big amount of adhesive joining both sides of the blade, improves performance.

- **Adhesive**

  The adhesive is displayed in red in figure 2.2, although the joints between the spar caps and the shear webs are hardly appreciated in the figure. Adhesive is modeled by a geometrically thin layer of cohesive elements in Abaqus. Their mechanical response is governed by a linear elastic traction-separation model prior to damage and the failure of elements is due to progressive degradation of adhesive stiffness [13]. The linear traction-separation behaviour is defined by an elastic matrix that relates nominal stresses to nominal strains. The former are the external force components divided by the initial area and the latter are the relative displacements divided by the original thickness. Stresses and strains are both evaluated at each integration point and they consist of three components (one for each space direction). The elastic behaviour is then defined as in equation 2.1, where K is the elasticity matrix and t and ε are the nominal stresses and strains vectors, respectively.

  $$t = K\varepsilon \tag{2.1}$$

  Furthermore, the traction-separation behaviour for the adhesive parts of this study has been defined to be uncoupled, which is specified when defining the adhesive properties in Abaqus. This specification sets in Abaqus the off-diagonal terms of the elasticity matrix K to zero [13]. This is the simplest way to specify the linear traction-separation law, as usually normal separation over cohesive elements do not lead to forces in the shear direction or shear slip does not cause forces in the normal direction. This way, only the elastic stiffness in the three main spatial directions (diagonal of K matrix) must be specified for Abaqus.

  The initial linear elastic behaviour of the traction-separation model is followed by the initiation and evolution of damage. All specified materials in Abaqus follow a general framework for damage propagation and failure. Abaqus even allows to study diverse damage mechanisms simultaneously. For each of the damage mechanisms specified, it is necessary to provide the damage initiation criterion for certain stress and strain values. The criterion considered in this report is the quadratic nominal stress criterion (QUADS in Abaqus), shown in equation 2.2, where damage initiates when this quadratic relation between

the nominal stresses ratios occurs. This criterion is the one used to determine adhesive failure, as explained in a later subsection.

$$\left[\frac{t_1}{t_1^o}\right]^2 + \left[\frac{t_2}{t_2^o}\right]^2 + \left[\frac{t_3}{t_3^o}\right]^2 = 1 \tag{2.2}$$

Once the damage initiation criterion is satisfied, the damage evolution law can also be specified, which shows the rate at which the material stiffness diminishes when the damage initiates. As this analysis is examined with the first-ply failure criterion (explained later in section 2.2.4), the evolution of the damage is not relevant for the study. Thus, the damage evolution law is omitted, and the relevant results are taken when the damage initiation criterion is reached.

2.1.4 Load conditions

As mentioned before, this project mainly focuses in the static buckling analysis over the considered blade section. The input loads used for the study are taken from a previous study of the same blade [11] which investigates its structural collapse through a full-scale test. The input data considered from this research are the uncoupled flapwise and edgewise bending moments experienced in section 19 during the blade test.

Flapwise load is produced by wind pressure; therefore, the upcoming wind is approaching the hub in the y-axis direction (Y_B in figure 2.3 [1]). The edgewise load is caused by gravitational forces and torque load. In figure 2.3 this load is experienced by the blade if the upcoming wind approaches the turbine in the X_B direction.

Depending on the bending moment direction experienced by the blade, it is possible to create a total loading envelope, as shown in figure 2.4. The four points of the loading envelope that intersect with the axes represent the uncoupled flapwise and edgewise movement. In addition, θ, in the same figure, represents the rotational angle from the flapwise load from pressure to suction in order to configure different load directions over the load envelope. According to the Rotor Blades for Wind Turbines Standard [1] (DNVGL-ST-0376), any blade design has to bear these pure loads at any static bending study:

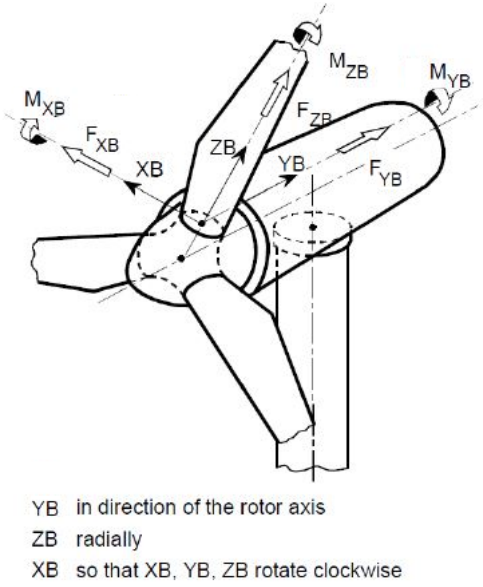

Figure 2.3: Blade coordinate system, with its origin at the blade root. This coordinate system is taken to move along with the blade in its rotation and the X and Y axes are exchanged from the ones considered in the DNV GL Standard [1], in order to match the blade model.

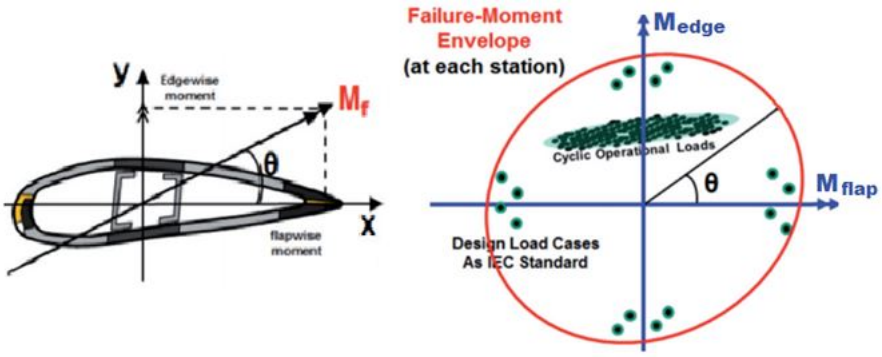

Figure 2.4: Generic loading envelope for a blade section [2].

- Positive flapwise direction, from pressure side to suction side (P2S from now on). It is produced at θ=0° on figure 2.4.

- Negative flapwise direction, from suction side to pressure side (S2P). It is produced at θ=180°.

- Positive edgewise direction, from trailing edge to leading edge (T2L). It is produced at θ=90°.

- Negative edgewise direction, from leading edge to trailing edge (L2T). It is produced at θ=270°.

Even though these loads are the ones considered for blade design, combined loading (flapwise + edgewise) can also be a source of high failure and further analysis should be carried on which is the aim of this study. Figure 2.5 shows several loading envelopes of a full-scale blade that is computed under 24 different load directions. The present study experimentally tries to obtain better structural design of wind turbine blades [3] and demonstrates that the maximum bending moments for ultimate limit state do not occur at pure flap or edgewise directions, but at a given angle with respect to the flapwise direction [3] (combined loading).

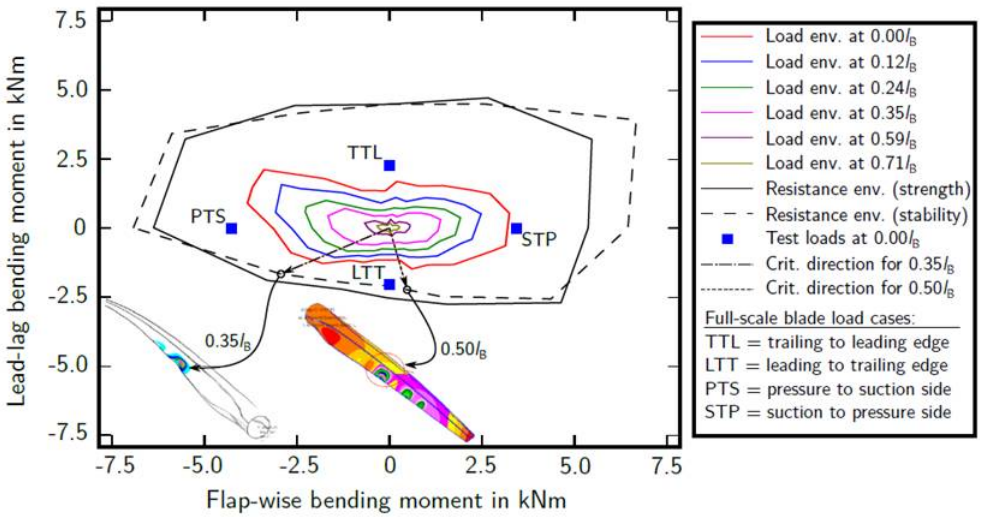

Figure 2.5: Different loading envelopes depending on the type of study/type of loads. Reproduced from [3].

This project examines combined loading in a similar way as [3] and different loading envelopes are created in order to evaluate blade performance. They can provide a comparison between different design criteria for the blade. In this analysis, three different loading envelopes are considered:

- **Design loads:** calculated from the input loads for this study [5]. According to the static bending tests requirements specified in the DNVGL-ST-0376 Standard [1], design loads F_d are inversely proportional to test loads by certain established factors, as shown in equation 2.3; F_t is the test load and γ_{1t} and γ_{2t} are the proportional factors. γ_{1t} accounts for scattering of the rotor in series production and it is fixed to 1.1 for static tests. γ_{2t} accounts for the favourable conditions that may exist in the test facility in comparison to the

actual operation. This is 1.0 in most cases [1].

$$F_d = \frac{F_t}{\gamma_{1t} \cdot \gamma_{2t}} \tag{2.3}$$

This way, from the input test loads [11], design loads can be calculated for this study. Design loads are the inputs from which buckling and material failure analyses are developed.

- **Buckling loads:** stability study. This study is necessary, according to the Standard [1] for loading design and buckling analysis. Both linear or nonlinear buckling are analyzed.
- **Ultimate loads:** strength study. Failure criteria determine the critical load at which the structure would fail. Two failure criteria are considered in this project: Tsai-Wu and adhesive failure.

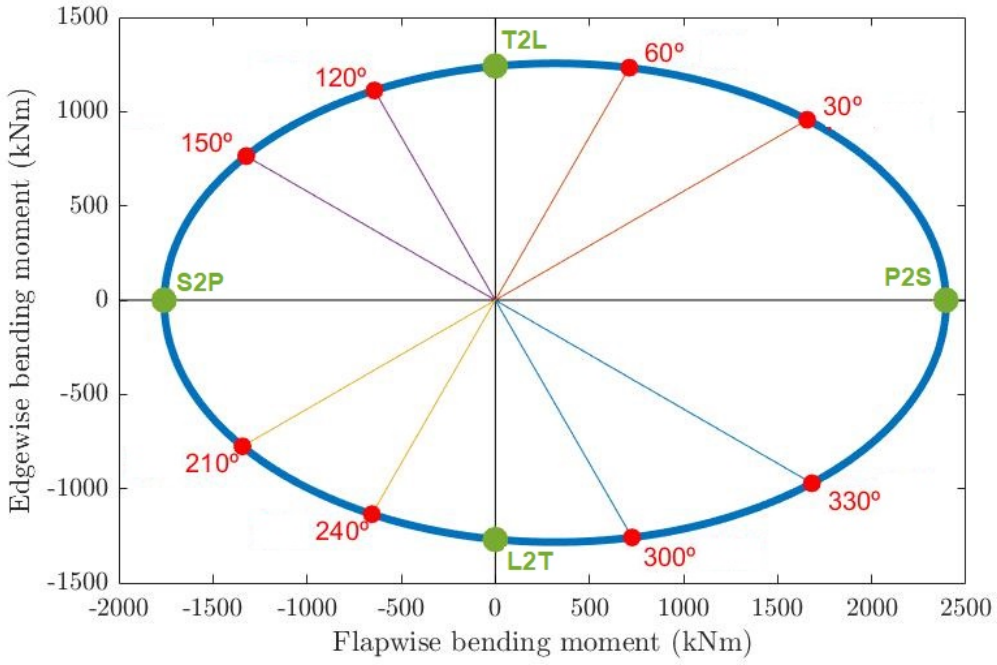

Figure 2.6: Loading envelope of the design loads for the buckling analysis.

In order to create the design loads envelope, only the uncoupled flapwise and edgewise design loads of this blade are known from equation 2.3. Therefore, it is necessary to approximate the shape of the overall loading envelope. It is assumed that the

Load direction	Design load (Nm)
P2S 0°	2.39E+06
30°	1.91E+06
60°	1.42E+06
T2L 90°	1.24E+06
120°	1.28E+06
150°	1.53E+06
S2P 180°	1.76E+06
210°	1.55E+06
240°	1.31E+06
L2T 270°	1.27E+06
300°	1.45E+06
330°	1.94E+06

Table 2.2: Design loads taken for the study from the approximation of the loading envelope.

loading envelope forms an ellipse through the known four points. This approximation is based on the loading envelope shape of former studies like [3], as the ellipse is the easier generic approximation. Furthermore, 12 points of the loading envelope are studied, separated by θ=30° between each other. The loading envelope with the design loads that has been considered in this project can be seen in figure 2.6. In the figure, the extreme flapwise and edgewise loads are represented with green dots whereas the combined loading points are represented with red dots. The specific magnitudes of all design loads are shown under table 2.2.

2.1.5 Different coordinate systems: from the test to the blade

It is important to note that the reference coordinate system of the test, where loads were measured and used as inputs for this study, is different from the one of the global blade section modelled in Abaqus. In order to ensure consistency between the test loads and the Abaqus blade model, the coordinate systems have to match with each other.

These coordinate systems are shown in figure 2.7. The blade test was developed 6.6° from the chord line reference axis, shown in black dashed lines in this figure. Taking into account the existing angle difference between the global axes coordinate system and the reference chord line, it is possible to calculate the angle between

both reference coordinate systems, being 12.3°.

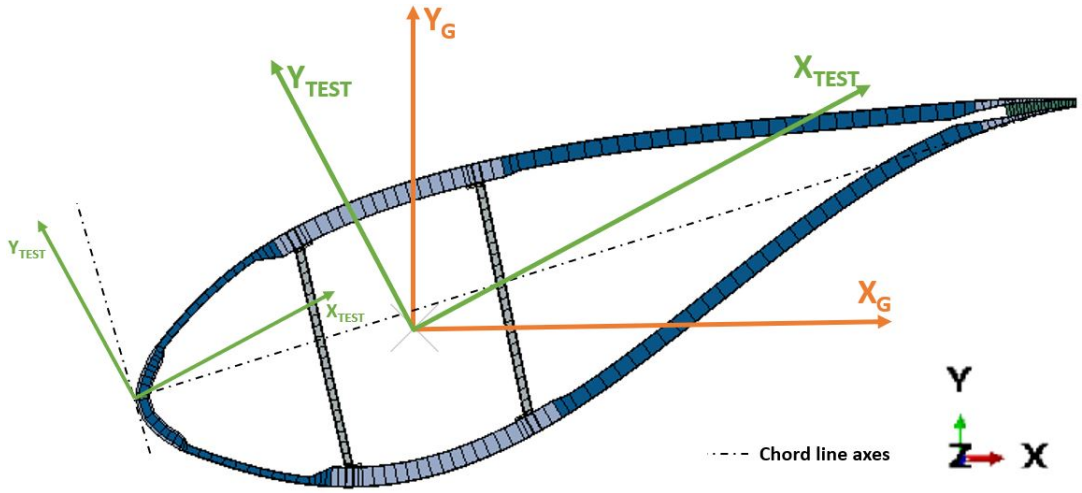

Figure 2.7: Different coordinate systems between the blade test and the blade model considered in Abaqus.

In the input file realization the Abaqus global reference system can be rotated into the test reference system by means of the *TRANSFORM keyword. This tool enables rotation by giving, as an input, the global coordinates of points for the aimed reference systems. This way, as illustrated in figure 2.8, the points a and b can be transformed from the initial reference system to the aimed one. Therefore, as Z axis is the same for both reference systems, the global X and Y axes are rotated 12.3° to match the test axes.

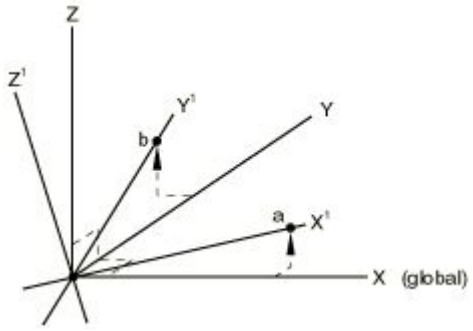

Figure 2.8: Cartesian transformation when *TRANSFORM keyword is used. [4]

To carry out the transformation, a_x is fixed as the slope between the complementary angle of both reference systems ($\tan(90° - 12.3°)$=4.482) and so, from basic trigonometric, a_y magnitude can be set to 1. (b_x,b_y) can be calculated following the same initiative. These inputs for the *TRANSFORM keyword are shown in table 2.3.

Point	a			b		
Coordinates	x	y	z	x	y	z
P2S	4.482	1	0	-1	4.482	0

Table 2.3: Inputs for *TRANSFORM keyword to rotate the global Abaqus reference axes into the ones of the test conditions.

In order to implement different loading directions, the test reference system can be rotated once more with the specific load direction increment from the initial one (P2S 0° flapwise load). Therefore, loading rotations are possible making use of the keyword *TRANSFORM. Rotating the reference system implies an automation of the coding in the input files as all load directions share the same characteristics and boundary conditions, as explained in the next subsection. Equation 2.4 shows how the counterclockwise rotation from the 0° load direction takes place. Rotating the former slope $m = 4.482$ from table 2.3 and setting the correspondent angle θ for each case, all the global reference systems can be known.

$$\begin{bmatrix} X \\ Y \end{bmatrix} = \begin{bmatrix} cos(\theta) & -sin(\theta) \\ sin(\theta) & cos(\theta) \end{bmatrix} \begin{bmatrix} m \\ 1 \end{bmatrix} \tag{2.4}$$

The bending moments magnitudes for each case are found by determining the coordinates of the loading points showed in figure 2.6. These coordinates are simply the intersection between the ellipse (calculated with the uncoupled flapwise and edgewise points) and the line with the correspondent angle slope from the center of the reference system (shown in figure 2.6).

2.1.6 Boundary conditions

In Abaqus, all loading directions share the same boundary conditions as, when rotating the reference system for each of them, the same geometry, blade characteristics and boundary conditions are maintained. However, the boundary conditions specifications depend on the type of loading that the blade is subjected to. Let one consider the P2S 0° flapwise design case to clarify why the boundary conditions are shared between all loading cases.

The full wind turbine blade can be considered as a cantilever beam structural problem. However, the boundary conditions vary from this one as a middle section of the full blade is considered. The boundary conditions for the studied blade section

are illustrated in figure 2.9. The input loads (explained in previous section) are applied in the 19 and 24m cross sections in order to represent this as a middle section. The magnitudes for the bending moment over both cross sections is the same and they stand for the correspondent design load over cross section 19. Furthermore, since the static buckling analysis specified in the Standard [1] does not require the study of shear stresses, those are omitted. Moreover, their addition would not have much variation on the blade buckling response.

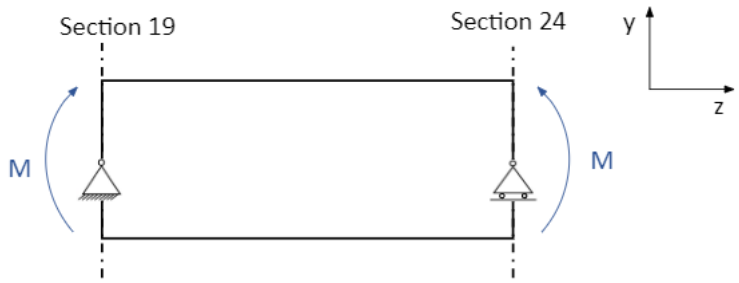

Figure 2.9: 2D sketch of the blade section studied with boundary conditions. The external bending moments for uncoupled flapwise and edgewise loads in section 19 are also shown in the blade section.

In the case of flapwise loading, the input bending moment is applied over the x axis, as shown in figure 2.9. Thus, in order to allow movement around x axis in the cross section, this is the only degree of freedom of the boundary conditions assigned to section 19. At first, it was considered to set the same boundary conditions to section 24, under the assumption that the horizontal projection of a deflected beam under loading remains very similar to the intact beam length (Bernoulli-Euler beam theory). Nevertheless, this is not a realistic case in a wind turbine blade, especially taking into account the high magnitude of tip deflection. As the blade deflects, all the cross sections do not have the same initial horizontal projection as if no load is applied. As a consequence, it is considered to free the longitudinal displacement on the z-axis as well as the x-axis rotation for section 24.

In edgewise loading, the P2S design case is rotated by 90°, so the rotation around x-axis is now constrained and the rotation around y-axis is enabled. As in edgewise movement the input bending takes place around y-axis, these boundary conditions free the rotation around this axis to evaluate the structure response. As Z coordinates are not changed over the different load cases, the longitudinal displacement on the z-axis of the 24m section is maintained. This fact enlightens why boundary conditions can remain the same for all load cases if the references systems are

rotated.

2.2 Buckling analysis and procedures

This section covers the linear and nonlinear buckling study. Their detailed definition and different operating procedures are discussed. Finally, Tsai-Wu and adhesive failure criteria, results from nonlinear analysis, are presented as well.

2.2.1 Configuring the buckling analysis

The buckling analysis is based on the DNVGL-ST-0376 Standard [1]. According to this legislation, all parts of the blade, such as spar caps, shells or shear webs shall be checked for buckling failure at all locations. The design criterion that needs to be satisfied for all analyses is shown in equation 2.5, where S_d is the structural response (stress or strain), R_d is the characteristic material design value and γ_m is the reduction factor.

$$S_d \leq \frac{R_d}{\gamma_m} \tag{2.5}$$

The reduction factor γ_m, for all verification analyses, is determined as follows:

$$\gamma_m = \gamma_{m0} \cdot \gamma_{mc} \cdot \gamma_{m1} \cdot \gamma_{m2} \cdot \gamma_{m3} \cdot \gamma_{m4} \cdot \gamma_{m5}$$

γ_{m0} is the base factor and is fixed to 1.2 for all type of design analyses. For each of the design analyses the partial reduction factors γ_{mc} and γ_{m1-m5} are specified in the Standard. Therefore, in the case of this study, buckling and stability static analyses have the following partial reduction factors:

- Criticality of failure mode γ_{mc}: 1.08 for all buckling analyses.
- Irreversible long term degradation γ_{m1}: 1.05, as stiffness degradation effects are not considered.
- Temperature effects γ_{m2}: 1.05, as stiffness degradation and temperature effects are not accounted for this study.
- Manufacturing effects γ_{m3}: 1.1, as nominal material properties are used.
- Accuracy of analysis methods γ_{m4}: 1.4 for linear buckling analysis and 1.05 for nonlinear buckling analysis. FEA is evaluated in a blade cross section and not in the full blade scale test.

- Accuracy of load assumptions γ_{m5}: 1, as loads have been studied in 12 different directions.

Moreover, buckling analyses may be carried out by either analytical or numerical methods. This project sticks to a numerical approach and takes into consideration both linear and nonlinear buckling analyses, further detailed in the following section. Two different reduction factors apply in each case: $\gamma_m = 2.200$ and $\gamma_m = 1.650$ for linear and nonlinear buckling, respectively. These factors are shown in table 2.4. As a consequence, the relation between the material response to external loading and the initial design loads sets a safety factor that can be compared to the correspondent reduction factor from the Standard. Hence, the buckling analysis of defects is based on this comparison to show the compliance of the design with the current legislation.

Linear Buckling	2.200
Nonlinear Buckling	1.650

Table 2.4: Reduction factors requested by the Standard [1] for static buckling analyses over the extreme flapwise and edgewise loads.

Finally, when a buckling analysis is performed, particular attention shall be given to the definition of the boundary conditions [1], as their variance will affect the final displacements that the structure accomplishes.

2.2.2 Linear buckling

Linear buckling analysis determines the critical buckling load solving the eigenvalue problem for the stiffness matrix K (equation 2.6), being $M$and N the degrees of freedom of the model.

$$K^{MN} v^M = 0 \tag{2.6}$$

The buckling loads are calculated according to the base stiffness state of the structure K_0, this is to say, at the initial conditions. Buckling sensitivity is investigated by introducing an incremental loading pattern in the model which is defined at each step, scaled by the eigenvalues λ_i found in the problem [13]. The eigenvalue problem is then defined as in equation 2.7. K_Δ^{NM} represents the stiffness matrix created with the incremental loads included in the model.

$$(K_0^{NM} + \lambda_i K_\Delta^{NM}) v_i^M = 0 \qquad \text{for } i \,\epsilon\, [1, size(v)] \tag{2.7}$$

Each eigenvalue λ_i coincides with the critical buckling failure and the correspondent eigenvector v_i^M defines the buckling mode shapes. The former multiplied by the applied load provides the critical load which would cause stability failure in a perfect system. The latter is a normalized vector and does not represent actual magnitudes of deformation [13]. In other words, the first obtained eigenvalue is the safety factor that the structure would have when applying the imposed load.

In Abaqus, linear buckling is carried out with the *BUCKLE keyword. Number of eigenvalues, maximum eigenvalue or the maximum number of iterations are parameters that can be fixed.

Abaqus returns the lowest eigenvalues as an output because the lower they are the more critical is the load at which buckling occurs. However, if the closer eigenvalues to zero are searched, they might be negative. Negative eigenvalues indicate that the structure would buckle under reverse loading, which would give additional unnecesary information. There are two possible algorithms to solve the eigenvalue problems. Lanczos eigensolver is chosen as it is the one enabling to specify the absolute value for the eigenvalues.

Linear buckling analysis contains some limitations. Firstly, even if the minimum eigenvalue is higher than the required safety factor, this does not ensure the absence of failure. Linear buckling represents an ideal situation, ignoring influential factors. On top of considering an ideal situation, lower eigenvalues are found in specific nodes or elements. However, the study does not consider the structure as a whole as it is not an incremental study. Moreover, the eigenvalue problem is based on the linear elastic stiffness; plasticity and other inelastic effects are ignored, such as temperature, field or materials nonlinearities [13]. Finally, as in mode analyses, the deformations obtained from the buckling analysis are normalized, leading to unreal values that have no physical meaning. Therefore, nonlinear buckling is necessary in order to enlighten results and include non linearities. In addition, this type of analysis is specially interesting when defects are introduced in the model.

Overall, the main advantage of linear buckling is to determine structural stability in short computing time. It is a fast way to verify if a model response is correct. However, as justified, it should be backed up with a nonlinear buckling analysis.

2.2.3 Nonlinear buckling

Nonlinear buckling bases the procedure on an incremental analysis. The imposed external load is reached after various load increments as a function of time in which mechanical equilibrium is found. Each increment influences the result of the next increment and, this way, displacements and stiffness vary at each of them. A comparison between linear and nonlinear buckling is shown in figure 2.10, where the variation in deformation with nonlinear buckling is clearly perceived. The equilibrium at each increment is found from an iterative process where convergence is achieved when external forces P equal internal loads I acting at a node. A residual value $R = P - I$ is then calculated at each iteration. Equilibrium is achieved if R is lower than 5%, being this value set by default in Abaqus [13]. Abaqus forces the simulation to stop if iterations start diverging.

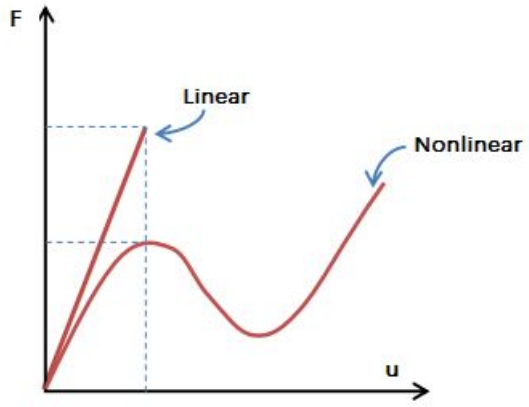

Figure 2.10: Linear and nonlinear buckling deformations according to applied load.

Nonlinear buckling analysis is performed under structures with geometrical or material imperfections. In the case of the intact blade or small defects, the structure may not have enough irregularities to develop a proper nonlinear analysis. Therefore, a small modification on the execution of the Abaqus input file is necessary. Artificial imperfections of maximum 1mm are distributed around the area where the major deformations over the first buckling mode are experienced in the linear buckling analysis. These small imperfections do not influence the final results but they ensure to successfully execute the nonlinear buckling study. Therefore, it has been decided to implement these procedures in all defect cases, to maintain consistency.

In Abaqus, the nonlinear buckling analysis is implemented by means of the *STATIC keyword, specifying that this is a nonlinear geometrical analysis with the

parameter NLGEOM. The first increment is a necessary input and the subsequent increments are automatically chosen by the program. Time period or minimum and maximum times allowed are other possible inputs but Abaqus can set them to default values if they are unknown. Furthermore, automatic stabilization can also be set for the computation. This stabilization is reached introducing viscous forces F_v in the targeted equilibrium: $P - I - F_v = 0$. Viscous forces are defined in equation 2.8, where c is the imposed constant damping factor, M is the mass matrix calculated with unity density and $v = \Delta u/\Delta t$ [13].

$$F_v = cMv \tag{2.8}$$

Stiffness matrix is calculated at each load increment. There can be a point where the program runs out if stiffness matrix takes many negative values or even zeros. At this point, it is impossible for the program to compute any deformations and the simulation is terminated. This is the case for many results of this study. If the analysis is able to continue running, post-buckling is produced. Post-buckling is not a point of interest for this study as first failure is aimed for the analysis of structure behaviour under defects.

Nonlinear buckling has the benefit of achieving robust results when incorporating geometry and material imperfections. As the analysis is more realistic than linear buckling, the critical load is lower than that of linear buckling analysis. Furthermore, the deformations calculated in each increment are not just shapes but real values. The main drawback of this analysis is the high computational time that it takes as well as possible problems of convergence. When divergence is found, some inputs for the *STATIC keyword need to be modified.

2.2.4 Failure criteria

Failure criteria is an important tool in the design of composite structures as they relate the lamina stresses and strains to the allowable values that the material can take. In other words, failure criteria determine if a structure can fail due to the applied loads. Failure is considered in the model when specific stress requirements within a failure criterion are reached or surpassed.

There are several existing failure criteria but they all define, in a way or another, the allowable stresses and strains for the specified structure. Depending on the criterion, a function F limiting stresses and strains is defined. The structure fails

if the stresses and strains created by the input loads make this function exceed or equal 1 (F≥1). In this project, the Tsai-Wu failure criterion and other focused on the adhesive failure are studied.

Furthermore, first-ply failure is taken in the analysis of failure criteria. The strength of the laminate is determined by the strength of each laminae [14]. The first-ply failure assumes that the final failure of the laminate occurs when the first laminae fails. This is a simplification of what happens in real life. After the first-ply failure, there is a change of stiffness in the laminate as the overall strength decreases. Final failure usually takes place later, when there is no more strength to support the input load. However, in some situations, the failure of a laminae leads to the apparition of cracks that end up triggering the complete failure. Thus, first-ply failure is taken as the strength limit in order to be highly restrictive.

In both failure criteria, the imposed boundary conditions may affect the final analysis so special caution is necessary. Boundary conditions create high stresses in specific points at their vicinity. In reality, as the blade is continuous, these stresses near the end sections do not exist. Therefore, for the present study, the elements close to the boundary conditions are not included when studying failure criteria. This point is clarified over the developed analyses.

2.2.4.1 Tsai-Wu failure criterion

It is a commonly used criterion described as the *Tensor Polynomial Criterion* or the *Quadratic Interaction Criterion* [14].

The Tsai-Wu failure criterion can be written as equation 2.9, evaluated in three dimensions as the studied model [5].

$$\begin{aligned} F_{TW} = F_1\sigma_{11} + F_2\sigma_{22} + F_3\sigma_{33} + 2F_{12}\sigma_{11}\sigma_{22} + 2F_{13}\sigma_{11}\sigma_{33} + 2F_{23}\sigma_{22}\sigma_{33} + \\ + F_{11}\sigma_{11}^2 + F_{22}\sigma_{22}^2 + F_{33}\sigma_{33}^2 + F_{44}\sigma_{23}^2 + F_{55}\sigma_{13}^2 + F_{66}\sigma_{12}^2 \end{aligned} \tag{2.9}$$

The proportional parameters on the equation relate the correspondent stresses with the ultimate strength of the material and their expressions are: $F_1 = 1/\sigma_{1t}^u + 1/\sigma_{1c}^u$, $F_2 = 1/\sigma_{2t}^u + 1/\sigma_{2c}^u$, $F_3 = 1/\sigma_{3t}^u + 1/\sigma_{3c}^u$, $F_{12} = -0.5/(\sigma_{1t}^u\sigma_{1c}^u\sigma_{2t}^u\sigma_{2c}^u)^{0.5}$, $F_{13} = -0.5/(\sigma_{1t}^u\sigma_{1c}^u\sigma_{3t}^u\sigma_{3c}^u)^{0.5}$, $F_{23} = -0.5/(\sigma_{2t}^u\sigma_{2c}^u\sigma_{3t}^u\sigma_{3c}^u)^{0.5}$, $F_{11} = 1/(\sigma_{1t}^u\sigma_{1c}^u)^2$, $F_{22} = 1/(\sigma_{2t}^u\sigma_{2c}^u)^2$, $F_{33} = 1/(\sigma_{3t}^u\sigma_{3c}^u)^2$, $F_{44} = 1/(\sigma_{23}^u)^2$, $F_{55} = 1/(\sigma_{13}^u)^2$ and $F_{66} = 1/(\sigma_{12}^u)^2$.

The superscript u represents the ultimate strength of the material and the subscripts t and c denote tensile and compressive directions, respectively. On the main failure criterion definition, σ_{11}, σ_{22} and σ_{33} are the normal stresses and σ_{12}, σ_{13} and σ_{23} are the shear stresses in the in-plane [5]. These stresses are illustrated in figure 2.11 for better comprehension. Therefore, material fails according to this criterion if $F_{TW} \geq 1$ once equation 2.9 is evaluated.

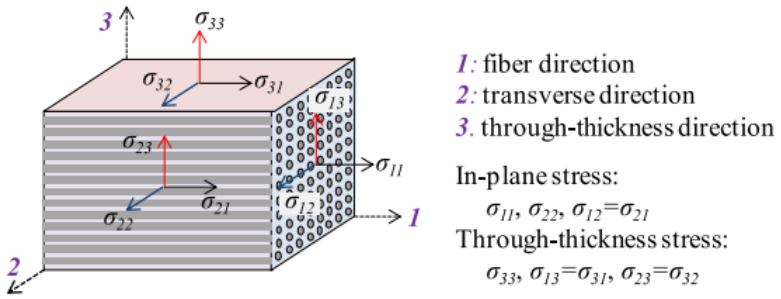

Figure 2.11: Representation of the strains and axes directions used in the Tsai-Wu failure criterion [5].

This criterion is an empirical model designed to fit failure strengths. However, this is exactly a flaw of this model, as the 3D boundaries created do not exactly resemble the physical behaviour because a structure can fail under different type of loadings. Consequently, physically based failure criteria (based on several measured points) are currently the main focus of researchers [14].

In Abaqus, this criterion can be applied to every element by stating the definition of F_{TW} in equation 2.9 gathering the different stresses at each increment. Nevertheless, whether or not the structure fails according to this criterion is not part of Abaqus' outputs. To solve this, a Fortran code has been used, which gives the F_{TW} estimation as an output variable (UVARM) for each increment.

2.2.4.2 Adhesive failure criterion

The failure criterion based on the adhesive performance can be directly obtained as a result output in Abaqus. As stated above, the cohesive sections fail when the first damage is initiated; in other words, when the quadratic nominal stress criterion is satisfied (left hand side of equation 2.2 is equal or higher than 1). Therefore, a value of this stress criterion for every element of the blade section is stored as an output in the database. As a result, if the output is less than 1, there has not been any

failure in that specific element whereas if the output is higher or equal to 1, there has been failure due to adhesive.

2.3 Assumptions

In order to implement the analyses, several assumptions have been made:

- Defects are configured with arbitrary rectangular shapes. Real defects would vary in shape and size.
- The four extreme flapwise and edgewise loads are the only known input for the study. Combined loading magnitudes are determined by the load envelope, which is approximated to an ellipse that includes the four extreme loads (figure 2.6).
- As mentioned in the previous section, first-ply failure criterion is considered for material failure.
- The blade model does not restrain the contact between plies. Therefore, when the blade deforms, certain layers can penetrate in others. This behaviour is not realistic.
- The boundary conditions limiting the final sections of the blade provide higher stresses than the ones that would be created in a middle section of the blade. Therefore, the end region is not considered for the analysis of results and the area near these end regions with clamp elements are cut.
- Geometric imperfections of 1mm length are added to the nonlinear buckling analysis of the intact blade to trigger buckling and provide trustful results from this method. To maintain consistency, these imperfections are also applied to the defect cases as it is assumed that they are very small to be noticeable compared to the effect of defects.

These assumptions have been the same for all studied cases so that consistency is maintained. However, they affect the final structural response of the blade section. In fact, some of the assumptions can lead to problems in the interpretations of results if they are not taken into consideration. Some of the cases that are thought to be highly influenced by these assumptions are more extensively presented in Chapter 5.

CHAPTER 3

Defects design

This chapter covers the design of potential common defects in wind turbine blades and their definition in Abaqus. Two types of defects are chosen to be examined: missing adhesive in the trailing edge (TR) and in the contact between spar caps and shear webs (SW).

3.1 Selection of defects

The trailing edge of wind turbine blades is a critical region of the blade. Furthermore, it has the greater contact of adhesive connecting the upper and lower part of the blade, so the existence of defects highly influences blade performance. It is for these reasons that this is an important starting point for the study of defects.

Another vital part of the blade is its box girder, composed of two spar caps and two shear webs. The objective of the box girder is to provide sufficient strength and stiffness to the blade, both globally and locally. Globally, as the blade should not collide with the tower during operation. Locally, the box girder ensures that the shape of the blade structure is maintained [15]. As it is also an important load carrier member of the blade, there is high interest in checking its dependence on missing adhesive defects. Specific regions of the box girder are the ones where this defect is studied, as discussed later on the development of the project.

Finally, a third type of defect was also considered under this project. This defect is debonding, as it is a very common type of defect on wind turbine blades. However, it is not detailed under the analysis as the final results turned out to be incoherent and the duration of the project has not been enough to identify a justification. Appendix A shows the followed procedure to create the defects as well as the obtained results.

3.2 Creation of missing adhesive defects

The defect of missing adhesive is generated in Abaqus by the modification of the correspondent adhesive element set: the one over the trailing edge or the one con-

necting shear webs with spar caps. As stated previously, an element set is created by means of a master element (indicated in red in figure 2.1), which is copied a certain amount of times selected by the user.

The adhesive layer has 20 elements in a row (x direction) and the total number of rows (z direction) coincides with the length of the airfoil section studied (200 elements). In order to implement the missing adhesive defect, the initial adhesive element set can be parted into two element sets, letting a space for the missing adhesive between them. Figure 3.1 illustrates this explanation. Set 1 is defined by the initial master element but its length (number of elements) in the z direction is shortened until the defect. After the defect, another set is implemented, implying the creation of another master element.

Several study cases for this type of defect can be developed by creating more element sets or modifying these. However, for simplicity and generalization, the former is the type of defect analyzed.

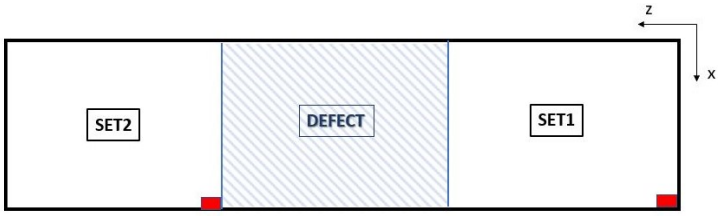

Figure 3.1: Creation of missing adhesive defect in Abaqus. Master elements from each element set are indicated in red.

Spar caps and shear webs are joined by four points of adhesive, two in the upper part of the blade section and two in the lower part of it. The specific location of the studied defects is detailed and justified under the analysis.

3.3 Design and sizing of defects

Specific sizes and positions of the explained defects have to be chosen in order to start the analysis. As the overall influence is unknown, especially for combined loading, arbitrary sizing is implemented in the first simulations. The initial size and positions of defects is shown in figure 3.2. These defects are also illustrated in the blade section in figure 3.3 for better understanding.

As seen in these figures, all the defects are going to be placed in the center of all studied element sets. The main reason is that, by centering the defects, the blade

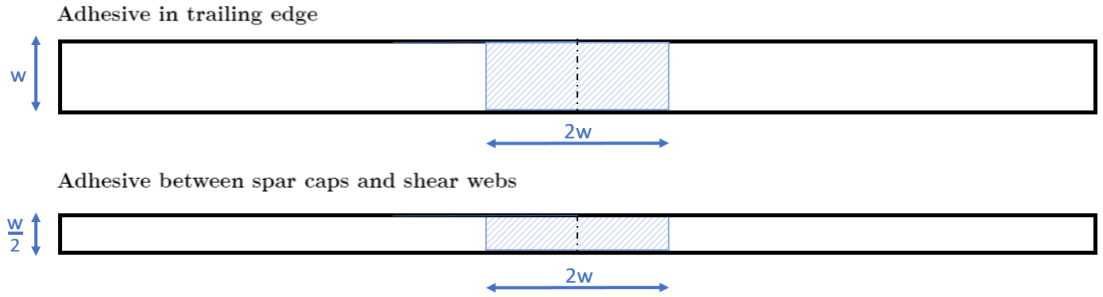

Figure 3.2: Initial dimensions of studied defects of missing adhesive.

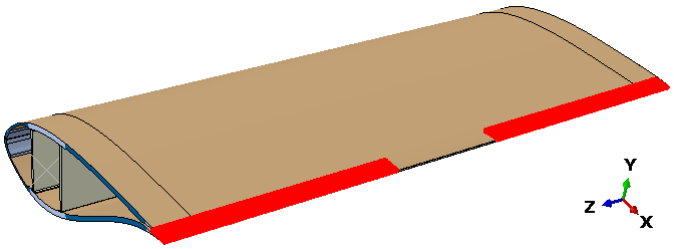

(a) TR defect

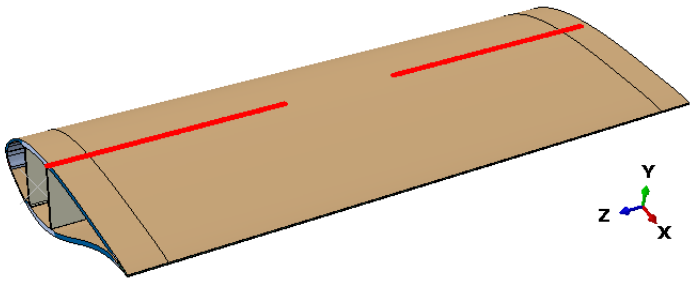

(b) SW defect

Figure 3.3: Initial TR and SW adhesive defects representation in the blade model.

section is symmetric. Otherwise, varying the position of defects, more variables would come into play when studying the response. Therefore, the present is a general analysis from which other specific studies can be developed. Furthermore, all the row elements of the adhesive in the trailing edge section (w in figure 3.2) is taken as an initial reference to model the size of defects. The width of all defects along the blade length is taken to be the same: $2w$=1m over the total 5m of the current blade. Even though this length might seem big for the blade section length, it is important to note that the purpose of this project is to get to a better understanding of buckling behavior and understand its progress.

The proposed size of defects is varied in further simulations when their effects are analyzed. Furthermore, the specific shear webs where the missing adhesive defect is analyzed is detailed under Chapter 5. The aim is to identify the variations and

behaviour between different defect cases.

CHAPTER 4

Intact blade analysis

This chapter focuses on the full exposition of results for the intact blade. Linear and nonlinear buckling analyses are detailed as well as the failure criteria, following the conditions and requirements specified in Chapter 2. Moreover, a damage prediction combining all former studies is developed, comparing the results.

The analysis procedure to draw final comparisons is carefully detailed under this intact blade analysis. Therefore, this chapter sets the base understanding for the later defects study as the explained analysis procedures are the same for all defect cases.

4.1 Linear buckling

Once the intact blade is subjected to linear buckling analysis with the input design loads described in Chapter 2 (table 2.2), the three main buckling modes are evaluated and shown in table 4.1. All cases share an increase in eigenvalues when increasing eigenmode. As it can be seen, Abaqus gives the eigenvalues in an increasing order, and the difference between the three first eigenmodes can be appreciated. However, the first eigenvalue is the one considered for this study, as it provides the most restrictive critical buckling load which is given by multiplying this eigenvalue with the applied load. Thus, the eigenvalue is indeed a safety factor for the blade section at each loading direction. Hence, eigenvalues can be compared to the reduction factor imposed by the Standard as they share the same definition.

It can be appreciated that the extreme loading points present eigenvalues higher than the requested reduction factor $\gamma_m = 2.200$, satisfying the Standard [1]. However, there are some eigenvalues over the combined loading directions that are lower than this reduction factor. This is the case for 30°, 210°, 240°, 300° and 330°, highlighted in yellow and orange in table 4.1. In this specific design, even though the intact blade is a good design according to the Standard, buckling may still occur when combined loading is experienced. These results prove that combined loading can sometimes result in higher damages than pure flapwise or edgewise loads. For instance, the safety factor for 330° case is extremely low for a linear buckling analysis, as well as the other cases highlighted in orange.

Study case	P2S 0°	30°	60°	T2L 90°	120°	150°
Design Load (kNm)	2394.250	1913.356	1423.721	1242.170	1284.186	1527.978
1^{st} eigen.	2.610	2.120	2.897	3.725	3.712	3.168
2^{nd} eigen.	2.612	2.120	2.905	3.728	3.712	3.179
3^{rd} eigen.	2.706	2.12	3.115	4.132	4.134	3.558

Study case	S2P 180°	210°	240°	L2T 270°	300°	330°
Design Load (kNm)	1759.245	1550.910	1310.865	1269.555	1453.299	1942.071
1^{st} eigen.	3.755	2.171	2.195	2.456	2.150	1.576
2^{nd} eigen.	3.756	2.181	2.208	2.468	2.162	1.583
3^{rd} eigen.	3.858	2.434	2.469	2.758	2.414	1.765

Table 4.1: Eigenvalues from linear buckling analysis for intact blade section at each studied load direction. Cells highlighted in green are the requested load directions by the Standard [1]. In yellow and orange are highlighted the cases for which the Standard is not satisfied ($\gamma_m \leq 2.200$), being the latter the most critical cases.

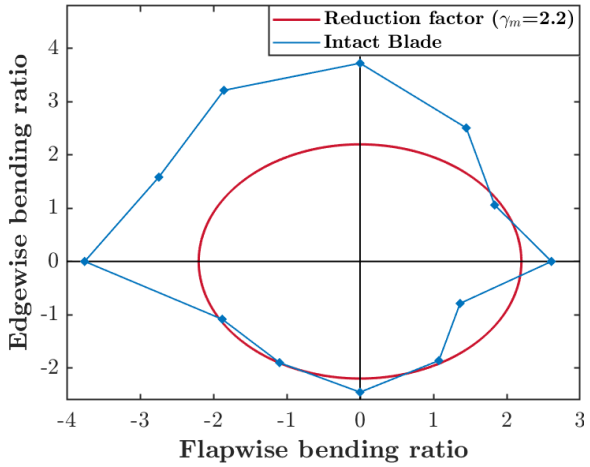

Figure 4.1: Linear buckling envelope of the intact blade case compared to the reduction factor requested by the Standard.

A visual representation of these results is shown in figure 4.1. The magnitudes of the eigenvalues in each load direction are shown at their respective rotation angles θ, forming a loading envelope similar to the one of the design loads for this buckling analysis (figure 2.6). The main difference is that, instead of bending loads, eigenvalues are forming the envelope in order to be compared to the reduction factor requested by the Standard. Therefore, the cases in which the eigenvalues are lower than the reduction factor (do not satisfy the Standard) are enclosed in the reduction factor boundary (red ellipse). On the contrary, the eigenvalues that satisfy the Standard and are higher than the reduction factor are on the outskirts of the ellipse.

Figures 4.2 to 4.5 show the deformations due to buckling of the four uncoupled flapwise and edgewise cases. As clarified in Chapter 2, linear buckling analysis does

not show real deformations on the structure. In the figures, each load case shows the three dimensional perspective of the blade model together with its cross section so the behaviour can be comprehended.

In all loading directions, the location where buckling occurs depends on several aspects. First, each point of the loading envelope varies its reference system and so, the bending moment direction. Buckling occurs where compression is experienced by the blade section so this varies according to the bending moment direction applied. Second, maximum distance to neutral axis and material strength explains the specific location of buckling maximum deflections, as the total bending moment is greater. More specific explanations follow next for which it is especially important to pay attention to the cross sections of each load case. In these, the x-axis of the test reference system is named Neutral Axis (NA from now on) and so, it is the direction in which the input bending moment is applied.

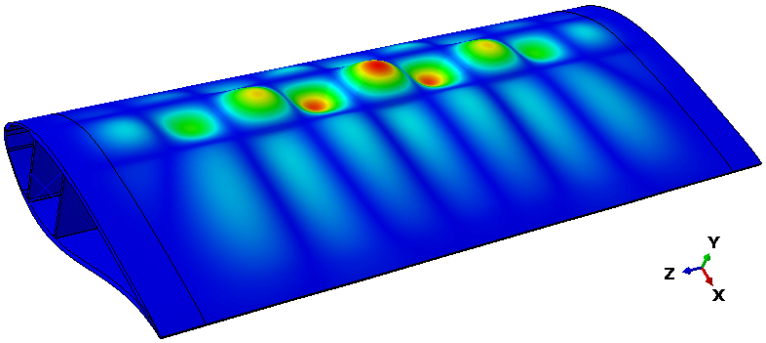

(a) Three dimensional perspective of the first buckling mode over the blade model. Scaling factor=0.12.

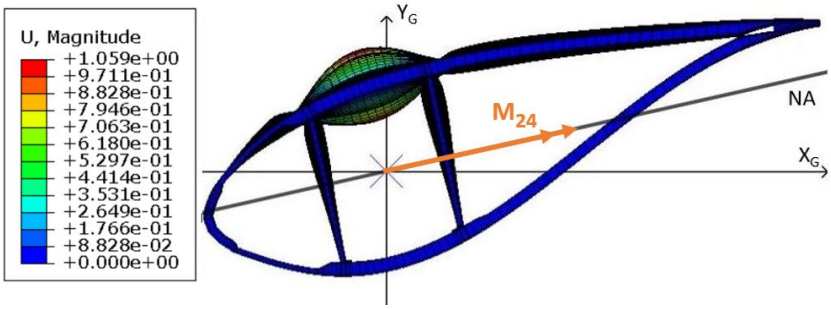

(b) First buckling mode over blade cross section

Figure 4.2: Linear buckling analysis for P2S 0° load direction over the intact blade.

Figure 4.2 shows the linear buckling response of the blade section for P2S 0° flapwise bending. Buckling takes place on the upper part of the cross section (4.2b) as it is where compression is experienced by the blade section. The bending moment's direction follows the NA towards the trailing edge, as illustrated in the figure. How-

ever, it is important to be careful with the bending moment sign convention. The positive bending moment is established to be in section 19 of the studied blade. Figure 4.2b is taken from section 24, meaning that this section experiences a negative bending moment. Therefore, the opposite sign convention is taken, justifying the buckling behaviour on the pressure side, where compression is experienced. From now on, this sign convention is applied to the rest of the load directions. Furthermore, in this case, buckling is held at the spar cap as it carries the flapwise load and its distance to the NA is maximum.

Figure 4.3 shows the deformation due to buckling when applying S2P 180° flapwise bending load. Buckling occurs in the lower part of the cross section as the bending moment has now the opposite direction from the previous case. Compression is now experienced in the suction side of the cross section and the main carrying capacity is also in the spar cap as in the previous case.

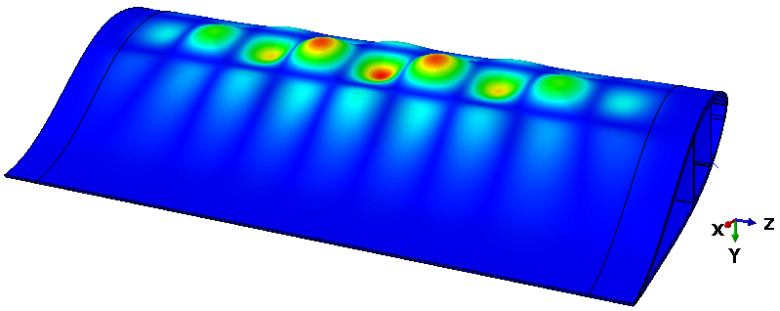

(a) Three dimensional perspective of the first buckling mode over the blade model. Buckling is shown in blade's suction side. Scaling factor=0.12.

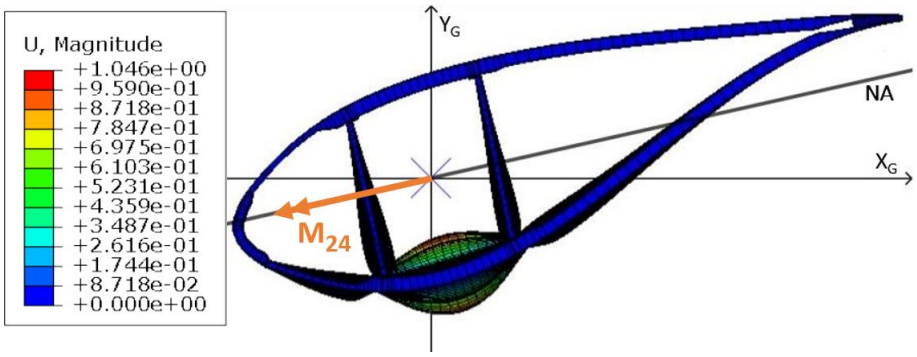

(b) First buckling mode over blade cross section

Figure 4.3: Linear buckling analysis for S2P 180° load direction over the intact blade.

Let one now focus on the edgewise loading cases. The results can be found in figures 4.4 and 4.5. Taking the same reasoning as before, buckling occurs where

compression is experienced. As the negative sign convention is taken, deformations are observed in the leading edge for T2L 90° load and in the trailing edge in L2T 270° load as they are the furthest areas from the NA.

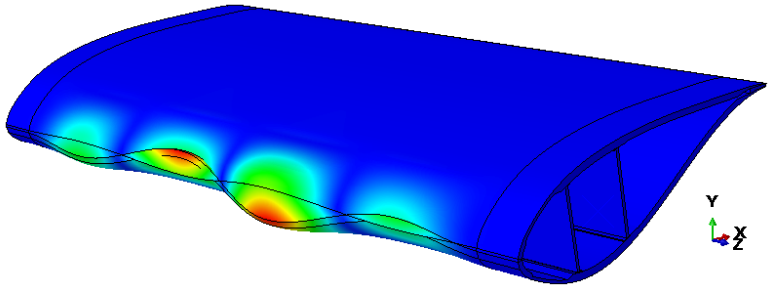

(a) Three dimensional perspective of the first buckling mode over the blade model. Scaling factor=0.12.

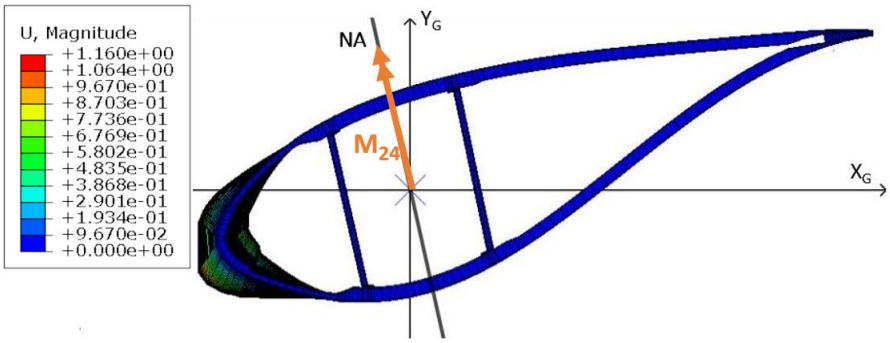

(b) First buckling mode over blade cross section

Figure 4.4: Linear buckling analysis for T2L 90° load direction over the intact blade.

Combined loading follows the same reasoning as the extreme loading directions, with the advantage that it clarifies how materials influence blade response. A clear example can be seen in figure 4.6, where the buckling behaviour at 30° direction is displayed. Similarly to P2S flapwise loading, compression is perceived in the upper part of the cross section (figure 4.6b). However, as this axis is tilted 30° from the previous case, the upper spar cap is no longer the longest distance to NA. Consequently, buckling needs to occur between the leading edge and the spar cap. Even though it seems that the sandwich panel (element set 911) has greater distance to the NA, the higher buckling deflections are experienced in the upper part of set 113. The reason behind this behaviour can be explained by the fact that the spar cap has greater bending stiffness than that of sets 911 and 113. Therefore, the low bending stiffness of set 911 is compensated with the one of the spar cap. However, the part of set 113 that is further away from the neutral axis takes the maximum deflection as its bending stiffness is lower.

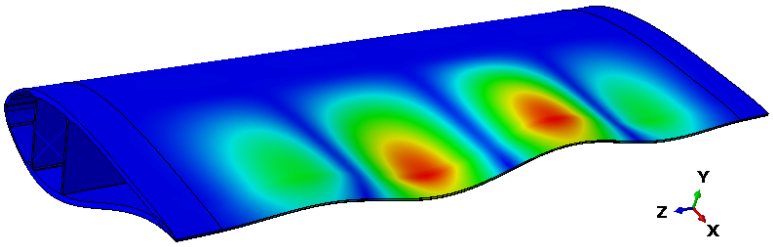

(a) Three dimensional perspective of the first buckling mode over the blade model. Scaling factor=0.12.

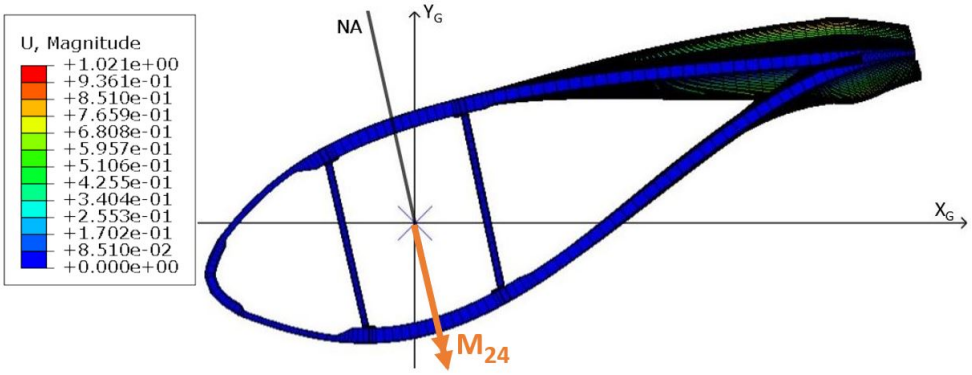

(b) First buckling mode over blade cross section

Figure 4.5: Linear buckling analysis for L2T 270° load direction over the intact blade.

If now the NA is tilted another 30° figure 4.7 is obtained, where the 60° load direction is applied. It is proven that buckling occurs close to the leading edge (similarly to the T2L case explained before) as this is now the bigger distance to the section from the NA.

The buckling behaviour of the rest of the combined loading directions is very similar to the previous ones. Buckling at 120° and 150° is alike T2L edgewise loading as the element set 113 is in compression and it has the lowest stiffness of this part of the cross section. The same way, once 180° is exceeded, all loads can perfectly resemble the buckling behaviour from pure L2T edgewise loading. From 210° to 330°, as the NA rotates in each direction, the spar caps no longer hold the greatest distance to the NA. Furthermore, buckling deflections increase through the sandwich panel (material element set 36) until the furthest element from the NA and, after this element, they decrease in set 13. The peak is produced at those specific elements due to the change of material. The sandwich panel has lower bending stiffness than the material of set 13.

The results from this linear buckling analysis need to be backed up with the

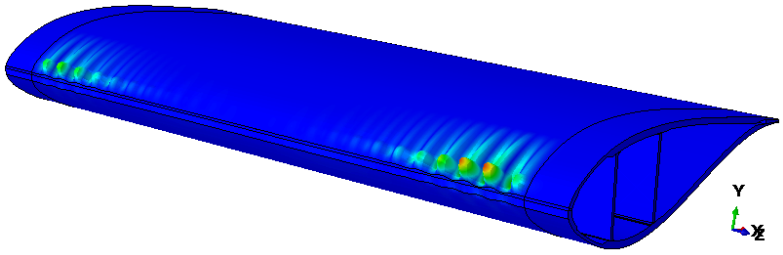

(a) Three dimensional perspective of the first buckling mode over the blade model. Scaling factor=0.12.

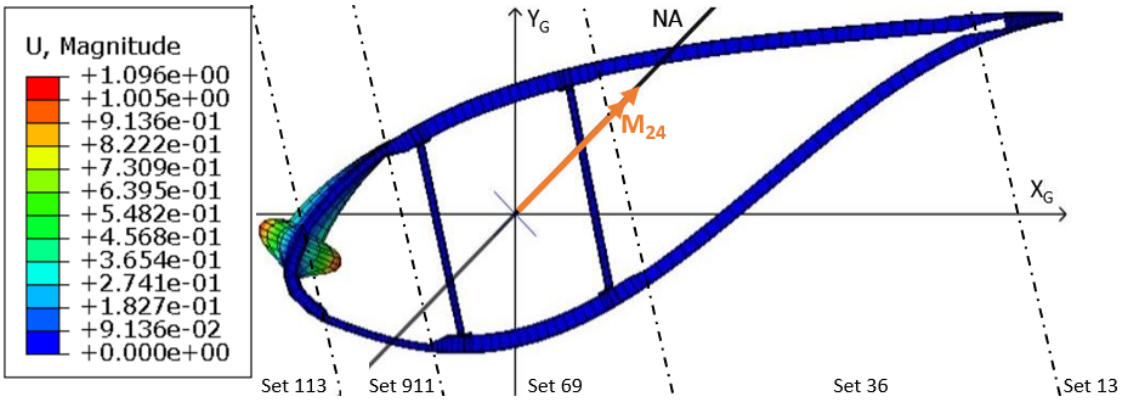

(b) First buckling mode over blade cross section

Figure 4.6: Linear buckling analysis for 30° load direction over the intact blade. Element sets according to different type of material configuration in the blade are indicated.

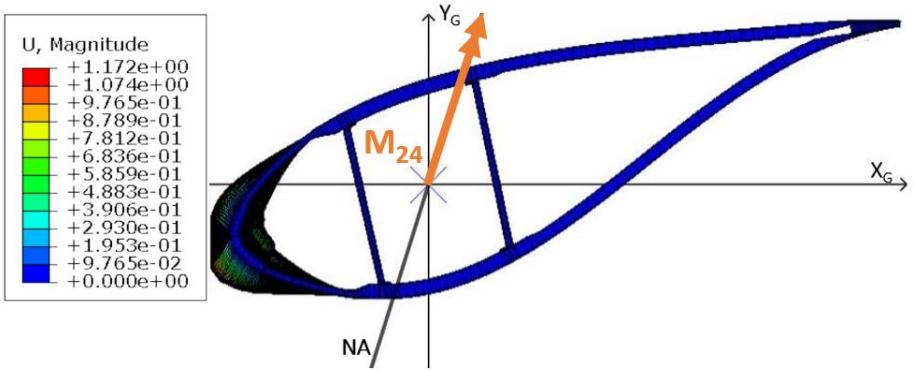

Figure 4.7: Linear buckling analysis for 60° load direction over the intact blade.

later nonlinear buckling analysis in order to provide a more realistic response.

4.2 Nonlinear buckling

The load experienced over the structure through the simulation increments can be simply taken as the bending reaction load at any point of the blade length. In this case, the reaction bending moment is saved as an output for section 19, where it can be evaluated as a function of time and as a function of the rotational angle at that same section. The rotational angle is a measurement of the deformation that the structure experiences. The load reaction at section 19 is the one studied as the results are positive from the reference system considered. In section 24, the results have the same module but negative sign as the input moment has opposite direction from the one imposed to section 19 (in positive x-axis direction).

The critical load for the blade section is determined from the peak on the bending moment reaction and rotational angle relation. An example can be seen in figures 4.10 and 4.8. In the first one, one can see that the bending moment is directly proportional to the rotational angle until the critical load is achieved. However, the second one is different, the peak is produced at a lower load but, after it, the bending moment and rotational angle relation continues following a linear curve. The first peak is a local failure of the blade section. The overall bending moment diminishes when a certain part of the blade fails but, afterwards, the blade can still take further load until the nonlinear analysis stops. Even if the blade can still bear more load, the first local failure is taken for this study, as first-ply failure criterion is taken into account.

Figure 4.9 shows the same bending moment and rotational angle relation but for 210° loading direction. It can be appreciated that there is a small peak near 3500 kNm loading but the maximum bearable load is produced at 4910 kNm. The first peak is again a local failure but the structure can still take more load. Once more, the local failure is taken as the structural failure for this study. A more detailed explanation about the load carrying capacity of the blade between the first local failure and final failure is explained later through failure criteria. In addition, the response of the blade model is also shown later in order to comprehend the behaviour under nonlinear buckling analysis.

In some cases, the simulation terminates before the structure has a first local or total failure. In fact, as the loading/displacement relation of these cases is a straight slope, it is assumed that the critical load occurs at a higher load than the one known when the analysis is over. This is the case for loads between 30° and 150° directions.

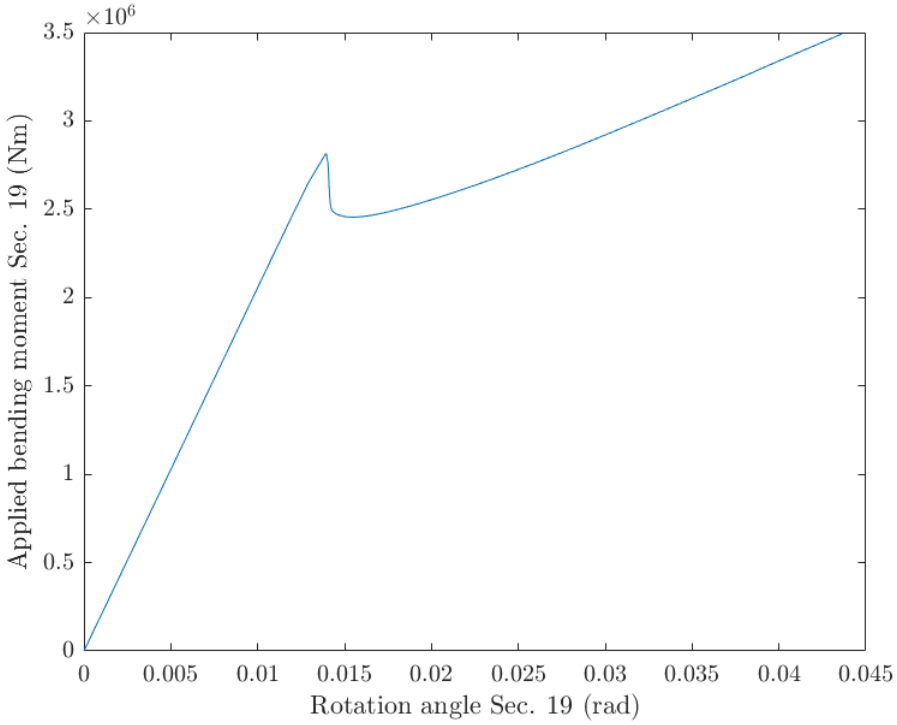

Figure 4.8: Nonlinear buckling analysis of L2T 270° edgewise loading for the intact blade.

Study Case	Design load (Nm)	Ultimate load (Nm)	Load ratio
P2S 0°	2.39E+06	5.20E+06	2.174
30°	1.91E+06	4.33E+06	2.264
60°	1.42E+06	4.39E+06	3.084
T2L 90°	1.24E+06	3.86E+06	3.110
120°	1.28E+06	4.69E+06	3.656
150°	1.53E+06	4.23E+06	2.767
S2P 180°	1.76E+06	5.28E+06	3.003
210°	1.55E+06	3.27E+06	2.111
240°	1.31E+06	2.64E+06	2.017
L2T 270°	1.27E+06	2.82E+06	2.217
300°	1.45E+06	2.78E+06	1.912
330°	1.94E+06	2.67E+06	1.373

Table 4.2: Loads from nonlinear buckling analysis for each loading direction for the intact blade. Loading ratios not satisfying the Standard ($\gamma_m \geq 1.650$) are shown in red.

As for the other cases, S2P 180° loading case shares a similar bending moment to rotational angle relation as P2S 0°, whereas all the cases from 210° to 330° share a similar relation to figure 4.8 (local failure occurs first).

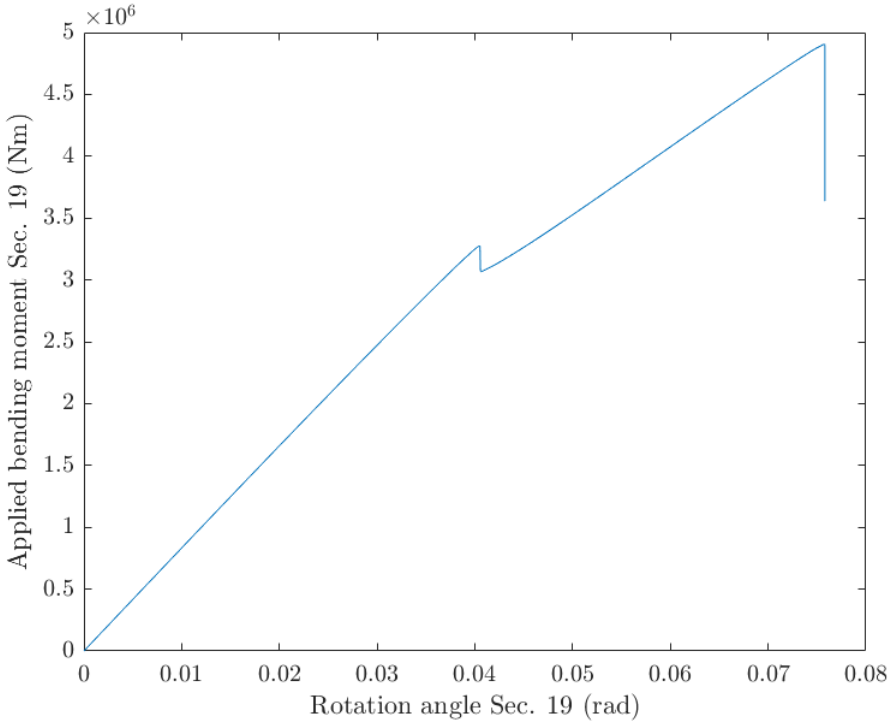

Figure 4.9: Nonlinear buckling analysis of 210° loading direction for the intact blade.

Once nonlinear buckling analysis has been computed, the load incrimination in relation to the rotational angle for each loading direction can be calculated. The ultimate load is obtained as that when the stiffness starts decreasing in this graph. Therefore, the a load ratio for this ultimate load can be calculated as a relation between the ultimate load and the design load in order to be compared to the nonlinear reduction factor specified by the Standard (table 2.4. These results are displayed in table 4.2. As seen in this table, there is only one case that is not satisfying the Standard, with lower reduction factor than the one requested ($\gamma_m = 1.650$). However, even though it is just one case, it is important to note that the combined loading case that is further from satisfying the design requirements is in 330° direction, agreeing with the previous linear analysis.

4.3 Failure Criteria

Two failure criteria are considered for nonlinear buckling analysis results: Tsai-Wu and adhesive failure. They can determine if the material strength bears the load that the nonlinear analysis has identified as critical. Consequently, the critical bending

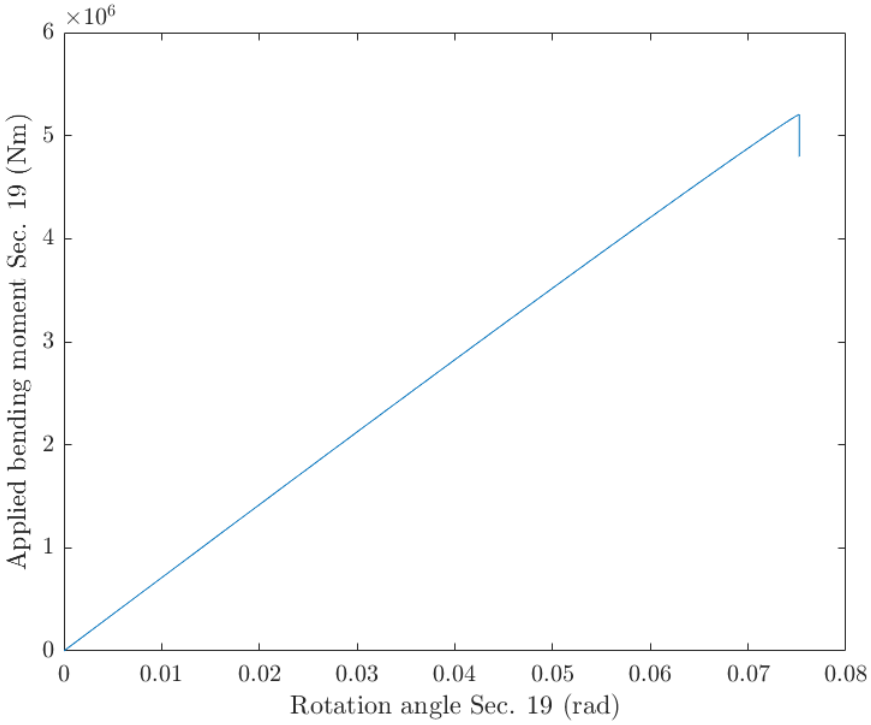

Figure 4.10: Nonlinear buckling analysis of P2S 0° flapwise loading for the intact blade.

moments from each criterion are compared later.

In order to find out which bending moment is causing material failure, the time at which material fails is introduced into the previous nonlinear buckling study and the correspondent bending load can be obtained. The bending moment reaction and rotational angle relation follows the same behaviour as the bending moment - time relation. Figures 4.11 to 4.15 show an example of the application of the failure criteria to the previous nonlinear analyses. It can be appreciated how bending moments due to material failure are lower than the critical load considered in the previous case (peaks in figures). Therefore, this project retains the results given by the failure criteria over nonlinear buckling as they provide more restricting loads.

Figure 4.11 show the material failure criteria for the P2S 0° loading direction. If the Tsai-Wu failure criterion is considered, the first failure accounted in the structure is produced in the upper spar cap of the blade section. This can be observed in figure 4.12a. The parts of the blade where material fails according to the Tsai-Wu failure criterion are shown in red, which coincide with the higher deformations experienced in the first buckling mode of the linear analysis of this same load direction (figure 4.2a). Furthermore, the final material failure (after the peak in 4.11

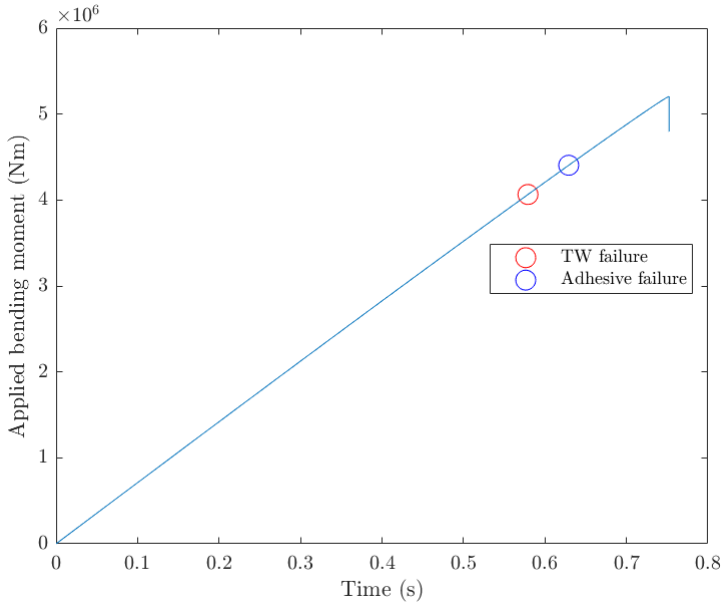

Figure 4.11: TW and adhesive failure criteria over the P2S 0° load direction for the intact blade.

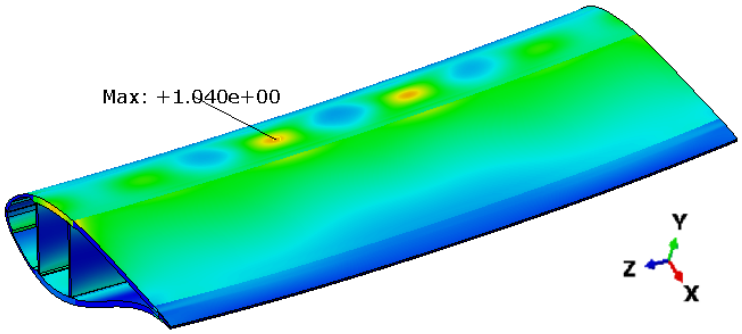

(a) First failure. Scaling factor=1.

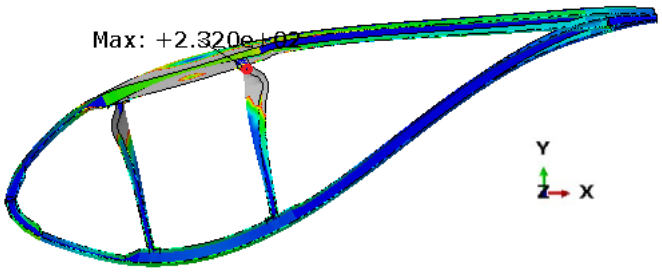

(b) Final failure. Scaling factor=1.

Figure 4.12: Comparison between first-ply failure and final material failure on the blade section, considering the Tsai-Wu failure criterion. P2S 0° load direction for the intact blade.

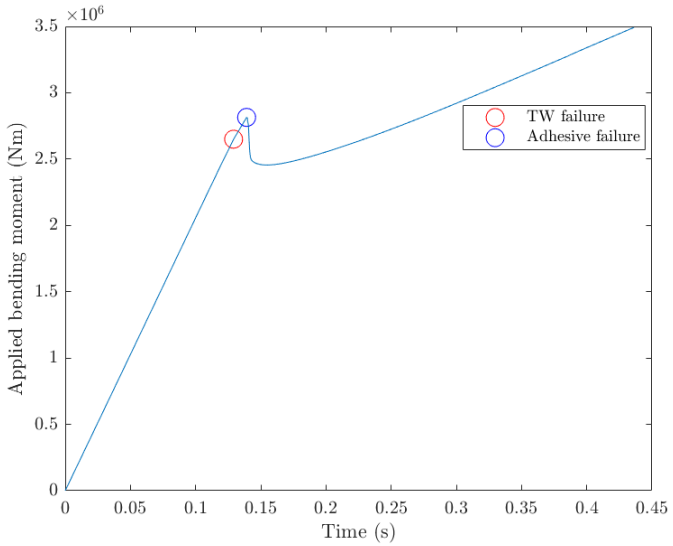

Figure 4.13: TW and adhesive failure criteria over the L2T 270° load direction for the intact blade.

is reached) is shown in figure 4.12b. It is appreciated that the upper part of the shear web is the one failing as it is where more carrying capacity is needed to bear the flapwise bending load. However, the critical buckling load considered for the study corresponds to the first failure, as first-ply criterion is considered. Moreover, according to the adhesive failure criterion in this case, the first failure in adhesive is produced over the upper part of one of the shear webs. The failure due to adhesive occurs later than the one given by the Tsai-Wu failure criterion, being the latter more restrictive for the study.

It is important to note that all failure criteria results are computed in Abaqus once the element sets that are located near the blade boundary conditions (shell elements) are removed, as mentioned in Chapter 2. Once these parts are arbitrarily removed, the results are taken as reliable.

In addition, the failure criteria are also studied for L2T loading direction and this can be seen in figure 4.13. The structural behaviour for this load case is detailed in figure 4.14 which shows different material failures according to the Tsai-Wu failure criterion. The first failure is produced before the first peak of the bending moment variation over the analysis, as seen in figure 4.13. Despite this first failure, the structure stiffness increases for a bit until the second failure is achieved at the peak of this graph, coinciding with the first failure encountered by the adhesive failure criterion. These first two failures occur at the same regions as the maximum deformations from the linear buckling analysis with the same loading direction. Finally, as both

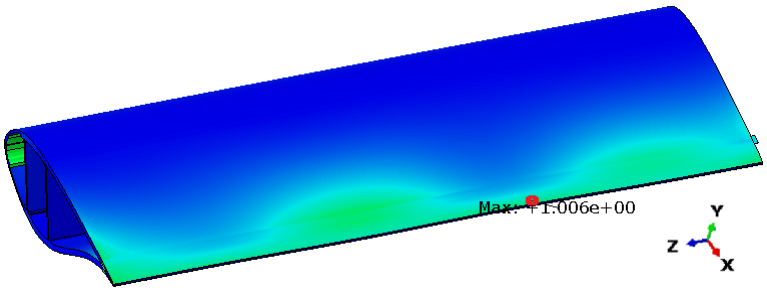

(a) First TW failure. Scaling factor=1.

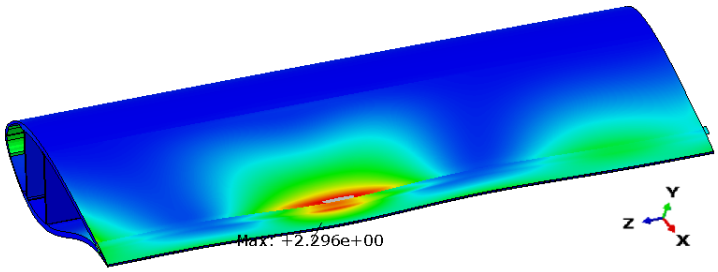

(b) Second TW failure. Scaling factor=1.

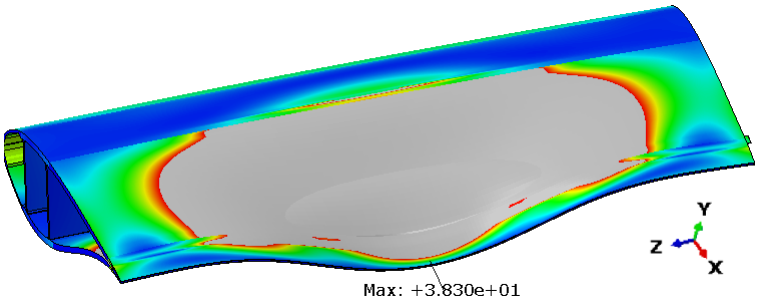

(c) Final TW failure. Scaling factor=1.

Figure 4.14: Comparison between different material failure locations over the blade section, considering the Tsai-Wu failure criterion. L2T 270° load direction for the intact blade.

failures enlarge, the final load before the simulation finishes shows the failure in the center of the blade section (figure 4.14c). Logically, the first failure due to adhesive is also proven to take place at the trailing edge. However, as seen in figure 4.13, the Tsai-Wu failure criterion is still more restrictive than the adhesive failure criterion in this case.

Finally, failure criteria are also applied to the 210° loading direction showed in the previous section. It can be seen in figure 4.15. The experienced behaviour is similar to the previous case, where the two initial failures due to the Tsai-Wu failure criterion are experienced in the trailing edge, finishing with a total failure in the middle region of the trailing edge element set. Similarly to the previous case,

first failure due to adhesive occurs later than the one found by the Tsai-Wu failure criterion, but in the same region (trailing edge).

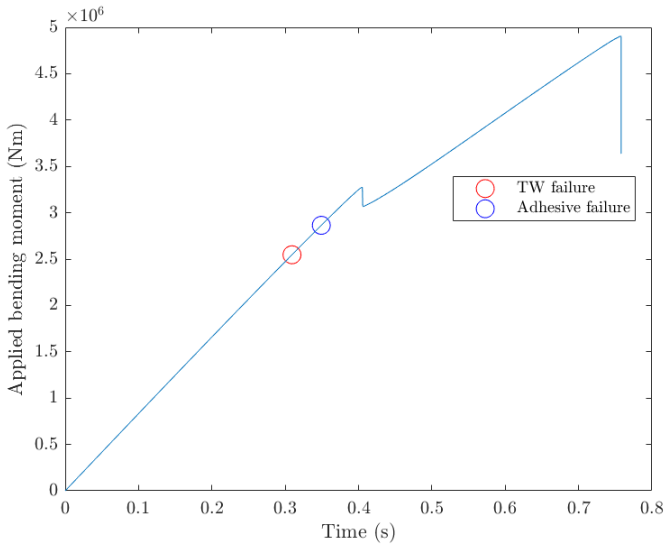

Figure 4.15: TW and adhesive failure criteria over the 210° load direction for the intact blade.

Once Tsai-Wu and adhesive failure criteria are evaluated over the intact blade structure, the results meeting the criteria are indicated in table 4.3. As mentioned before, critical loads due to material strength are lower than the critical loads due to nonlinear buckling.

According to the Tsai-Wu failure criterion, the ratio between the critical failure load and the design load shows that three cases do not satisfy the Standard requirements. This is a general outcome that is important to consider when analyzing the structure of the blade as it fails due to material failure in the first place. As seen from the nonlinear buckling study, even after material fails, the structure can still bear more load as nonlinear buckling analysis can overestimate the critical load carrying capacity. However, if the first-ply criterion is taken as a design path, the critical load from failure criteria should be highly decisive.

As stated in the adhesive failure criterion, two load directions are now the ones that do not satisfy the Standard: 30° and 330°. The Tsai-Wu failure criterion is proven again to be more restrictive than the adhesive failure criterion in the intact blade.

Study Case	Design load (Nm)	TW Load (Nm)	TW Ratio	Adh. Load (Nm)	Adh. Ratio
P2S 0°	2.39E+06	4.40E+06	1.840	4.06E+06	1.698
30	1.91E+06	1.50E+06	0.781	2.82E+06	1.472
60°	1.42E+06	2.38E+06	1.672	3.16E+06	2.220
T2L 90°	1.24E+06	3.03E+06	2.443	3.82E+06	3.072
120°	1.28E+06	2.86E+06	2.224	4.37E+06	3.403
150°	1.53E+06	2.75E+06	1.797	4.23E+06	2.767
S2P 180°	1.76E+06	4.31E+06	2.453	3.97E+06	2.255
210°	1.55E+06	2.55E+06	1.642	2.86E+06	1.847
240°	1.31E+06	2.39E+06	1.824	2.54E+06	1.935
L2T 270°	1.27E+06	2.65E+06	2.087	2.81E+06	2.217
300°	1.45E+06	2.72E+06	1.869	2.67E+06	1.840
330°	1.94E+06	2.60E+06	1.338	2.60E+06	1.338

Table 4.3: Tsai-Wu and adhesive failure criteria for each loading direction of the intact blade model. Loading ratios not satisfying the Standard requirements are shown in red.

4.4 Comparison between numerical studies

From the previous detailed procedures a final comparison between linear and non-linear buckling procedures can be seen in figure 4.16. Both studies are examined with regards to the compliance with the Standard.

Linear buckling analysis represents the first eigenvalue from each load direction as they are the more restrictive buckling ratio. Nonlinear buckling is illustrated in the same way as the linear buckling study: bending ratios are shown at the correspondent rotation angles θ from the P2S flapwise case (0°). This way, the Standard is satisfied when bending ratios are greater than the Standard reduction factor (outside of the red ellipse representing this factor). In addition, nonlinear buckling analysis is represented by the material failure criteria, as it has also been proven to be more restraining than the critical loads from the nonlinear buckling study.

The visual representation of the buckling analysis in figure 4.16 allows to prove that the intact blade is an acceptable design with regards to the current Standard, as both linear and nonlinear analyses satisfy the uncoupled flapwise and edgewise loading directions. However, both analyses also show that some combined loading directions are far from complying with the Standard. The extent at which some combined loading cases are not satisfying the Standard requirements is clearly shown. 30° and 300° are proven to have the worse buckling response, far behind from the aimed reduction factor, specially for nonlinear buckling.

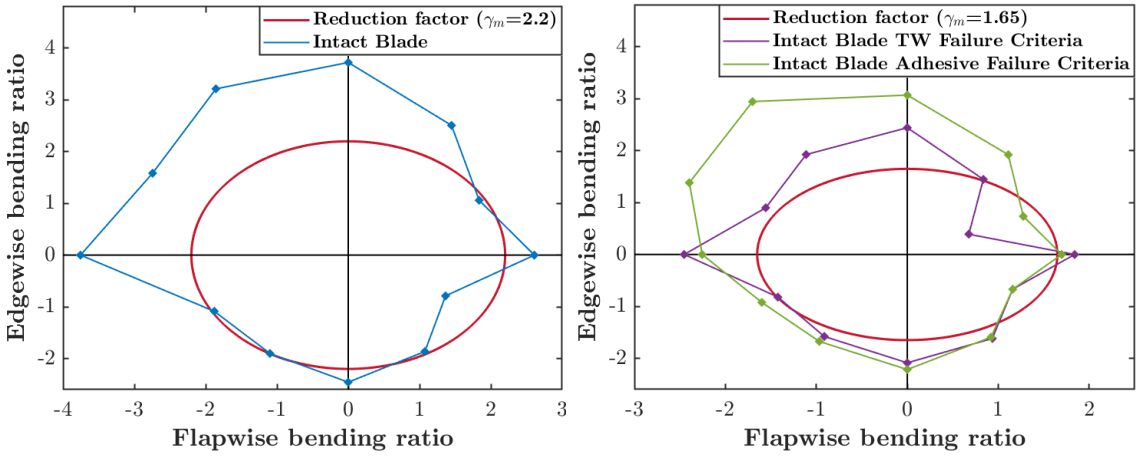

(a) Linear buckling (b) Nonlinear buckling

Figure 4.16: Linear and nonlinear buckling envelopes for the intact blade.

Furthermore, as appreciated in the figure, the Tsai-Wu failure criterion is found to be more restrictive than the adhesive failure criterion. In the majority of the loading directions the composites would fail before the load reaches the value given by the adhesive criterion. However, as it is also proven when analyzing the defects that some specific loading directions experience the opposite behaviour when the particular failure mode directly affects adhesive. For instance, in the intact blade, failure due to adhesive is clearly produced before failure due to Tsai-Wu failure criterion under both directions of pure flapwise loading. The main reason is that the maximum deformation from the external loads is directly produced over the spar caps, which are the main load carriers, as showed in figures 4.2 and 4.3. These regions have maximum distance from the NA so the adhesives in both edges experience great load which leads to its sooner failure.

CHAPTER 5

Analysis of defects

All base analyses schemes explained over the intact blade study are implemented now over the parametric study of defects. Selected cases of defects are studied and compared to the intact blade results from Chapter 4.

Linear buckling is analyzed with the first eigenvalues from each load direction, as done in the intact blade study. Nonlinear buckling compares the failure criteria of each defect case with the intact blade. For this comparison, Tsai-Wu and adhesive failure criterion have been gathered in one material failure criterion, where the most restrictive failure criteria is considered. In most cases, as seen in the intact blade study, Tsai-Wu failure criterion provides a lower critical load than that from adhesive failure criterion. However, the cases in which the opposite scenario is perceived are explained and detailed under this chapter.

5.1 Missing adhesive in the trailing edge

Several defect cases are examined in the trailing edge. As a first approach and understanding of the response, the defect case proposed in Chapter 3 is analyzed (TR1 defect case now). Later, other study cases are created for comparison. In total, three study cases are proposed and sketched in figure 5.1. The reason behind the decreasing size of the defect is explained through the analysis.

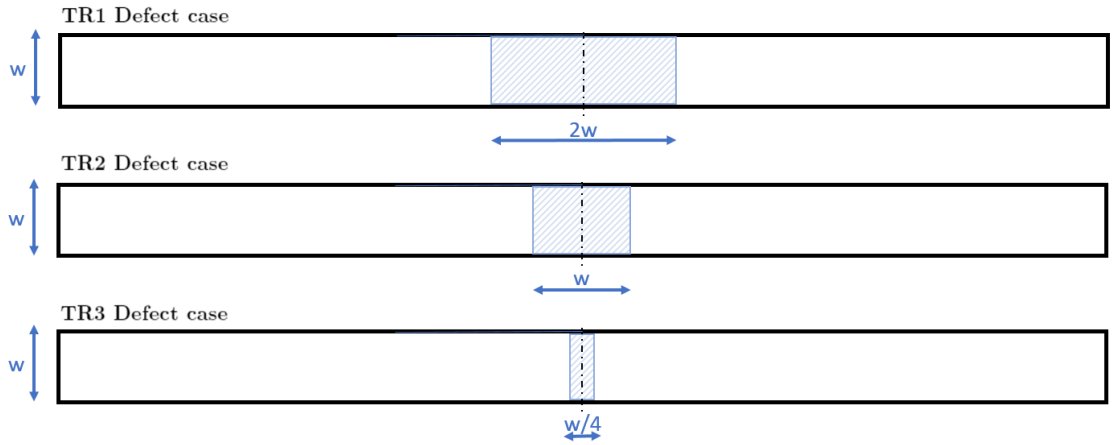

Figure 5.1: Sketch of trailing edge defect cases.

5.1.1 TR1 defect case

If linear buckling analysis is studied under this defect case, the obtained results can be compared to those of the intact blade, as shown in figure 5.2. The limit load directions at which the buckling response is the same for the intact blade and the defect case study are illustrated in green whereas, when there is mismatch between the buckling analyses, the limit cases are presented in red. This way, the loading directions between 30° and 180°, including these, have the same load carrying capacity as in the case of the intact blade. Nevertheless, the rest of the cases are extremely influenced by the defect and they are far from satisfying the Standard. Same procedure as in the intact blade is followed so the Standard is not satisfied by the bending ratios that are confined within the required reduction factor boundaries. Furthermore, the grey part of the represented cross sections illustrates the compression part for each load direction, with the same sign convention as in the intact blade analysis.

The buckling response between 30° and 180° directions is not influenced by the defect at the trailing edge defect as this does not lay on the compression side of the cross section on these loading directions. This can be appreciated in figure 5.2, where the defect (circled in red) lays on the white region which coincides with the tension side. However, loading directions between 210° and 0° allow the defect to be in the compression side, lowering the critical buckling load. The higher mismatch between the linear studies is due to the position of the defect with respect to the NA. If the defect is in a region with greater distance from the NA, the critical load is lower as the deformations around that part are high and blade performance is worsen.

Logically, the cases where the defect does not affect blade performance have the same linear buckling response as the intact blade, explained in the former section. On the contrary, the cases where the defects highly affect the performance swift their linear buckling response to the region where the defect exists. This can be appreciated in figure 5.3, where the linear buckling response for the P2S load case is originated over the region of missing adhesive. The rest of the cases encounter their first failure mode in the same shape and location where the defect is set.

The nonlinear buckling analysis (figure 5.4) shows a comparison between the material failure of the intact blade with that from the failure criteria applied to the TR1 defect case. The cross sections with the pure extreme loads are illustrated as well.

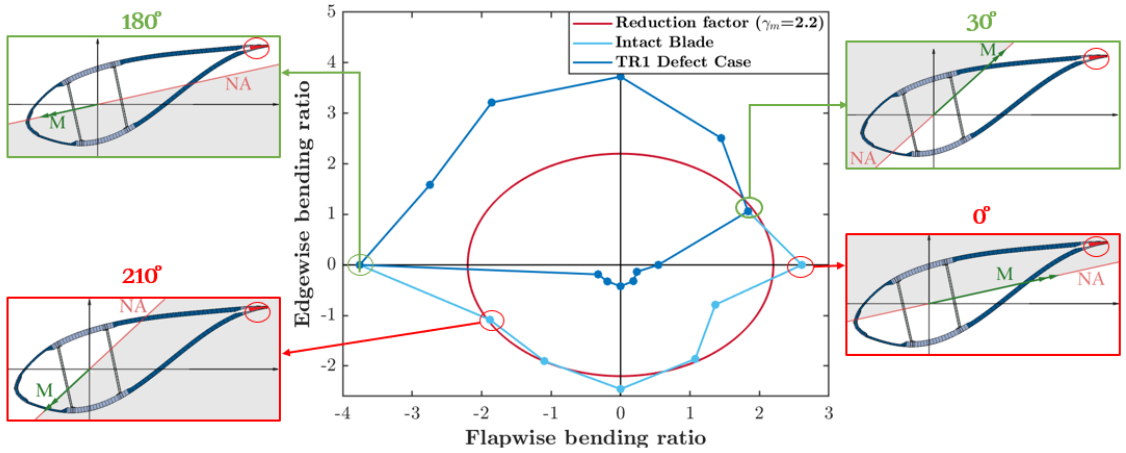

Figure 5.2: Linear buckling envelope comparing TR1 defect case with the intact blade. Specific load directions are illustrated over the blade cross section to clarify the mismatch between the intact blade and the defect buckling analyses. Grey colour under these cross sections indicate compression side and the defect is highlighted with a red circle.

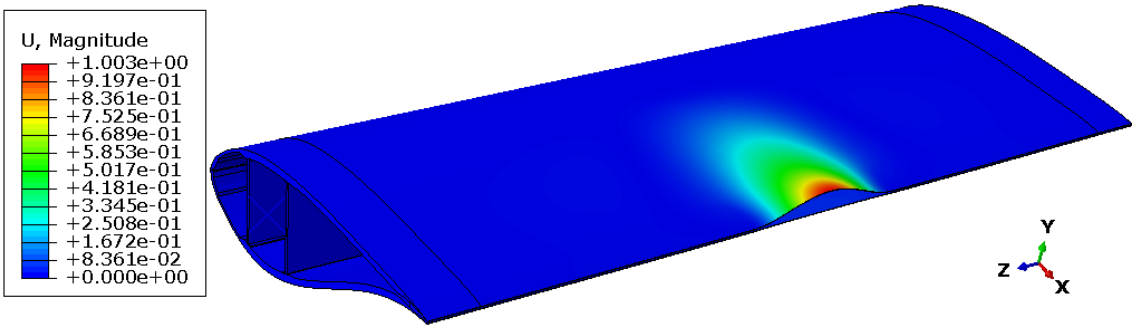

Figure 5.3: Linear buckling analysis of TR1 defect case with P2S 0° loading direction. First buckling mode is shown.

According to the nonlinear buckling analysis, the blade design with the defect does not satisfy the Standard in the same cases as in the linear analysis. This can be seen in figure 5.4 as the loading directions that do not meet the Standard requirements are inside the reduction factor boundaries. However, nonlinear buckling analysis presents one difference with respect to linear buckling analysis: the defect also reduces blade performance over the load in T2L 90° direction. Even though the critical buckling load under this direction still meets the Standard requests, performance is affected by having the defect in the tension side of the cross section. The reason behind this dissonance is that linear buckling analysis evaluates the lowest eigenvalue over the first buckling mode in each element/node of the blade, without evaluating the blade as a whole. Nevertheless, as the nonlinear buckling study is

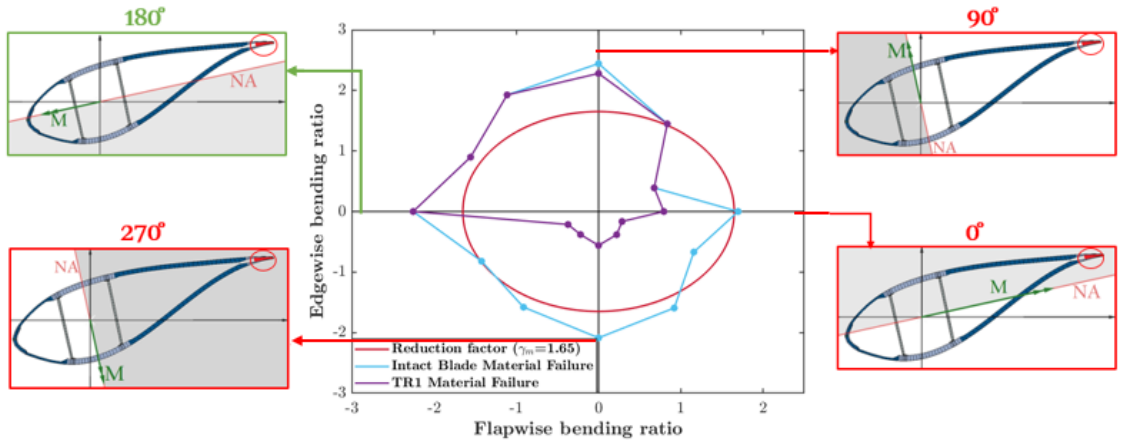

Figure 5.4: Nonlinear buckling envelope comparing TR1 defect case with the intact blade. Extreme load directions are illustrated over the blade cross section. Grey colour under these cross sections indicates compression side and the defect is highlighted with a red circle.

divided into increments, the outcome of the analysis contrasts all the blade elements. In this manner, it is reasonable to find that, the performance of the blade is affected by the presence of this defect in some directions, even if it is in the tension side. Furthermore, the reason why 90° is the only direction that has the defect in tension and slightly reduces performance is that this is the loading direction with the longest distance from the defect to the NA. This way, despite the defect lies on the tension side, the buckling capacity of the whole blade section is diminished.

In this defect case, Tsai-Wu is the most restrictive failure criterion in all loading directions from 30° to 180°, counterclockwise. However, under the loading directions where the defect experiences compression, the adhesive failure criterion is slightly more restrictive than the Tsai-Wu failure criterion. This is due to the fact that this type of defect highly affects blade performance and its size is considerable. In addition, most of these loading directions encounter their higher deformations on the trailing edge in the intact blade analysis. Consequently, an adhesive defect in the same region leads to a sooner failure in this adhesive region.

Figures 5.5 to 5.7 exhibit the final deformation of the blade section when 100% of the design load is applied (last increment of the nonlinear buckling analysis) for three of the extreme loads. In addition, the first failure encountered by the Tsai-Wu failure criterion is illustrated.

When P2S 0° loading direction is applied, the first failure is found by the adhesive failure criterion over the trailing edge. Figure 5.5a shows the first composite failure

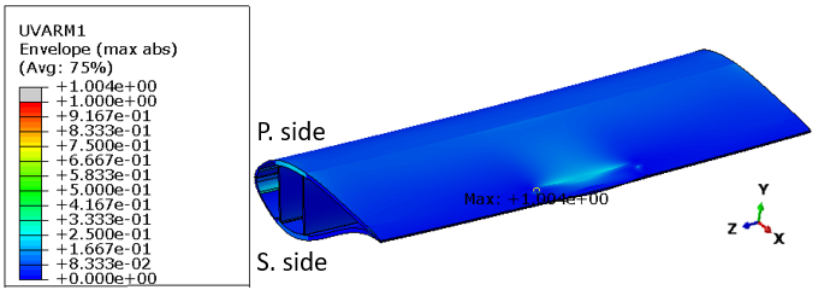

(a) First failure from TW failure criterion over blade section. Scaling factor=1.

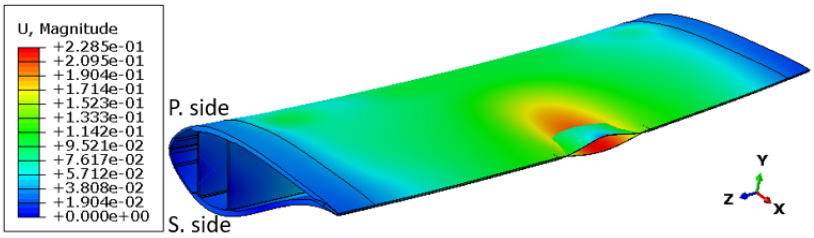

(b) Blade deformation when 100% of the design load is applied. Scaling factor=0.7.

Figure 5.5: Final blade deformation and first failure under the TW failure criterion over the nonlinear analysis of P2S 0° loading direction for TR1 defect case. Pressure (P.) and suction (S.) side indicated in the figures.

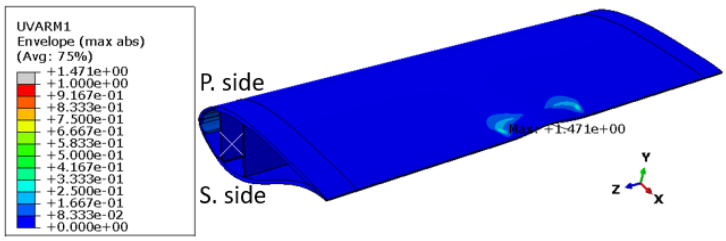

(a) First failure from TW failure criterion over blade section. Scaling factor=1.

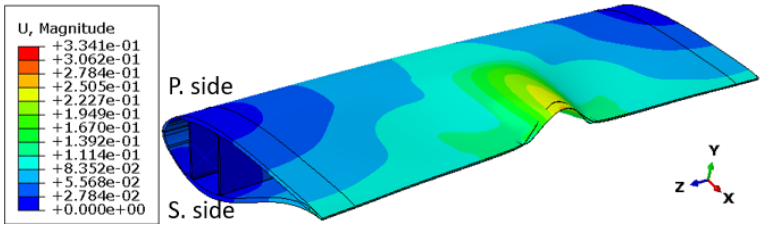

(b) Blade deformation when 100% of the design load is applied. Scaling factor=1.

Figure 5.6: Final blade deformation and first failure under the TW failure criterion over the nonlinear analysis of L2T 270° loading direction for TR1 defect case. Pressure (P.) and suction (S.) side indicated in the figures.

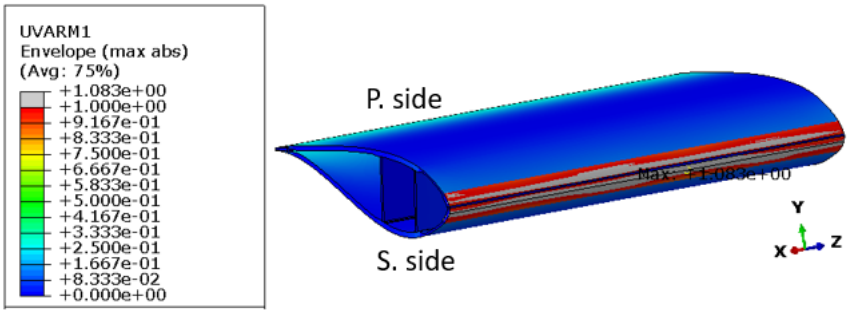

(a) First failure from TW failure criterion over blade section. Scaling factor=1.

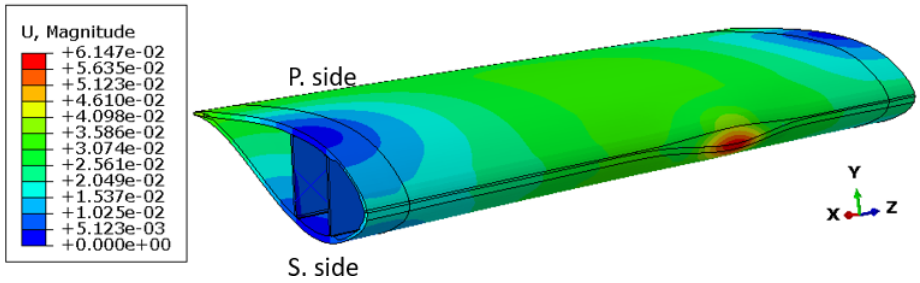

(b) Blade deformation when 100% of the design load is applied. Scaling factor=1.

Figure 5.7: Final blade deformation and first failure under the TW failure criterion over the nonlinear analysis of T2L 90° loading direction for TR1 defect case. Pressure (P.) and suction (S.) side indicated in the figures.

when the Tsai-Wu failure criterion is considered. When the adhesive first fails it can no longer transmit the load to the shear webs and so, the part of the shear web that is closer to that failing adhesive is the one that fails next. As this failure increases with increasing load, the blade encounters maximum deformation at the area of the trailing edge where the defect takes place, as presented in figure 5.5b. Due to the lack of contact restrictions between the blade model plies, the final deformation provokes the penetration of the upper and lower part of the trailing edge. Even though this phenomena is not realistic, it does not affect the final results of this case as it is clearly shown that the defect affects the trailing edge region and first-ply failure criterion is taken for the material failure study.

Other interesting loading points are the pure edgewise load directions, which suffer an extreme decrease in blade performance. As expected, L2T 270° direction (figure 5.6b) shows its maximum deformation around the area of the defect as this is under compression for this load. Reasonably, as in the P2S 0° load, the first failure also occurs slightly before in the adhesive than in the composite material. However,

as the defect is now at maximum distance from the NA and the trailing edge is bearing the major load, the first failure of composites is produced in the center of the blade section, where the defect is located. T2L 90° loading direction encounters higher deformation at the leading edge, as shown in figure 5.7b. As the defect is in tension for this loading direction, despite having an appreciable distance from the NA to the defect, the behaviour towards failure resembles the intact blade. However, due to the lack of carrying load lost by the defect, this failure occurs before it would happen for the intact blade.

It is clearly seen that this first proposed defect leads to a complete failure of blade performance when the defect is under compression. The defect size is reduced in the next study case in order to show the variations over these results.

5.1.2 TR2 defect case

In this second case the previous defect is diminished to half of its length (0.5m). Both linear and nonlinear buckling studies can be seen in figure 5.8.

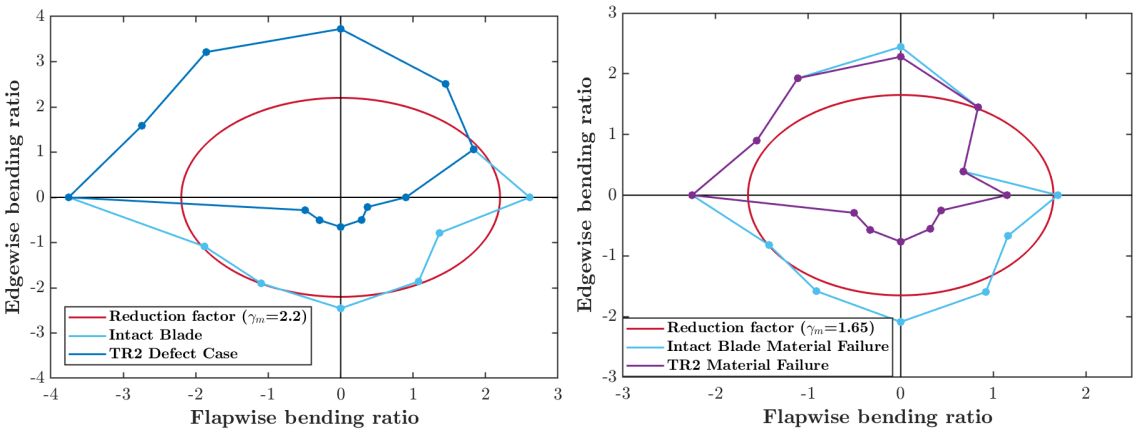

(a) Linear buckling (b) Nonlinear buckling

Figure 5.8: Buckling envelope comparing TR2 defect case with the intact blade.

The linear analysis presents a similar response to that of the previous case. The loading directions having the defect in the tension side are not affected by it as the defect is smaller now. The same way, the critical buckling loads are now higher as the load carrying capacity increases with a smaller defect. Even if the defect is reduced, the load in the affected directions is still very low compared to the Standard requirements.

Furthermore, the nonlinear buckling study also shows a slightly better response from that of the previous case. As in the linear case, the critical loads are now higher with the decrease of the defect. In addition, the blade continues to fail the Standard requirements in the loading directions where the defect encounters compression. In addition, the adhesive failure criterion takes the same critical load as the Tsai-Wu failure criterion in these loading directions, meaning that both composite and adhesive would bear the same critical load at which the structure would fail. The Tsai-Wu failure criterion dominates material failure over the rest of the load directions.

5.1.3 TR3 defect case

As a last analysis of the structural response of this type of defect, the length of the defect is reduced to $w/4 = 12.5$cm. The linear and nonlinear buckling envelopes are exhibited in figure 5.9.

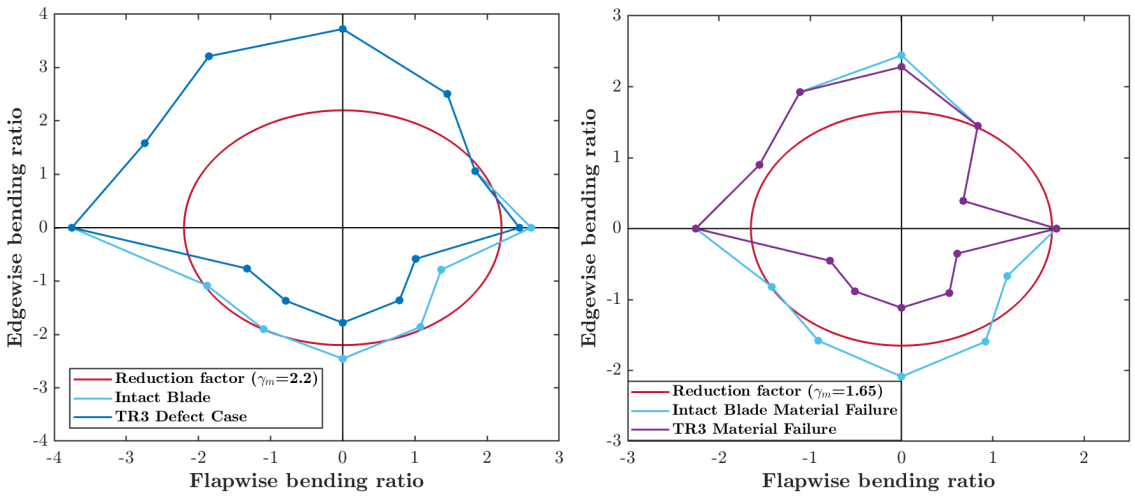

(a) Linear buckling (b) Nonlinear buckling

Figure 5.9: Buckling envelope comparing TR3 defect case with the intact blade.

The structural response is very similar to that of the previous defect case as the blade would still fail under the loading directions where the defect experiences compression. However, this scenario allows flapwise P2S extreme loading direction to satisfy the Standard requirements in both linear and nonlinear buckling analyses. Furthermore, despite the reduction of the defect size, T2L 90° is still affected by the defect location.

Even though this type of defect is very small, the blade performance is unacceptable as the loading directions with the defect under compression have critical bending ratios lower than 1, failing to comply by far with the requirements of the Standard (higher than 1.65).

5.2 Missing adhesive between spar caps and shear webs

The missing adhesive defects between spar caps and shear webs can take place at any of the upper or lower contacts of the shear webs. Nevertheless, in order to reduce the variety of possibilities, the adhesive that is studied for potential defects is the one marked on figure 5.10. As the blade section is quite symmetric, there would not be much dissonance between the effect of a defect in the upper or lower part of the same shear web. This way, the adhesive in the upper side of the right shear web (UR in figure) is taken arbitrarily and the one in the lower part of the left shear web (LL) is chosen to investigate the change on results. In addition, it is interesting to analyze the defects over LL shear web as it is closer to the leading edge.

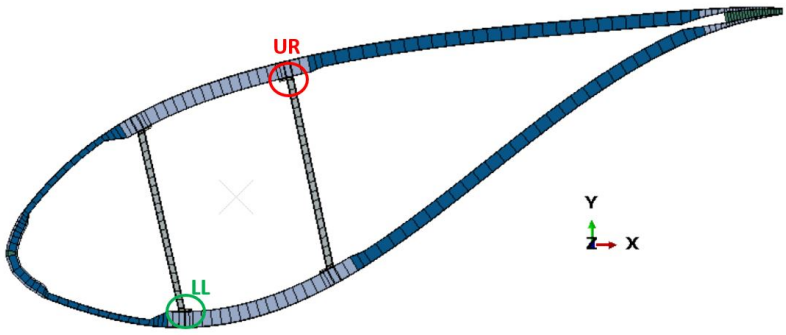

Figure 5.10: Location of upper-right (UR) and lower-left (LL) adhesive between shear webs and spar caps in blade model.

For both UR and LL adhesive in shear webs, two defect cases are considered starting from the one proposed in Chapter 3. These defect cases are illustrated in figure 5.11 and their sizes are common for both UR and LL adhesives. Consequently, four defect cases are considered in total under this section: SW1 and SW2 for the missing adhesive in the UR shear web and SW3 and SW4 for the missing adhesive in the LL shear web.

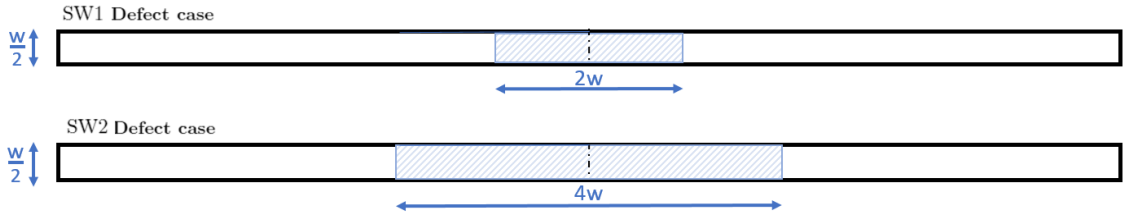

Figure 5.11: Sketch of missing adhesive between spar caps and shear webs defects for UR shear web. SW3 and SW4 LL missing adhesive defects share the same size with SW1 and SW2, respectively.

5.2.1 SW1 defect case

The linear buckling analysis of this defect case differs from the one of the intact blade in two loading directions, 0° and 30°, as shown in figure 5.12. The 60° cross section is coloured in green as the defect is present in the tension side of the NA; therefore, it is not affected by the linear buckling study. 240° is shown to be the direction at which the defect first starts to be in the compression side of the NA. Consequently, 240° and 30° loading directions are the load limits at which the defect is under compression.

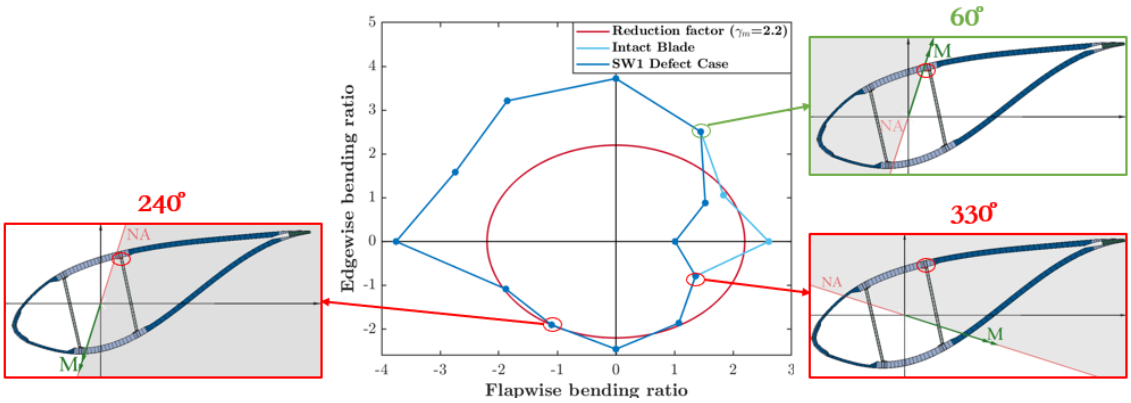

Figure 5.12: Linear buckling envelope comparing SW1 defect case with the intact blade. Specific load directions are illustrated over the blade cross section to clarify the mismatch between the intact blade and the defect buckling analyses. Grey colour under these cross sections indicates compression side and the defect is highlighted with a red circle.

The buckling ratios of the intact blade and the defect seem to be different only at 0° and 30° loading directions. The reason is that the loading directions from 240° to 300° are very close to pure edgewise movement. This way, the higher deformations are experienced in the trailing edge as it is much further from the NA than the area where the defect is located. In addition, as the major bending load is carried by

the trailing edge, the box girder is carrying less load capacity. Therefore, the defect on the shear web is not bearing as much load on those directions. 330° direction is slightly influenced as more box girder surface is under compression; despite this, the maximum deformation is still held under the trailing edge, leading to a low effect of the defect over blade performance.

P2S flapwise extreme loading presents the highest decrease on its critical buckling load, failing to comply with the Standard. The first buckling mode from the linear analysis can be seen in figure 5.13. As the upper box girder bears flapwise bending, it is reasonable that a defect in one of its shear webs creates a buckle in the spar cap where the defect takes place. 30° loading case diminishes blade performance as the upper part of the box girder is lowering the bending load at the further region from NA which is closer to leading edge. Therefore, it is reasonable that this load direction is also affected by the imposed defect.

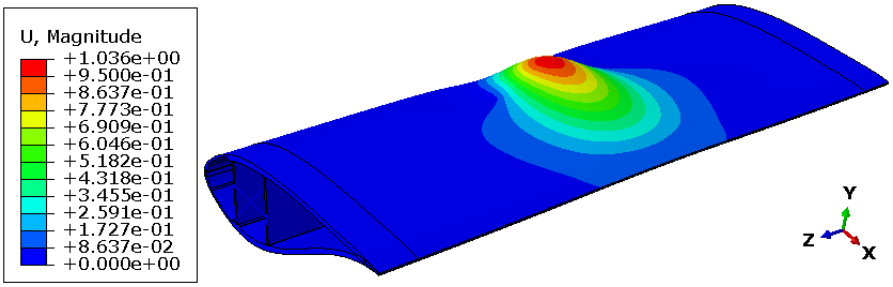

Figure 5.13: First buckling mode of the linear analysis on the blade section with SW1 defect case. Flapwise P2S 0° loading direction is applied. Scaling factor=0.12.

Nonlinear buckling analysis is shown in figure 5.14 and, as demonstrated by the trailing edge defect cases, this deviates from the linear buckling analysis. Firstly, the structure mismatches the intact blade failure criteria in one different loading direction from the ones stated before. This direction is 180°, meaning that this type of defect has an influence on both types of pure flapwise movements.

Once more, the Tsai-Wu failure criterion is dominating over the adhesive failure criterion. However, the adhesive failure criterion is slightly more restrictive under the P2S 0° loading case, as this is the direction where the defect mostly affects blade performance. The decrease in loading capacity is mainly due to the missing adhesive defect (in compression) and the fact that it is at almost maximum distance from the NA.

Even though the defect is under tension with S2P 180° loading direction, its first failure is produced over the defect region. In fact, as the applied load gets higher,

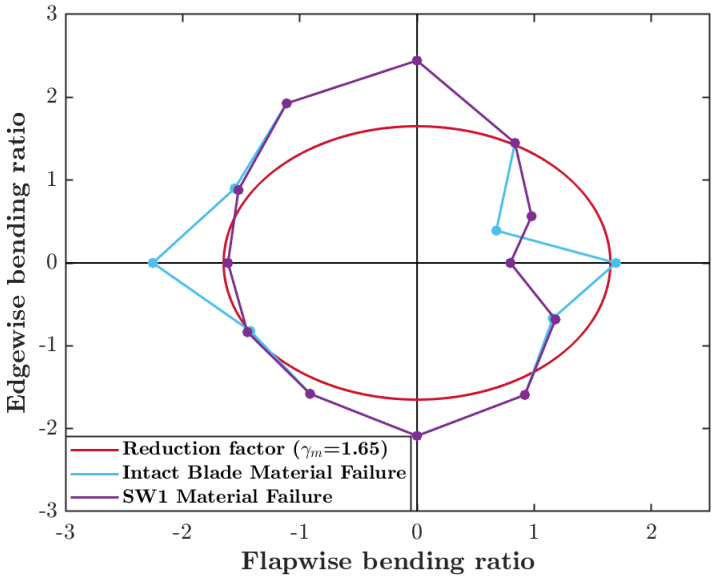

Figure 5.14: Nonlinear buckling envelope comparing SW1 defect case with the intact blade.

the failure increases over the defect region. Not until the load prior to final failure is reached, the failure is produced under the lower part of the box girder where compression is held. As a consequence, this type of defect has a great influence on this loading direction as even in the tension side of its NA, the defect affects the overall response of the structure. The behaviour of both flapwise directions on the blade model is more detailed under the next type of defect, as it is bigger and its effects are larger.

The 30° loading direction is a special case for this study. As it can be seen in figure 5.14, the results show that the blade would perform better with the presence of this defect than without it (intact blade).

Different failure points are shown in figure 5.15 to visualize the structural response of this load direction. The first failure of this loading direction is found by the Tsai-Wu failure criterion in the upper part of the leading edge, coinciding with the first failure on the intact blade, as seen in figure 5.15a. However, even though the first failure takes place at the same region as in the intact blade, it is produced later than this one. As the load is incremented, the failure through the leading edge (grey elements in the figure) spreads all over the leading edge. Later on, the first failure found by the adhesive failure criterion is produced on the UR shear web, where the defect is located. Finally, shortly after this failure, the composite failure over the leading edge turns to be higher over the defect region, where the adhesive

has failed. This failure point can be seen in figure 5.15b. Therefore, as the load continues increasing until the last increment, the failure continues spreading over the defect region, causing a final deformation as the one illustrated in figure 5.16.

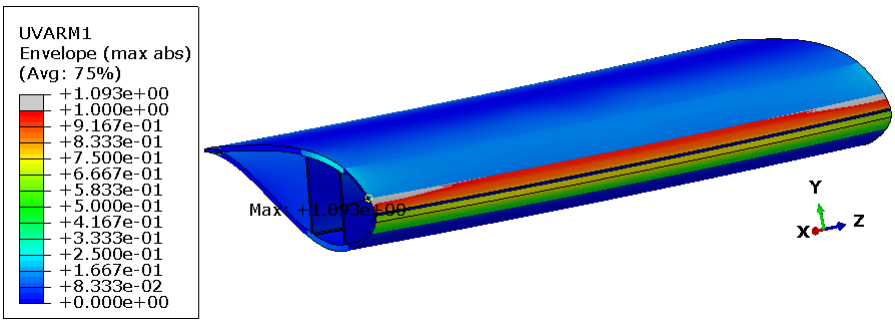

(a) First failure in the leading edge area. Grey areas spread over the leading edge when the first failure increases.

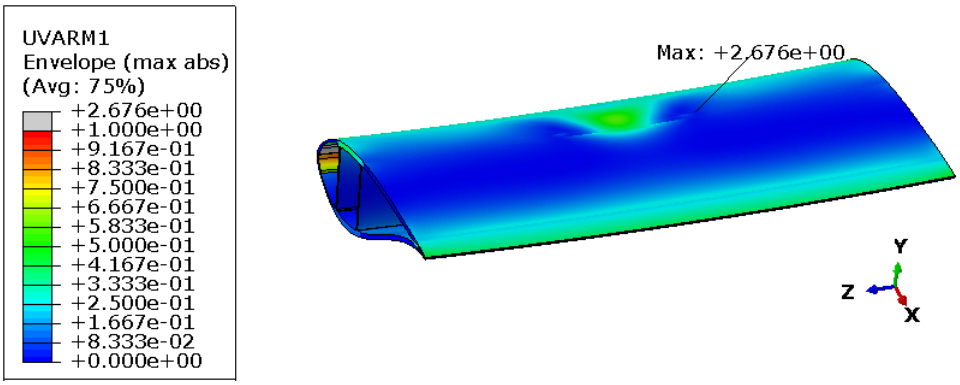

(b) First failure over the defect region

Figure 5.15: The Tsai-Wu failure criterion applied at different increments of the 30° loading direction to the blade section with SW1 type of defect.

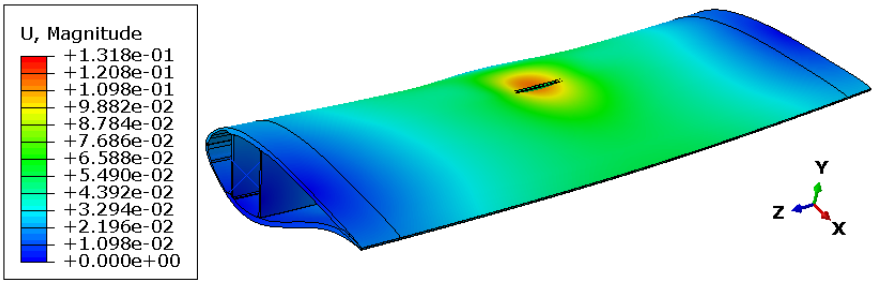

Figure 5.16: Final deformation when 100% of the design load is applied to the blade section with 30° loading direction and SW1 defect case.

The justification towards the results under this load directions must be related to the characteristics and assumptions of the studied blade model. In addition, a similar behaviour is also observed in an extra type of defect that was investigated

on this project: debonding in the blade aft panels. The defect design and implementation together with the results is exhibited in Appendix A. However, the project duration has not been long enough to trigger the reason of these results. Thus, further research is needed to examine these special cases.

5.2.2 SW2 defect case

This case enlarges the length of the previous defect so a bigger failure is analyzed, specially to check the consequences over the loading directions in compression at a greater failure situation. Both linear and nonlinear buckling analyses are shown in figure 5.17. The linear analysis is very similar to the one of the previous case but, as expected, critical loads are now smaller as the defect is increased. 330° loading direction shows a higher change with respect to the previous case. Even though the loading directions from 240° to 300° do not seem to differentiate the buckling behaviour from the intact blade to the defects, these loads are slightly lower on the defect case as a matter of having the defect under compression.

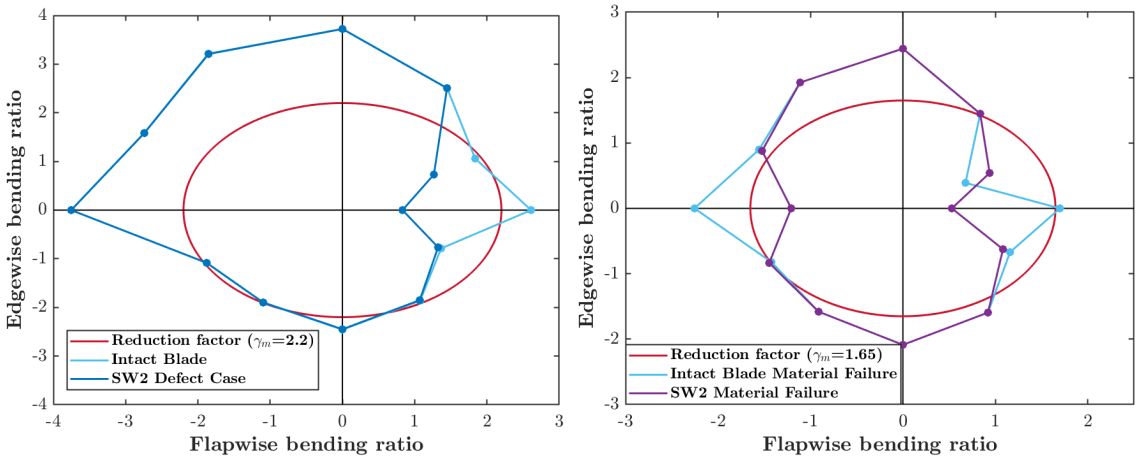

(a) Linear buckling (b) Nonlinear buckling

Figure 5.17: Buckling envelope comparing SW2 defect case with the intact blade.

A similar effect in loads is experienced in the nonlinear buckling analysis compared to the previous case. 30° loading case continues to be incoherent although the critical load has decreased from the previous case. The adhesive failure criterion is now a bit more restrictive than in the previous case, as more adhesive is missing. In fact, the adhesive failure criterion is closer to the Tsai-Wu failure criterion in the loading directions where the defect is under compression.

Moreover, it is remarkable that the S2P 180° extreme loading ratio decreases much more with respect to the previous case, showing that the extreme loads are indeed likely to be affected by performance losses, even when the defect is in tension. The mechanical behaviour under P2S an S2P loading directions is extended next.

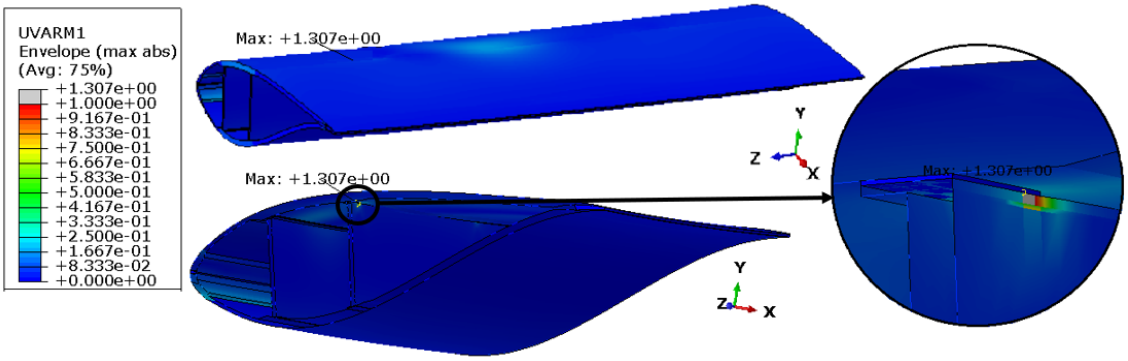

Figure 5.18: First failure from the Tsai-Wu failure criterion for the P2S 0° loading direction of SW2 defect case. Figure on top shows the complete blade section and the lower figure is a cut of the former image in order to locate the failure, which is enlarged for better visualization. Scaling factor=1.

As mentioned before, when P2S 0° loading direction is applied, the first material failure takes place over the adhesive. The first failure in adhesive is produced near to the defect, as it has to transmit more load between spar cap and shear web. After this first failure, the blade section encounters its next failure over the composite material just on top of the failing adhesive. This second failure is actually the first failure from the Tsai-Wu failure criterion and it is shown in figure 5.18. This figure shows the location of the failure on the blade model as well as a section of this to visualize the failure position. It can be appreciated that the failing point belongs to the shear web right underneath the first failure in adhesive as, once the adhesive first fails, the load carrying capacity can not be transmitted from spar cap to shear web. When the load is incremented, the failure increases until the right shear web collapses. Afterwards, the failure starts to be held over the upper-left shear web as it is the main load carrier when the right shear web can not bear any more load. The final deformation when 100% of the design load is applied can be appreciated in figure 5.19a. It is reasonable that the maximum deformation is held in the middle of the blade section as it is where the adhesive is missing.

S2P loading direction encounters a very similar behaviour as in the previous load direction. Even though the defect is under tension now, it highly affects blade performance as explained in the previous defect type. Its first failure is found by the

Tsai-Wu failure criterion close to the missing adhesive defect. Similarly, adhesive fails later on. After the shear web completely fails, the failure moves towards the lower shear webs of the blade model (in compression). This is the reason why the final failure is produced in the same place as the intact blade as seen in figure 5.19b.

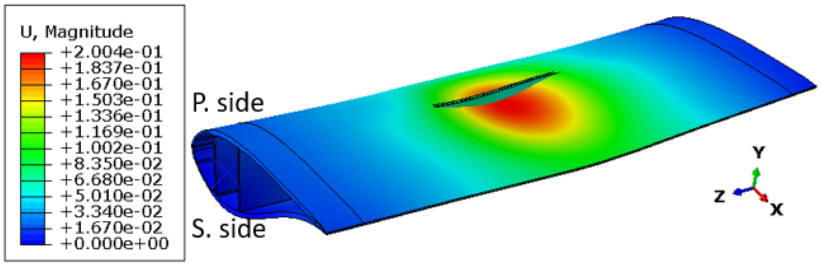

(a) P2S 0° loading direction

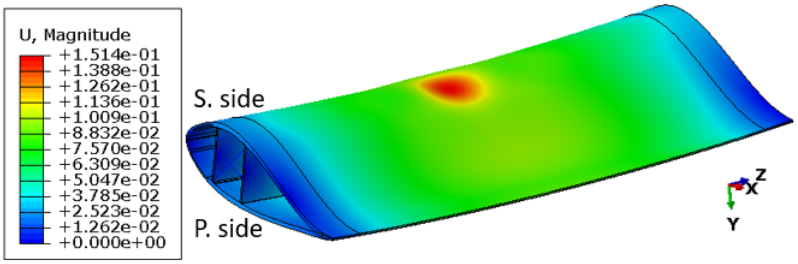

(b) S2P 180° loading direction

Figure 5.19: Final deformation when 100% of the design load is applied at 0° and 180° loading directions with SW2 type of defect. Pressure (P.) and suction (S.) side indicated in the figures. Scaling factor=1.

Consequently, it is seen that first-ply failure reports the same location and type of failure when the defect is under both tension (S2P) and compression (P2S). However, the final failure is proven to be different as well as the critical load magnitude. All in all, as expected, the critical failure worsens when the defect is under compression.

At 30° loading direction, it can be seen a similar behaviour as that of the previous case (figure 5.17b). In this case, the first failure is still produced at the leading edge (same region as in intact blade) but, only after short time, there is a second local failure where the defect is located. This way, it is shown that the direction of the load is still causing the first failure as if the defect did not exist but, as this defect gets bigger, the failure takes place in its location.

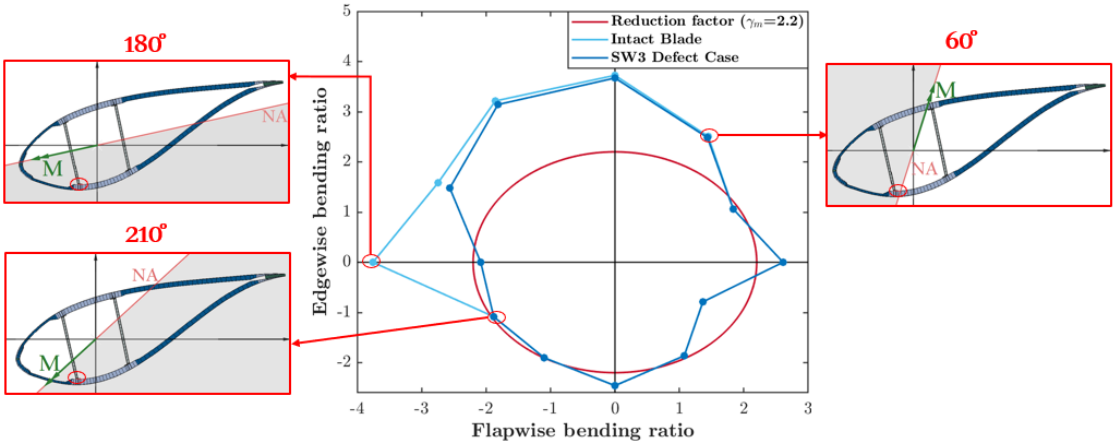

Figure 5.20: Linear buckling envelope comparing SW3 defect case with the intact blade. Specific load directions are illustrated over the blade cross section to clarify the mismatch between the intact blade and the defect buckling analyses. Grey colour under these cross sections indicates compression side and the defect is highlighted with a red circle.

5.2.3 SW3 defect case

Examining now the first case of defects in the LL adhesive of the box girder, the linear buckling analysis is represented in figure 5.20. As seen, 60° and 210° loading directions are the load limits at which the defect is under compression. Therefore, from 60° to 210° counterclockwise, the defect affects the performance of the blade and the critical load in these directions.

The 60° cross section presented in figure 5.20 shows that the defect lays very close to the NA in the compression area. Due to this short distance, it is reasonable that buckling is not affected much by the defect, encountering maximum deformations in the leading edge area as presented in the intact blade. The following directions (from 90° to 150°) gradually decrease their critical buckling load from the intact blade analysis as the defect increases the distance to the NA. However, the first buckling mode is produced in the same way as the intact blade for both 90° and 120°, whereas at 150° the first buckling mode is affected by the location of the defect. The variance in the first buckling load for 150° can be perceived in figure 5.21 where, apart from the buckles near the leading edge encountered in the intact blade analysis, there is also an influence of the defect.

Once pure S2P 180° loading is experienced, the defect is almost at maximum distance from the NA and the box girder bears maximum deformations. Under this direction the defect highly decreases the critical buckling load, failing to comply with

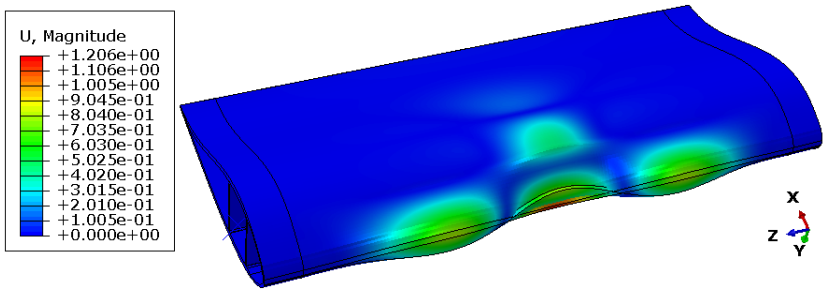

Figure 5.21: First buckling mode of the linear analysis on the blade section with SW3 defect case. 150° loading direction is applied. Scaling factor=0.12.

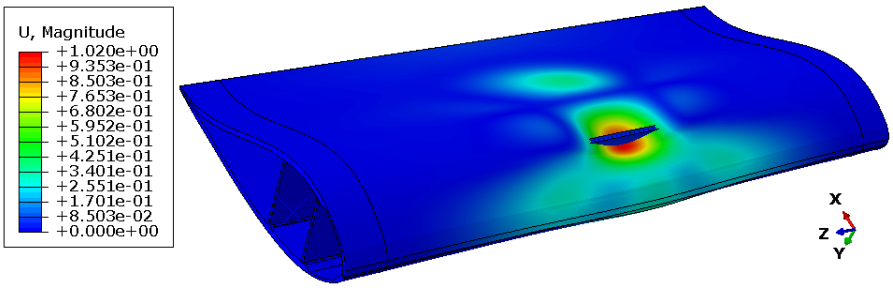

Figure 5.22: First buckling mode of the linear analysis on the blade section with SW3 defect case. Edgewise S2P 180° loading is applied. Scaling factor=0.12.

the Standard. The first buckling mode of the analysis is shown in figure 5.22 where it can be seen that the major deformation occurs where the defect is implemented. Finally, at 210° loading direction, the higher buckling is experienced at the trailing edge as the defect is very close to the NA. As a consequence, under this direction, the blade performance is also similar to that of the intact blade.

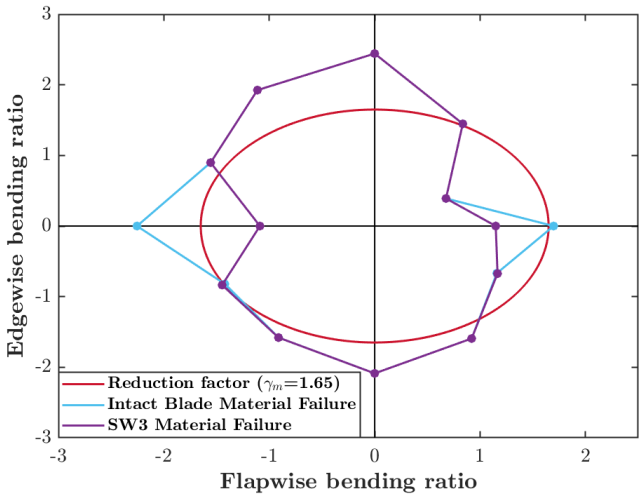

Figure 5.23: Nonlinear buckling envelope comparing SW3 defect case with the intact blade.

The nonlinear study of this type of defect is shown in figure 5.23. The greatest difference from the intact blade is that the flapwise movement of the blade (both S2P 180° and P2S 0° loading directions) fails to comply with the Standard. As in the previous defect cases, even though the P2S loading direction experiences the defect under tension, this is at maximum distance from the NA and it affects the overall performance of the blade. The manner at which the blade fails is examined under the next type of defect, as this is bigger and consequences are clearer.

In addition, the Tsai-Wu failure criterion is more restrictive than the adhesive failure criterion in all cases but in the S2P flapwise bending direction. This is reasonable as it is the direction at which the blade performance is decreased the most. In addition, under this direction, the region with the missing adhesive defect is in compression at a great distance from NA, experiencing higher buckling.

5.2.4 SW4 defect case

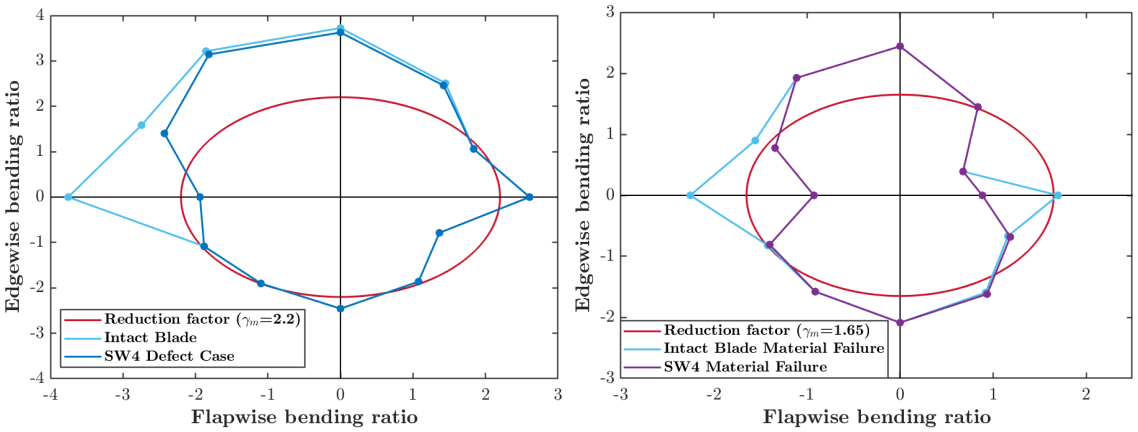

(a) Linear buckling (b) Nonlinear buckling

Figure 5.24: Buckling envelope comparing SW4 defect case with the intact blade.

The buckling envelope for the second case of defect in the LL adhesive of the box girder is presented in figure 5.24. The linear analysis shows a very similar behaviour to that of the previous design case. As one would expect, the loading envelope between the intact blade and the defect maintains the same tendency or shape but, as the defect is greater in this case, the critical loads are more restrictive than those of the former case. It is a bit clearer now the influence of the defect over the loading directions that allow the defect to be in compression.

The nonlinear buckling analysis also shows a similar behaviour to the previous case. Under this defect case, not only flapwise bending movement leads to the unsatisfactory compliance of the Standard but also the 150° loading direction. A comparison between these three failing points is studied next.

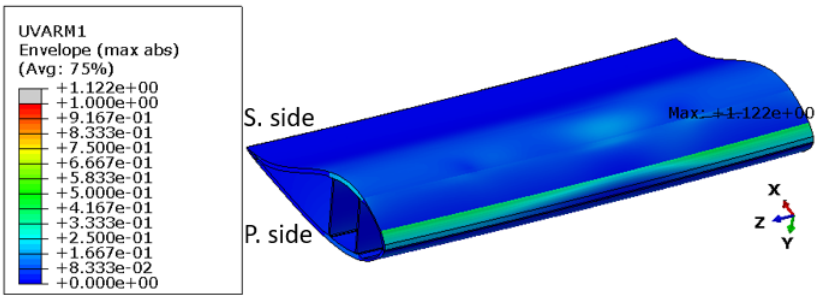

(a) First failure from TW failure criterion over blade section.

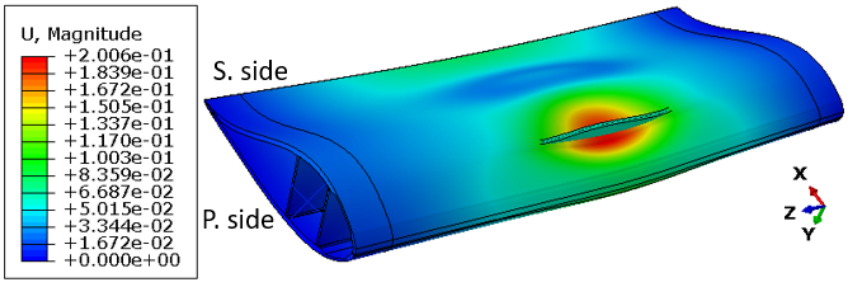

(b) Blade deformation when 100% of the design load is applied.

Figure 5.25: Final blade deformation and first failure under TW failure criterion over the nonlinear analysis of S2P 180° loading direction for SW4 defect case. Pressure (P.) and suction (S.) side indicated in the figures. Scaling factor=1.

The adhesive failure criterion is more restrictive than the Tsai-Wu criterion in 180° and 150° loading directions. Both loading directions encounter first failure applying adhesive failure criterion over the defect region. The first failure according to the Tsai-Wu failure criterion is also found over the defect region for S2P 180° loading direction. In fact, this failure occurs in the node of composite material that is just colliding with the correspondent adhesive node that fails first in the model. Adhesive transmits the carrying capacity from the spar caps to the shear webs. Therefore, it is reasonable that, if the adhesive fails, the immediate composite next to the failure is affected.

A different behaviour is found in the 150° loading direction. It encounters its first failure from the Tsai-Wu failure criterion in the leading edge, as experienced in the intact blade, as a matter of having the defect closer to the NA than in the 180° load direction. However, the location of this first composite failure is different

with respect to the intact blade. It occurs in the region of the leading edge that has shorter distance to the first failure due to adhesive in the defect area. The shift of the first composite failure from the center of the blade section (intact blade) to the failure point shown in figure 5.26a is due to the presence of the defect. Once the first failure due to adhesive is produced, the nearest region in the leading edge carries the load. Then, shortly after this first composite failure, the second failure takes place in the LL shear web adhesive where the defect takes place. Actually, this is produced in a composite region close to the first adhesive failure. This case is an example that shows that after considering first-ply failure, the internal stresses can be redistributed and lead to a second failure in other region of the blade. However, in this case the blade section would not meet the Standard requirements due to adhesive failure.

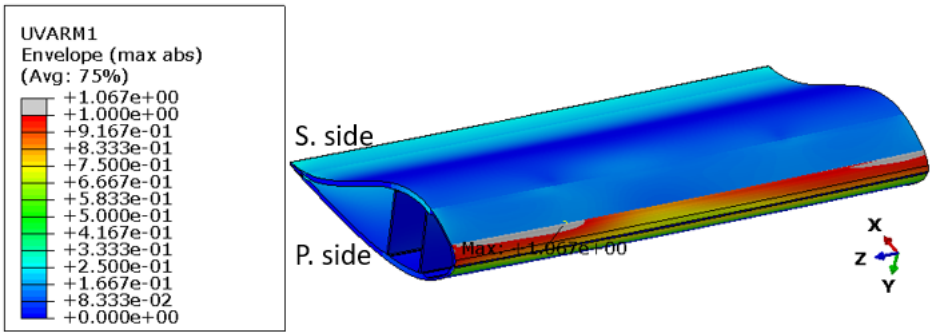

(a) First failure from TW failure criterion over blade section.

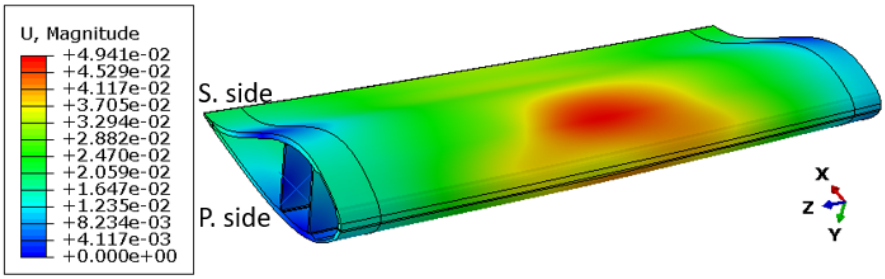

(b) Blade deformation when 100% of the design load is applied.

Figure 5.26: Final blade deformation and first failure under TW failure criterion over the nonlinear analysis of 150° loading direction for SW4 defect case. Pressure (P.) and suction (S.) side indicated in the figures. Scaling factor=1.

Final deformations when 100% of the design load is applied can be seen in figures 5.25b and 5.26b for S2P 180° and 150° loading directions, respectively. It is appreciated how in both scenarios, the maximum deformation is experienced over the defect region. As the defect is under the compression side for both load

directions, it is reasonable to observe the final failure where the defect takes place as well as to have a bigger deformation under the S2P load as it increases the distance between defect and NA.

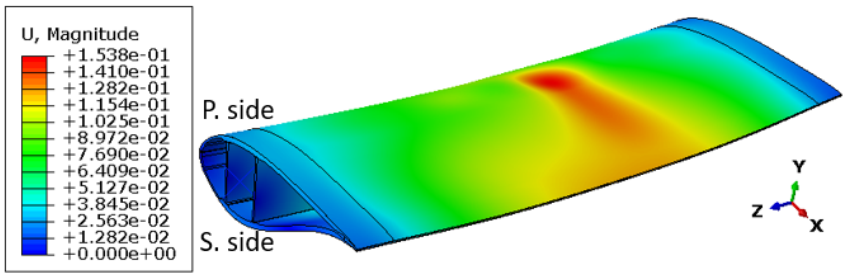

Figure 5.27: Blade deformation when 100% of the design load is applied the non-linear analysis of P2S 0° loading direction for SW4 defect case. Pressure (P.) and suction (S.) side are indicated. Scaling factor=1.

The material failure for flapwise P2S loading direction is firstly determined by the Tsai-Wu failure criterion as it is dominating over the adhesive failure criterion. In this case, despite encountering the defect on the tension side, the first failure takes place at the same location as the defect, similarly to previous defect cases. Nevertheless, after several increments, the failure moves towards the upper spar cap (in compression), as it would happen in the intact blade. The deformation of the blade section when total load is applied can be seen in figure 5.27. The maximum deformation is smaller than in S2P direction as, even though the defect is at maximum distance from the NA, it is still in the tension side. All in all, as first-ply failure criterion is taken, the blade performance is really reduced with respect to the intact blade.

CHAPTER 6
Conclusions and future work

6.1 Conclusions

From this study several conclusions can be drawn:

- The design of wind turbine blades should consider combined loading as a requirement as it is shown that safety factors under combined loading can be considerably reduced from those of uncoupled flapwise and edgewise loads.
- It is found in this blade section that $\pm 30°$ from pure positive flapwise bending are the directions most prone to buckling failure, regardless the presence of defects.
- The defects over the trailing edge decrease blade performance in more load directions under compression than that with defects over the spar cap-shear web joints. Furthermore, defects in the trailing edge have been found to highly affect blade performance as small defects can reduce the structural performance of rotor blades. Therefore, special caution should be paid to the manufacturing of this trailing adhesive region.
- The Tsai-Wu failure criterion is found to dominate over the adhesive failure criterion except the cases where the adhesive is present under maximum compression.

6.2 Recommendations for future studies

First of all, it is important to note that the model has been configured so it can resemble as much as possible a general blade section. However, the results of this study are limited with the consideration of first-ply failure criterion and the specific characteristics of the model (specially material and boundary conditions). Therefore, if this study can be continued, more specific influence of blade characteristics over the results should be enlightened. This way, further analysis in debonding defects must be also developed, so the parametric study of the most common defects can be completed. Drawing further conclusions of these type of defects can prioritize repairs in wind turbine blades or even reduce the amount of time a wind turbine is stopped. Moreover, a very interesting future study can be to analyze the influence

of defects and combined loading on a full-scale blade. Developing this parametric FEA study in a full-scale blade will lead to a more realistic and complete analysis.

Furthermore, combined loading is shown to be as important for blade design as pure flapwise or edgewise loading. On this note, further studies could be developed to analyze more in detail which are the specific load directions and points of the load envelope that should be accounted in this future Standard modification. In addition, fatigue testing under combined loading can also be a matter of further research. This report enlightens static testing under combined loading; however, fatigue testing is a more complicated study due to load introduction points and load excitation [3].

APPENDIX A

Debonding defects

Debonding or delamination is one of the most common defects studied in wind turbine blades. Delaminations are areas of no bonding adjacent laminaes which can be caused by air traps or a problem with resin infusion (production process) [16]. They normally takes place between different layers over the aft panels. The aft panels are formed of composite sandwich structures and, sometimes, debonding occurs when one of the composite layers (upper or lower) is separated from the foam.

Debonding is studied between the external layer and the core, as a defect in the external part of the blade is more probable. This defect has a different approach to that of the previous defects. The debonding defect is represented in Abaqus by unlinking the nodes of the implied layers over certain region of the defect. Therefore, in the debonded area, the nodes between the layers to separate are no longer the same ones. The previous nodes are assigned to elements of one of the layers and further nodes are created to define nodes of the second layer. As a consequence, the debonded surface has the same node coordinates but different node numbers. A Matlab code is created to automatically generate an input file that contains the modification of node numbers to introduce in the Abaqus input file.

In order to create a region for the defect in the central part of the aft panels, each studied layer has been divided into 5 element sets, with a master element in each region to create them (figure A.1).

The sets for both external and core layers are:

- Set 1 is defined by the initial master element, it covers all the region in x direction and the distance until the defect in z direction.

- Set 2 is defined by increasing z1 in the z direction to the node numbers and coordinates from those of the initial master element.

- Set 3 is defined by increasing zSet3 in the z direction to the node numbers and coordinates from those of the initial master element.

- Set 4 is defined by increasing z1 in the z direction plus xySet4 in the x direction to the node numbers and coordinates from those of the initial master element.

- Set 5 is defined by increasing z1 in the z direction plus xy1 in the x direction to the node numbers and coordinates from those of the initial master element. The nodes that the second layer shares with the first one are incremented to simulate the debonding, even though they have the same spatial coordinates.

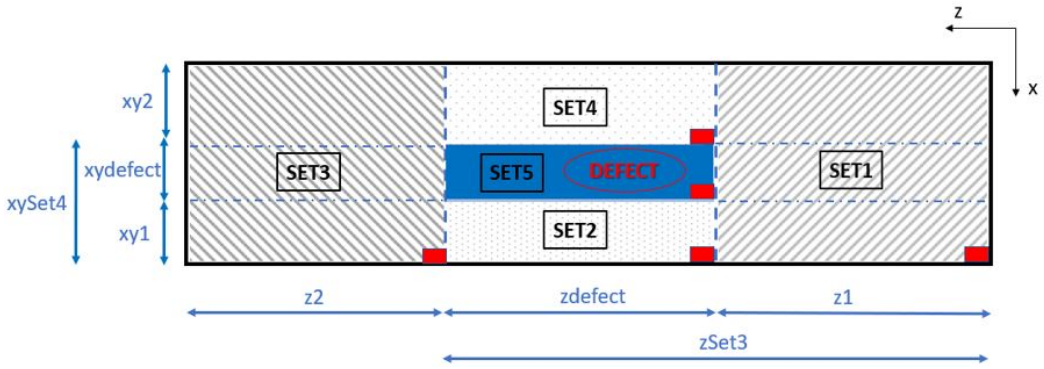

Figure A.1: Example of a layer when creating the debonding of the aft panels.

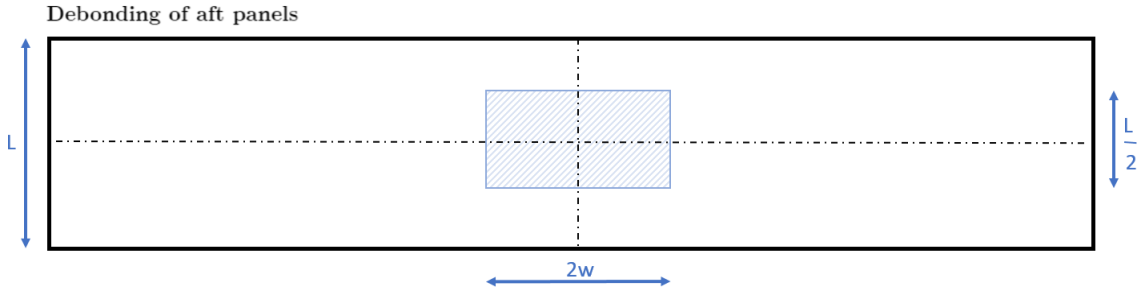

Figure A.2: Sketch of debonding defect.

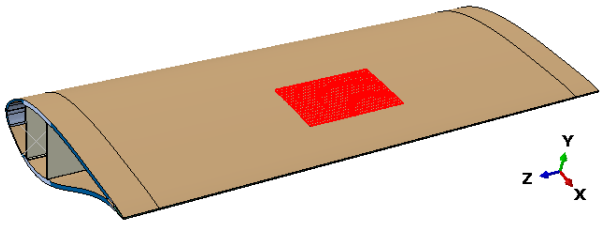

Figure A.3: Representation of the debonding defect in the blade model.

Debonding is investigated on the upper aft panel as the lower one would provide very similar results due to the relatively high symmetry of the present blade. The size of the defect considered is shown in figure A.2. As aft panels size is quite large, the defect has been taken over half of the whole height (x-axis) of the element set. The width of $2w$ is maintained as in the missing adhesive defects. The representation of this defect over the studied blade model is illustrated in figure A.3.

Analysis of the defect case

Figure A.4 shows the linear buckling analysis of this type of defect and the intact blade study differs from this one in the loading directions where the defect experiences compression. The defect is placed on the compression side from 210° to 0° loading directions, as shown in the figure. The aft panels do not contribute to the bending stiffness of the structure as much as the box girder or the leading and trailing edges. This way, the decrease of the performance in this kind of defect is lower than in the previous defects, having a similar response between the intact blade and the defect case. The greater difference is produced in the P2S extreme flapwise direction. The exception in this case is due to the increase of distance from the neutral axis to the defect when buckling is experienced. Even though the box girder bears the flapwise bending moment, the defect is proved to reduce performance in this extreme direction.

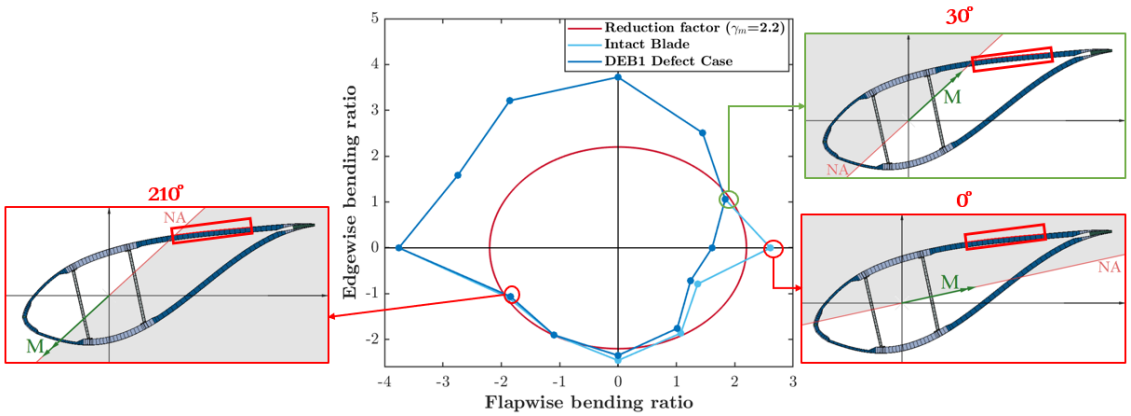

Figure A.4: Buckling envelope comparing the debonding defect with the intact blade. Specific load directions are illustrated over the blade cross section to clarify the mismatch between the intact blade and the defect buckling analyses. Grey colour under these cross sections indicates compression side and the defect is highlighted with a red rectangle.

The nonlinear analysis of this defect is illustrated in figure A.5. Only the loading directions that allow the defect to be in compression are affected by this one. However, the results are incorrect as the blade performance is better without defects that with them (intact blade has lower critical loads that those including the defect). The exact justification for this behaviour has not been triggered in the project time but some ideas for further studies have been considered.

The results must be produced according to specific characteristics of the current

blade model. Distribution of internal stresses or the configured boundary conditions might be having an influence over the results incoherence.

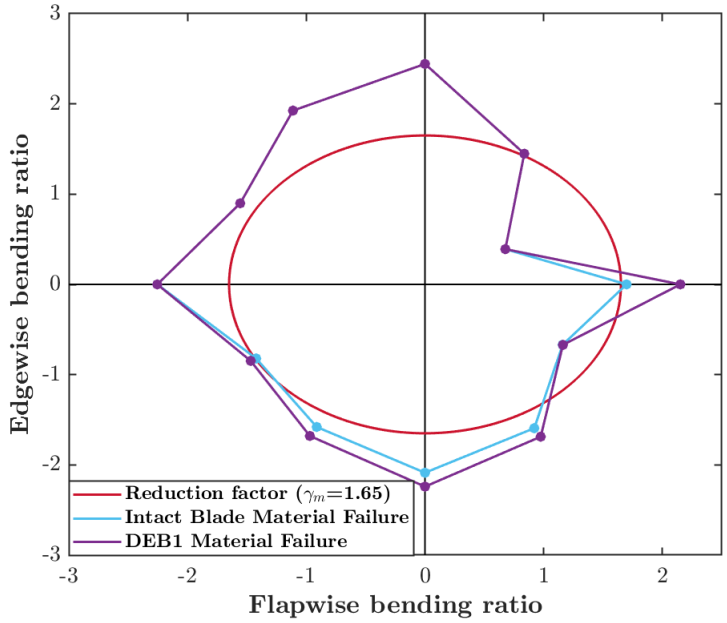

Figure A.5: Buckling envelope comparing the debonding defect with the intact blade.

Bibliography

[1] DNV GL. *Standard DNVGL-ST-0376, Rotor blades for wind turbines*. 2015.

[2] Sung Kyu Ha. Innovative design procedures for large-scale wind turbine blades. *JEC composites magazine*, (70):39–45, 2012.

[3] Martin Alexander Eder, Kim Branner, Peter Berring, Federico Belloni, Henrik Stensgaard Toft, John Dalsgaard Sørensen, Adrien Corre, Torben Lindby, Amilcar Quispitupa, and Thomas Karl Petersen. *Experimental Blade Research - phase 2*. DTU Wind Energy, Denmark, March 2015. Energiteknologisk udvikling og demonstration (EUDP), J.nr. 64011-0006.

[4] Abaqus keywords reference guide. `http://dsk.ippt.pan.pl/docs/abaqus/v6.13/books/key/default.htm`.

[5] Xiao Chen, Xiaolu Zhao, and Jianzhong Xu. Revisiting the structural collapse of a 52.3m composite wind turbine blade in a full-scale bending test. *Wind Energy*, 20(6):1111–1127, 2017.

[6] I. Amenabar, A. Mendikute, A. López-Arraiza, M. Lizaranzu, and J. Aurrekoetxea. Comparison and analysis of non-destructive testing techniques suitable for delamination inspection in wind turbine blades. *Composites Part B: Engineering*, 42(5):1298 – 1305, 2011.

[7] Kim Branner and Amin Ghadirian. *Database about blade faults*. DTU Wind Energy, Denmark, 2014.

[8] Jr. Charles E. Harris, James H. Starnes and Hampton Virginia Mark J. Shuart, Langley Research Center. Advanced durability and damage tolerance design and analysis methods for composite structures, 06 2003.

[9] Paul Dvorak. Listening for damage and flaws in wind turbines blades. *Wind Power Engineering and Development*, January2, year =.

[10] IRENA. *Renewable Power Generation Costs in 2017*. International Renewable Energy Agency, 2018.

[11] Xiao Chen. Experimental investigation on structural collapse of a large composite wind turbine blade under combined bending and torsion. *Composite Structures*, 160:435 – 445, 2017.

[12] L. Espinosa N. Koorn D. Smissaert. F. Lahuerta, M. J. de Ruiter. Assessment of wind turbine blade trailing edge failure with sub-component tests. 2017.

[13] Abaqus analysis user's manual. `http://130.149.89.49:2080/v6.8/books/key/default.htm?startat=ch02abk15.html#usb-kws-hbuckle`.

[14] Dan Zenkert and Mark Battley. *Laminate and Sandwich Structures. Foundations of fibre composites*. DTU Mechanical Engineering Department, 2^{nd} edition, 08 2009.

[15] George Balokas and E.E. Theotokoglou. Structural analysis and materials selection in cross-section of composite wind turbine blade. 06 2011.

[16] H.S. Toft, P Berring, Kim Branner, and John Sørensen. Distribution of defects in wind turbine blades and reliability assessment of blades containing defects. *European Wind Energy Conference and Exhibition 2009, EWEC 2009*, 1:344–371, 01 2009.